UNIVERSITÉ DE GENÈVE
FACULTÉ DES SCIENCES
Département de chimie minérale, analytique et appliquée
Professeur Michal Borkovec

Charging behavior of polyamines in solution and on surfaces: A potentiometric titration study

THÈSE

présentée à la Faculté des sciences de l'Université de Genève
pour obtenir la grade de Docteur ès sciences, mention chimique

par
Duško Čakara
de
Zagreb (Croatie)

Thèse N° 3555

GENÈVE
Atelier de reproduction de la Section de physique
2004

Contents

Résumé

La méthode des titrages potentiométriques est utilisée pour les études du comportement électrostatique des polyélectrolytes ou des interfaces colloïdales, en milieu aqueux. Le titrage potentiometrique nous permet de mesurer la

charge provenant des reactions acide-base. Les espèces participant à l'échange des protons avec l'eau, peuvent être libres dans la solution, présentes sous la forme d'un polyélectrolyte, ou encore se situer à une interface.

Au cours de la thèse, un titrateur automatique, complétement commandé par ordinateur, a été assemblé dans l'atelier d'électronique du département. Les programmes pour effectuer les titarages potentiométriques à forces ioniques constantes, ont été mis en œuvre. Le titrateur est composé de quatre burettes de haute précision, d'une cellulle permettant une grande augmentation du volume de la solution, d'un voltmètre de haute impédance, d'un couple d'électrodes pour la mesure du pH (électrode de verre et une électrode de référence Ag/AgCl) et d'un système de dégazage par l'azote. Un convertisseur analogique-digital a été incorporé avec le voltmètre. Le nouveau titrateur "Jonction" est représenté sur la figure à la page suivante et décrit dans l'annexe de la thèse.

Dans le premier chapitre sont présentées la méthodologie expérimentale, ainsi que l'analyse des données pour une évaluation de la charge présente sur une molécule subissant l'échange de protons avec l'eau. Pour obtenir les données de l'acidité en fonction du pH, un titrage est effectuée, durant lequel les volumes des solutions ajoutées (HCl, KOH, KCl) et le pH, sont mesurés. L'expérience est

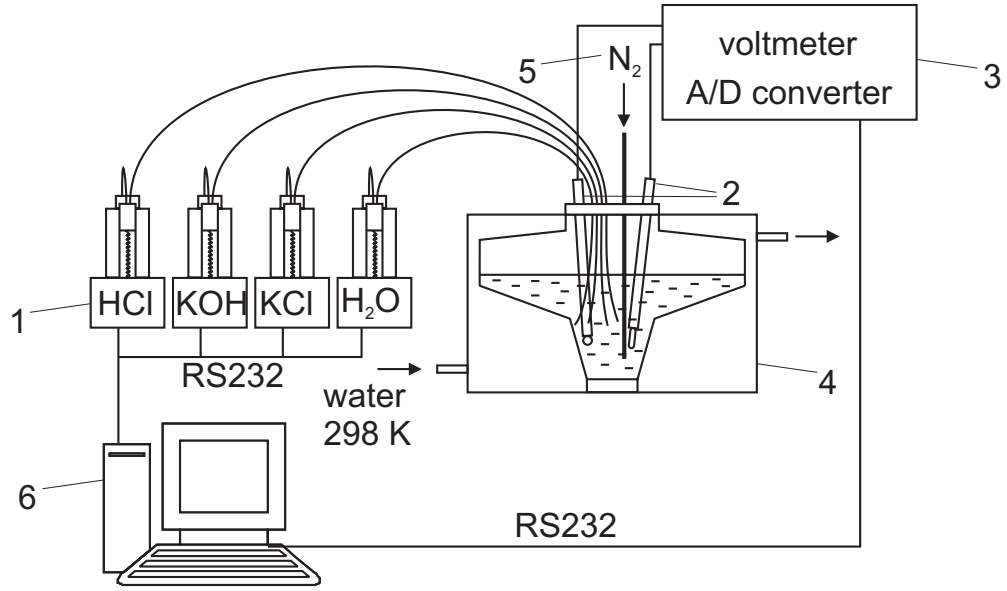

Le titrateur Jonction.

réalisée avec et sans la substance analysée. L'évaluation de la charge se base sur une soustraction de l'acidité de solution blanc, à l'acidité de solution contenant la molécule analysée. Une normalisation de la charge par la charge maximale donne le degré de protonation; et la dépendence de ce dernier avec le pH est nommée l'isotherme de liaison des protons. L'interprétation des courbes de titration du blanc est effectuée avec une fonction analytique dont les paramètres sont obtenus par régression non-linéaire. Cette procédure nous permet de vérifier les conditions d'expérience. En outre, la précision expérimentale est verifiée en analysant les substances standards dont les valeurs de pK apparaissent dans la littérature, en particulier l'acide acétique et l'éthylène diamine. De très satisfaisants résultats expérimentaux ont mis en évidence une grande précision de mesure avec des valeurs de pK très proches des valeurs théoriques.

Dans le deuxième chapitre, la méthode poténtiométrique est mise en œuvre pour analyser le comportement électrostatique du dendrimère poly(amidoamine). La structure chimique de cette molécule est representée sur la figure à la page

suivante. Un mécanisme de protonation est proposé: il se base sur un traitement statistique de toutes les espèces provenant de la protonation. Ceci inclut une distinction des espèces macroscopiques et des espèces microscopiques. L'espèce macroscopique est définie par le nombre des protons liés à la molécule, m. Ceci est aussi appellé l'état de protonation macroscopique. Les états microscopiques sont definis par la distribution des protons liés parmi les sites de protonation. Pour un macro-état donné, les états microscopiques peuvent être définis en utilisant un vecteur de dimension m, composé d'une variable binaire, s_i, assignée à chaque site i. Donc, les espèces microscopiques sont definies par le vecteur s_i, où $i = 1$ à m. L'énergie d'un état microscopique peut être modelisée en utilisant l'expansion:

$$\frac{\beta F(\{s_i\})}{\ln 10} = -\sum_i \mathrm{p}\hat{K}_i s_i + \frac{1}{2!}\sum_{i,j} \epsilon_{ij} s_i s_j + ...$$

où la sommation est effectuée sur tous les sites i, les $\mathrm{p}\hat{K}_i$ dénotent des constantes de protonation microscopiques, ϵ_{ij} dénotent des interactions entre les sites voisins, et $\beta = 1/kT$. Toutes les probabilités statistiques des espèces macroscopiques, ainsi que microscopiques, peuvent être calculées en utilisant l'équation ci-dessus. Dans ce cas-là, les probabilités statistiques correspondent aux abondances des espèces dans la solution. Par ailleurs, il est possible de calculer les constantes de protonation macroscopiques et microscopiques. Pour un micro-état donné, les constantes microscopiques sont la mesure de l'energie de liaison d'un proton à un site particulier, les $\mathrm{p}\hat{K}_i$ sont des microconstantes du micro-état dans lequel la molécule est complètement déprotonée, et avec ϵ_{ij}, ils forment les paramètres "cluster".

La symétrie moléculaire des dendrimères permet l'établissement des paramètres cluster, toujours selon le même principe, dont le nombre de ces paramètres reste modéré. Il est possible de calculer toutes les constantes de protonation en utilisant ces paramètres; et réciproquement, il est possible d'obtenir les paramètres cluster des isothermes de protonation, de manière similaire à la régression non-linéaire.

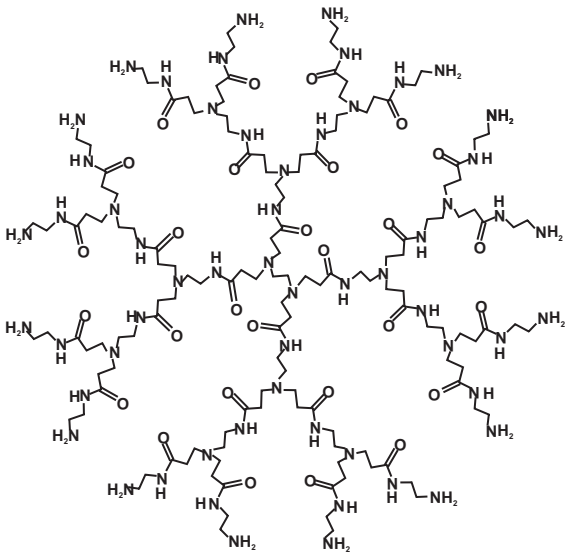

dendrimère poly(amidoamine)

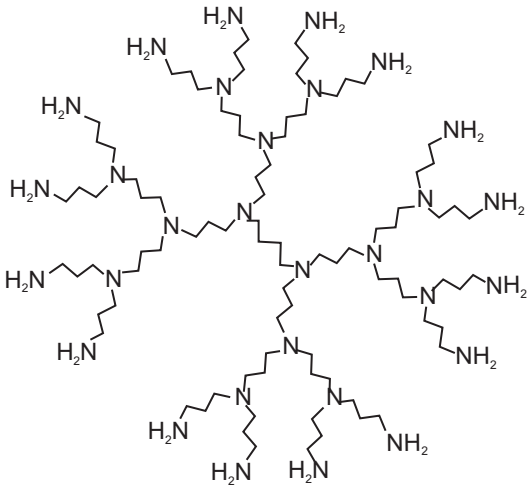

dendrimère poly(propylèneimine)

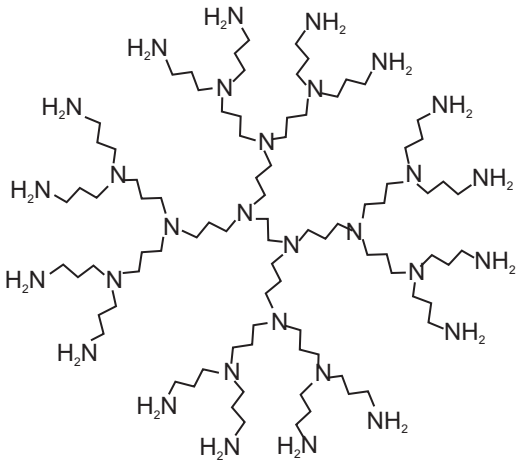

dendrimère (2,3)

Les dendrimères étudiés de génération G2.

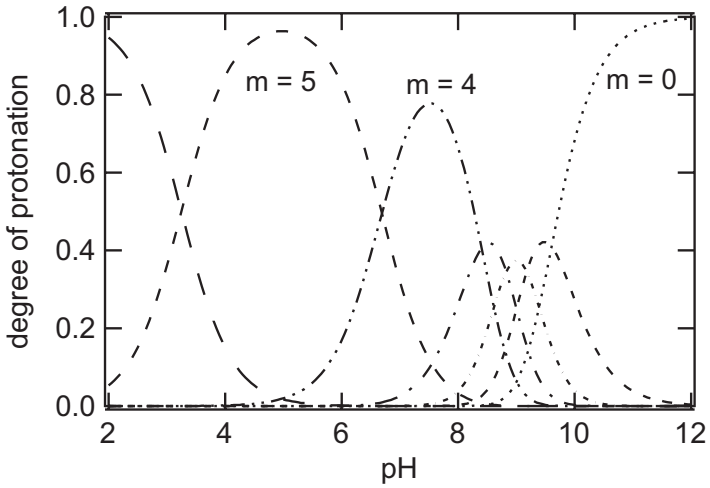

Mécanisme de protonation macroscopique de dendrimère poly(amidoamine) G1.

Par la suite, les isothermes de protonation des six premières générations du dendrimère poly(amidoamine) ont été analysées par le modèle. Six paramètres cluster sont déterminés, ceci suffisant pour une très bonne description des courbes expérimentales. Les constantes de protonation macroscopiques sont calculées en utilisant les paramètres cluster. Puis, la connaissance des constantes macroscopiques permet d'établir les diagrammes d'abondance des espèces macroscopiques par rapport au pH. On appelle ceci un mécanisme de protonation macroscopique. Pour les deux premières générations, pour lequelles le nombre de sites reste modéré, il est même possible d'obtenir ces constantes directement par régression non-linéaire. Les valeurs obtenues de cette façon, sont en très bon accord avec des valeurs calculées à partir des paramètres cluster. Un mécanisme de protonation macroscopique pour la première génération de dendrimère poly(amidoamine), est présenté sur la figure ci-dessus.

Les mécanismes de protonation microscopique tiennent compte des probabilités de présence de toutes les micro-espèces, en fonction du pH. Aussi pour

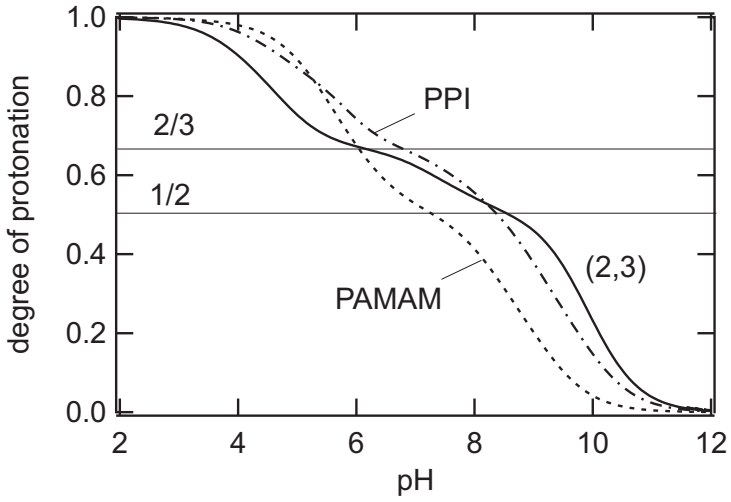

Isothermes de protonation de la quatrième génération des dendrimères poly(amidoamine), poly(propylèneimine) et (2,3).

les mécanismes macroscopiques, il est possible d'établir les mécanismes microscopiques en partant des paramètres cluster, cela en utilisant un traitement statistique, où l'équation 1 donne les probabilités de présence des micro-espèces.

Dans le troixième chapitre, les mécanismes de protonation sont comparés pour trois types de dendrimères polyamine, à savoir les dendrimères poly(amidoamine), poly(propyleneimine), et un dendrimère qui ressemble à ce dernier, mais avec une unité centrale plus longue. Au moment de la rédaction de la présente thèse, ce dernier dendrimère, n'est pas présent dans la litterature scientifique, car pas encore synthétisé. Nous le nommons alors ici, dendrimère (2,3). Les isothermes de protonation pour la quatrième génération des tous les dendrimères, sont répreésentées sur la figure ci-dessus. Les mécanismes de protonation de trois types de dendrimères se présentent différement. Le dendrimère poly(amidoamine) est protoné en deux étapes distinctes. Dans une première zone du pH comprise entre 10 et 7.5, les sites amines primaires sont protonés, et le reste l'est de pH 7 à 4. Dans la région de pH entre ces deux zones, apparaît une micro-espèce, avec

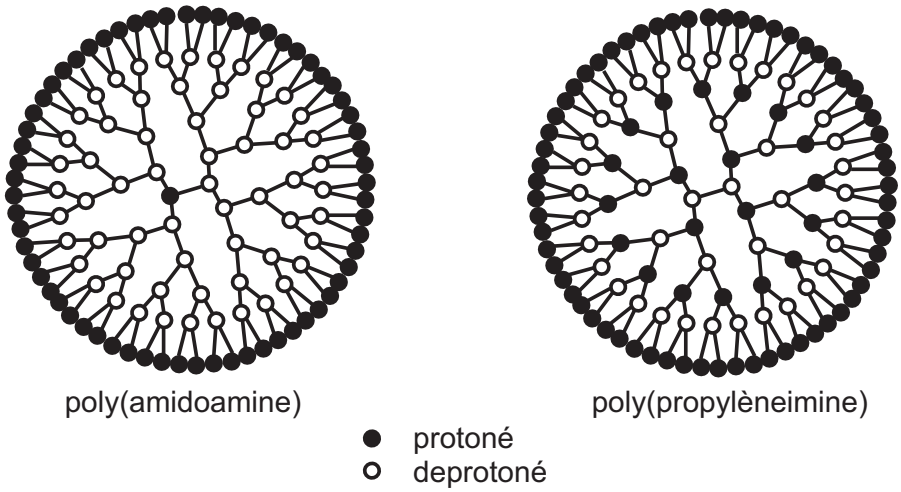

Micro-espèces intermédiaires présentes autour du pH=7, pour les dendrimères poly(amidoamine) et poly(propylèneimine).

des sites amines primaires protonés, ce qui donne un plateau dans l'isotherme de protonation au degré de protonation égal à un demi. Pour le dendrimère poly(propylèneimine), l'isothèrme du protonation montre deux zones. Le plateu intermédiaire se situe au degré du protonation égal à deux tiers. Là, les sites amines primaires et tous les autres sites qui se situent dans les anneaux impairs, en comptant l'anneau avec les sites primaires comme étant le premier, sont protonés. Le dendrimère (2,3) montre des caractéristiques dans le mécanisme de protonation, qui ont des ressemblances avec les deux dendrimères, poly(amidoamine) et poly(propylèneimine). Pour la génération zéro, le mécanisme est proche de celui du dendrimère poly(amidoamine), et pour les générations suivantes, il ressemble plus au mécanisme du dendrimère poly(prolpylèneimine). Les micro-espèces intermédiaires présentes autour de pH=7, données par les mécanismes microscopiques pour les dendrimères poly(amidoamine) et poly(propylèneimine) sont présentées sur la figure ci-dessus.

Le comportement électrostatique des surfaces colloïdales chargées, en absence

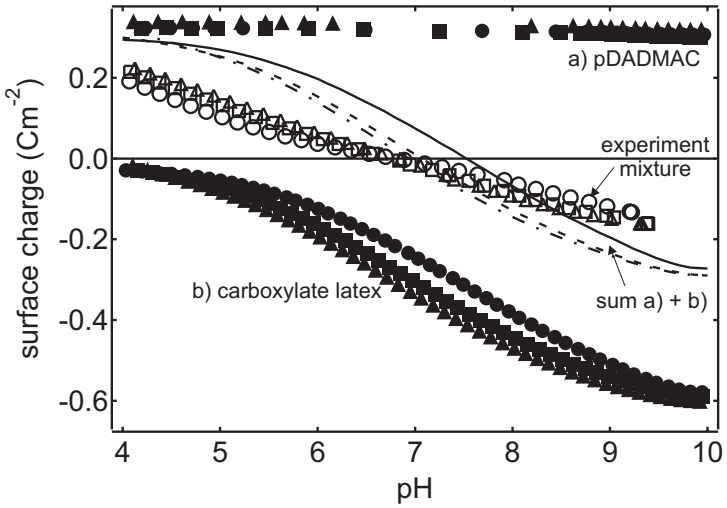

Isothermes de protonation de latex carboxil pur, de pDADMAC pur et de latex en présence de pDADMAC adsorbé. Les courbes représentent la somme des charges des composants purs.

et en présence d'un polyélectrolyte de charge opposée, est presenté dans les deux derniers chapitres. Dans le chapitre 4, les isothermes de protonation des particules de latex carboxylé sont étudiée en absence et en présence du poly(chlorure de dimethyldiallylammonium) (pDADMAC). La structure de la surface est presentée sur la figure 4. Les isothermes du protonation pour le latex en absence du pDADMAC, montrent le comportement typique d'une surface avec des sites acide faible. Les isothermes de protonation du pDADMAC pur, ne montrent aucune dépendance en charge, par rapport au pH. Par contre, les isothermes de protonation de la surface, avec le pDADMAC adsorbé, donc dans le cas d'un système mixte, montrent une inversion de charge autour d'une certaine valeur pH. Cette valeur peut être considérée comme le point de charge nulle (PCN), auquel de le potentiel électrostatique de surface est égal à zéro. Les isothermes des composants purs, ainsi que de système mixte, sont présentés sur la figure à la page suivante.

Le comportement électrostatique de la surface du latex carboxylé, en présence du pDADMAC, ressemble au comportement d'une surface d'un oxyde métallique, par le fait de la présence du point de charge nulle. La coïncidence existe entre celui-ci, et le point isoeléctrique trouvé par des mesures de mobilité électrophoretique du même système. De plus, le point de charge nulle du système mixte peut-être régi par la quantité de polyélectrolyte adsorbé. Cependant, le point de charge nulle est présent dans les isothermes d'adsorption, mais uniquement dans les cas d'adsorptions correspondant au rapport numérique entre les sites DADMAC et carboxylates < 1. Le comportement électrostatique de système mixte est bien en accord avec un modèle de Stern, modifié pour la présence du polyélectrolyte adsorbé.

Tout l'excès de charge dissout, y compris les sites DADMAC dans la solution, peut être détecté comme un excès de charge au point de charge nulle, en observant l'isotherme de protonation. Ceci est utile pour la détermination quantitative d'adsorption de pDADMAC sur la surface de latex. Observée de cette manière, l'adsorption coïncide bien avec celle mesurée par l'analyse de carbone et d'azote totaux dans la solution, comme le montre la figure à la page suivante.

Le même comportement électrostatique, précédemment observé pour le système mixte pDADMAC-latex carboxylé, est remarquable pour le système pDADMAC-silice. La surface de la silice exerce un comportement acide, dans la région de pH d'étude, ce qui est montré sur la figure à la page suivante. Cependant, quand le pDADMAC est présent à la surface, les isothermes de protonation font remarquable le point de charge nulle. Dans les expériences présentées dans le cinquième chapitre, l'effet de la masse molaire du pDADMAC sur la compensation de la charge de surface de la silice est étudié en comparant les dépendances du point de charge nulle, au taux de charge du DADMAC adsorbé, cela pour deux masses molaires, à savoir 100 et 500 kDa. La figure présentée à la page xi ne revèle aucun effet de masse molaire.

La méthode de titrage potentiométrique s'est montrée adaptée pour effectuer

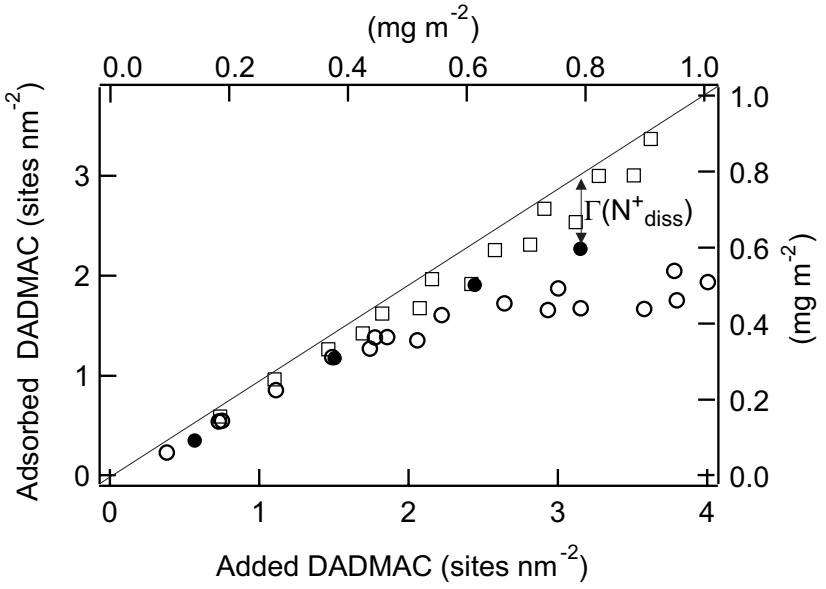

Comparaison entre l'adsorption déterminée à partir des isothermes de protonation (symboles noirs), et des mesures directes (symboles blancs).

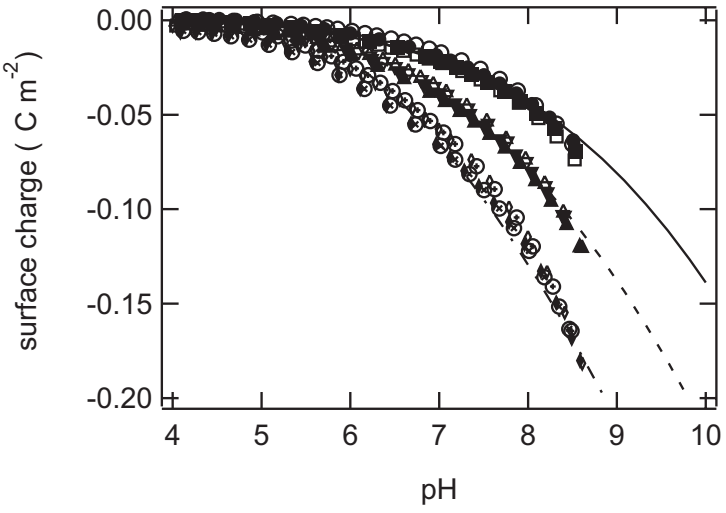

Isothermes de protnation de la silice à trois forces ioniques differentes. Les courbes dénotent du modèle de Stern.

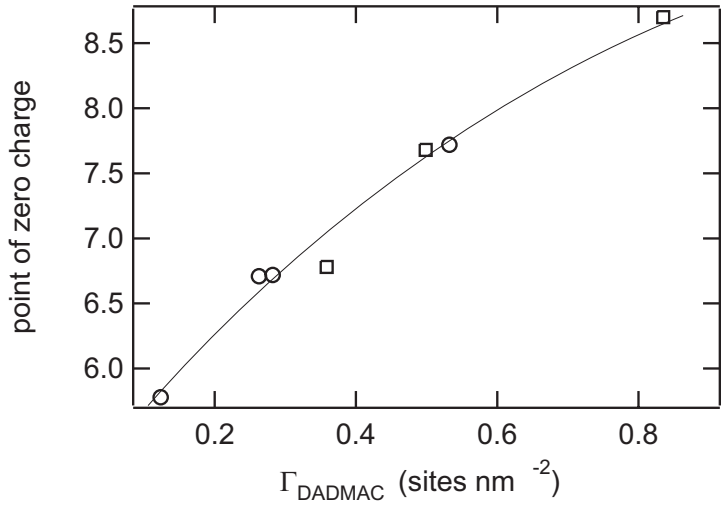

Point de charge nulle pour silice en présence du pDADMAC, en fonction d'adsorption.

les études du comportement électrostatique des espèces chargées en milieux aqueux, notamment des polyélectrolytes, des surfaces colloïdales, et des mélanges des deux.

Les études des mécanismes de protonation des dendrimères polyamines ont confirmé le modèle de protonation, suivant lequel les interactions électrostatiques entre les sites voisins jouent un rôle très important, ainsi que les valeurs des pK microscopiques inhérents aux sites eux-mêmes. Dans ce sens, le dendrimère poly(amidoamine), selon lequel les sites de protonation voisins sont distants, revèle un mécanisme de protonation determiné uniquement par les valeurs de pK microscopiques. Au contraire, le dendrimère poly(propylèneimine), dont les sites voisins sont plus proches, est caractérisé par un mécanisme où la protonation des sites voisins est évitée pour raison de répulsion électrostatique.

Le comportement électrostatique d'une surface faiblement acide, s'est montré très différent en présence, et en absence d'un polyélectrolyte de charge positive. En absence de celui-ci, le potentiel de surface est toujours négatif, et les

isothermes de protonation montrent toujours une charge négative, augmentent avec le pH. En présence du polyélectrolyte adsorbé, la charge de surface peut être inversée par les protons liés et le potentiel de surface est égal à zéro autour d'une valeur de pH donnée, soit au point de charge nulle. Pour cette raison, les isothermes de liaison des protons à forces ioniques différentes, se croisent dans une étroite région de pH. Le point de charge nulle peut être modulé par la quantité de polyélectrolyte adsorbé. D'ailleurs, la charge mesurée au pointe de charge nulle peut être utilisée pour déterminer le taux d'adsorption, et cela est en très bonne adéquation avec les mesures directes. La dépendance du point de charge nulle avec l'adsorption, pour deux masses molaires différentes, s'est montrée égale, ce qui ne souligne aucune influence de la masse molaire du polyélectrolyte sur le comportement électrostatique de l'interface.

Introduction

Polyelectrolytes are polymers which are charged in aqueous solutions. Strong and weak polyelectrolytes can be distinguished, one carrying strong, and the other weak acidic or basic moieties. In water solutions, polyelectrolyte molecules present a source of an excess charge, which stems from the conjugate pairs of acid or base groups. The conformation of polyelectrolytes, as well as their mutual interactions, are both closely related to the charge [1, 2]. This is important for many of the solution properties, such as the viscosity [1, 3], aggregation stability and aggregate structure [4], the response to the electrical and mechanical fields [5], etc. On the other hand, the charge present on weak polyelectrolytes is tunable by the solution conditions (pH, ionic strength), which can be used to control the solution properties [1, 6].

The behavior of polyelectrolytes at a solid/liquid interfaces is interesting partly due to the importance in industrial and environmental processes, and partly due to the complexity of such systems. For example, polyelectrolytes can be used to stabilize suspensions of particles, or induce their precipitation, which is extensively used in industry (paper production, construction materials, food production), purification of waste waters by flocculation, etc. As well, adsorption of polyelectrolytes at charged particles is important in production of spherical membranes by self-assembled monolayers, which gained huge interest during the past decade [7]. In all the above cases, a handful of colloidal properties, such as the viscosity, colloidal stability, electrophoretic mobility, permeability of the

polyelectrolyte layers for small molecules etc, strongly depend upon the surface charge. One of the goals of the present study, is to reduce the current deficit in experimental surface charge data, and contribute to the understanding of pH-dependent charging of surfaces in the presence of adsorbed polyelectrolytes.

The most straightforward method for measuring the equilibrium excess charge in a system, which contains acid or base, is the potentiometric titration [6, 8]. The methodology for estimating the solution excess charge from the potentiometric titration data will be presented in the first chapter of this thesis. This will include a thorough description of potentiometric data analysis, which will be supported with experimental examples, the tests of precision and accuracy, and discussions of error sources. Within the present thesis, a computer-controlled high-precision titrator was developed. A peculiarity of this setup is the facility of performing repeated titration experiments at constant ionic strengths, including real-time data monitoring. A thorough technical description of this setup, directions for programming and running, are presented in the appendix.

The focus of the second and the third chapter is on the protonation behavior of hyperbranched polyamines in solutions. In the second chapter, the proton binding isotherms of six different generations poly(amidoamine) dendrimers are reported at different ionic strength. The fact that the protonation state of one site can influence the protonation constant (pK) of another site, makes the solution of the acid-base equilibria for polyelectrolytes more complicated than in the case of simple or oligo-acids or bases, as was confirmed in numerous experimental studies [1]. In the present thesis, this problem is addressed by applying a simple site-binding model similar to the Ising model [9], which includes only several parameters, and can be resolved by applying statistical mechanics. Within this model, the same set of parameters can be applied for different types of molecules, and its usefulness is demonstrated in the third chapter, where a comparison of the detailed, microscopic charging mechanisms is presented for three types of dendritic polyamines, namely the poly(amidoamine), poly(propyleneimine), and

an imaginary dendrimer, which has a structure similar to poly(propyleneimine) dendrimer, but with a short core unit.

Fourth chapter presents a study of the charging properties of weakly acidic carboxylate latex particles, in the presence of poly(dimethyldiallylammonium chloride), which is a strong polycation. It is demonstrated, that the adsorbed amount of polyelectrolyte can be inferred from the proton binding isotherms. The applicability of the basic Stern model and a modified version of that model, was investigated for the interpretation of the experimental data. Particularly interesting results were obtained with the modified Stern model.

In the fifth chapter, the charging behavior of silica in the presence of adsorbed poly(dimethyl-diallylammonium chloride) is reported. There, the focus is on the influence of the polyelectrolyte molecular weight on the adsorption, and the protnation behavior of silica.

Chapter 1

Potentiometric titrations at constant ionic strengths

1.1 Introduction

In water solutions, charged species are produced through dissociation reactions. For monoprotic acids and bases, the dissociation can be noted as:

$$\mathrm{HA} \rightleftharpoons \mathrm{H^+} + \mathrm{A^-}; \qquad K_\mathrm{d}^a = \frac{a_{\mathrm{H^+}} a_{\mathrm{A^-}}}{a_{\mathrm{HA}}} \tag{1.1a}$$

$$\mathrm{B^+} + \mathrm{H_2O} \rightleftharpoons \mathrm{H^+} + \mathrm{BOH}\ ; \qquad K_\mathrm{d}^a = \frac{a_{\mathrm{H^+}} a_{\mathrm{BOH}}}{a_{\mathrm{B^+}}} \tag{1.1b}$$

where a_X represents the equilibrium activity of the species X (by definition, activity of water equals unity), and K_d^a represents the dissociation equilibrium constant. The analytical concentrations of the species X, c_X (or alternatively [X]), are related to their activities, through the activity coefficients

$$\gamma_\mathrm{X} = \frac{a_\mathrm{X}}{c_\mathrm{X}}. \tag{1.2}$$

It is also useful mentioning the mixed constants[8]:

$$K_\mathrm{d} = \frac{a_{\mathrm{H^+}}[\mathrm{A^-}]}{[\mathrm{HA}]} \tag{1.3}$$

$$K_{\mathrm{d}} = \frac{a_{\mathrm{H^+}}[\mathrm{BOH}]}{[\mathrm{B^+}]} \tag{1.4}$$

These constants are not the true thermodynamic constants, to which they can be related through the activity coefficients.

Equations (1.1a) and (1.1b) can be extended for polyprotic acids and bases, which will be discussed in the chapter 3. For example, for a simple diprotic acid, we can define the equilibirum constant for each step:

$$\mathrm{H_2A} \rightleftharpoons \mathrm{H^+} + \mathrm{HA^-}\ ; \qquad K^a_{\mathrm{d},1} = \frac{a_{\mathrm{H^+}} a_{\mathrm{HA^-}}}{a_{\mathrm{H_2A}}} \tag{1.5a}$$

$$\mathrm{HA^-} \rightleftharpoons \mathrm{H^+} + \mathrm{A^{2-}}\ ; \qquad K^a_{\mathrm{d},2} = \frac{a_{\mathrm{H^+}} a_{\mathrm{A^{2-}}}}{a_{\mathrm{HA^-}}} \tag{1.5b}$$

where $K^a_{\mathrm{d},i}$ denote the equilibrium constants for each step i.

The overall degree of protonation of a polyprotic acid or a base, θ, is defined as:

$$\theta = \frac{\frac{1}{[\mathrm{X}]_0} \sum\limits_n n[\mathrm{X_n}] - n_{\mathrm{min}}}{n_{\mathrm{max}} - n_{\mathrm{min}}} \tag{1.6}$$

where n denotes the charge number of a dissociation species, n_{min} and n_{max} are the minimum and maximum charge numbers, respectively (for acids, n is negative, and for bases it is positive). The total concentration is given by

$$[\mathrm{X}]_0 = \sum_n [\mathrm{X_n}] \tag{1.7}$$

To be able to compare the concentrations of species in different solutions, the relative concentrations, $[X]/[X]_0$, have to be used. The pH scale and the ionic product of water, K_{w}, are defined as:

$$\mathrm{pH} = -\log_{10} a_{\mathrm{H^+}},\ \text{and} \tag{1.8}$$

$$K_{\mathrm{w}} = a_{\mathrm{H^+}} \cdot a_{\mathrm{OH^-}}. \tag{1.9}$$

The electroneutrality condition is one of the most important concepts for resolving the speciation in water solutions [8]. It states that the net charge of the

solution as a whole equals zero:

$$\sum_n n[\mathrm{X_n}] + [\mathrm{H^+}] - [\mathrm{OH^-}] = 0 \tag{1.10}$$

where $[\mathrm{X}_n]$ is the analytical concentration of a species X_n. For example, if the solution contains HCl, KOH and KCl, the electroneutrality condition reads:

$$[\mathrm{H^+}] + [\mathrm{K^+}] - [\mathrm{OH^-}] - [\mathrm{Cl^-}] = 0 \tag{1.11}$$

H-Acidity and OH-Alkalinity are two quantities, which will be useful for the calculation of the proton binding isotherms. The H-Acidity ([H-Acy]) is the excess concentration of the protons, with respect to their concentration in a neutral solution. For example, in a solution of acetic acid, KOH, and HCl, the H-Acidity is:

$$[\text{H-Acy}] = [\mathrm{H^+}] - [\mathrm{OH^-}] - [\mathrm{CH_3COO^-}] = [\mathrm{Cl^-}] - [\mathrm{K^+}] \tag{1.12}$$

Conversely, the OH-Alkalinity ([OH-Alk]), is the negative H-Acidity, for example:

$$[\text{OH-Alk}] = [\mathrm{CH_3COO^-}] + [\mathrm{OH^-}] - [\mathrm{H^+}] = [\mathrm{K^+}] - [\mathrm{Cl^-}] \tag{1.13}$$

The activities of all the dissociation species are mutually dependent[10]. Therefore, at a fixed initial composition of the solution, the overall speciation can be regulated by changing the activity of one single species. Since the proton activity is easily measurable, it is convenient to express the concentrations of the dissociation species versus pH. This also enables a comparison of the speciation in different solutions (e.g. two different acids), with the same total concentrations (this is the reason for which pH is called the "master" variable[8]).

Proton binding isotherm is the dependency of the overall degree of protonation of an acid or a base, upon pH, $\theta(\mathrm{pH})$ (see figure 1.1). proton binding isotherm reflects the dissociation speciation in the solution, and is fully defined by $\mathrm{p}\bar{K}_{\mathrm{d},i}$ values and the pH. For example, for acetic acid, when $\mathrm{pH} < \mathrm{p}K_\mathrm{d}$, the protonated $\mathrm{CH_3COOH}$ species dominate over the deprotonated, charged $\mathrm{CH_3COO^-}$ species.

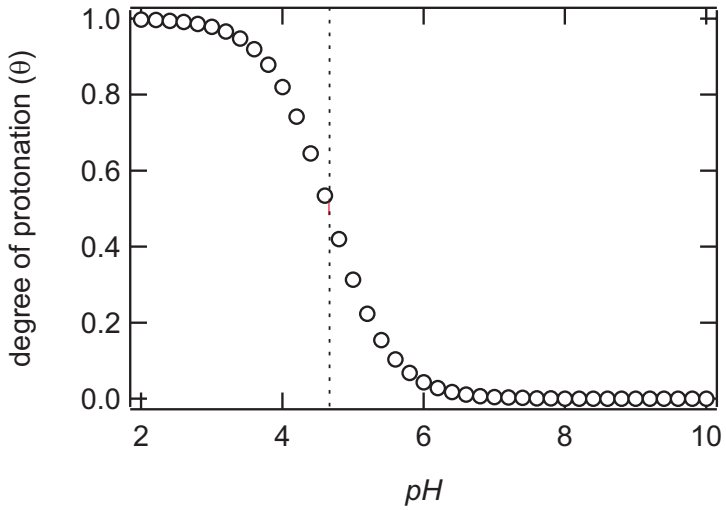

Figure 1.1: Example of a modeled proton binding isotherm of acetic acid at 0.1 M ionic strength. The dashed line denotes pH=pK_{d}=4.66[11].

When pH $>$ pK_{d}, the situation is reversed. In the case where the initial acid or base concentration is proportional to some other measurable quantity, e.g. the surface area of a particle with acidic or basic surface groups, the degree of protonation, θ, can be replaced with the charge (in Coulombs) per surface area, or the number (in moles) of elementary charges per surface area.

1.2 Potentiometric titration method

For the experimental determination of the proton binding isotherms, it is necessary to measure the concentrations of the charged dissociation species upon a variation of pH in the solution. Many quantitative analytical methods can serve for the measurement of the charged species equilibrium concentrations, for example, spectrophotometry, NMR, conductometry, voltammetry, etc. Nevertheless, the most common way to obtain the proton binding isotherm are the potentiometric titrations [8].

Potentiometric titration is a method, where the pH of the solution is varied by

controlled and measured additions of strong acid or base (e.g. HCl or KOH), and simultaneously measured by a pH-sensitive electrode couple. The usual (minimal) experimental setup includes a burette that contains a strong acid or base at a known concentration, a pH-measurement couple (combined glass electrode, or separated glass and reference electrodes) with a high-impedance voltmeter, the titration vessel and a stirrer [12]. Although the existence of the first automated titrators was reported already in the late sixties [13], the appearance of the personal computers triggered the wide use of such systems (one example of the first PC-controlled titrator stems from 1978 [14]). The earliest review of the automated potentiometric titration methodology, known to this author, originates from 1968 [15].

The measured quantities are the electromotive force of the pH-sensitive electrode couple, the volumes of the strong electrolyte(s) added to the system, and the total volume of the system (sum of the initial volume and the added volume(s)). From these data, the experimental titration curves (OH-Acidity versus pH) are calculated. The term "blank titration" will be used for a titration of a system, which contains only strong acid and strong base counterions at concentrations that are regulated through the additions from the burettes, protons and hydroxyle ions. For the system which, in addition to this, contains a substance for which the proton binding isotherm should be calculated (e.g. acetic acid), the term "analyte titration" will be used.

In the present work, a method for automated potentiometric titrations at constant ionic strengths was developed. The setup resembles to the Wallingford titrator [16], and includes four burettes, each containing strong acid, strong base, 1:1 salt solution at high concentration, and water. For each titration step, the additions of all of the burette solutions are calculated by the computer. The titrations were automatically performed at pre-defined and controlled constant ionic strengths. In particular, this means that the pH was swept in a controlled way, and the titration data (the glass electrode potential with respect to an Ag/AgCl

reference electrode, as measured by a high-impedance voltmeter, and the volumes of the added solutions) were collected at pre-defined ionic strengths, which were kept constant during one titration run. Successive forward and backward titration runs were performed (throughout this text, "forward" titration means the pH sweep from the initial to the final pre-defined pH value, and "backward" is the opposite direction), at different ionic strengths, which were adjusted after a forward and backward titration cycle.

1.3 Experimental setup

In this work, with an invaluable effort of Stephane Jeannerret, a computer-controlled high-precision titration setup was built from scratch. The experience with the Wallingford titrator [16] was very helpful to fulfill this task. The new titrator is called the "Jonction" titrator. The scheme of the Jonction titrator setup is presented in figure 1.2. All the technical details about the "Jonction" titrator, and the details about the software needed to run the constant ionic strength titrations, are presented in the appendix of this thesis.

The hardware of the Jonction titrator consists of the following (the numbers in the list correspond to the scheme presented in fig. 1.2):

1. Four Metrohm 712 Dosimat burettes with tubings
2. pH-measurement electrode couple
3. Voltmeter (with A/D converter)
4. Titration cell
5. Pure nitrogen degassing apparatus
6. PC

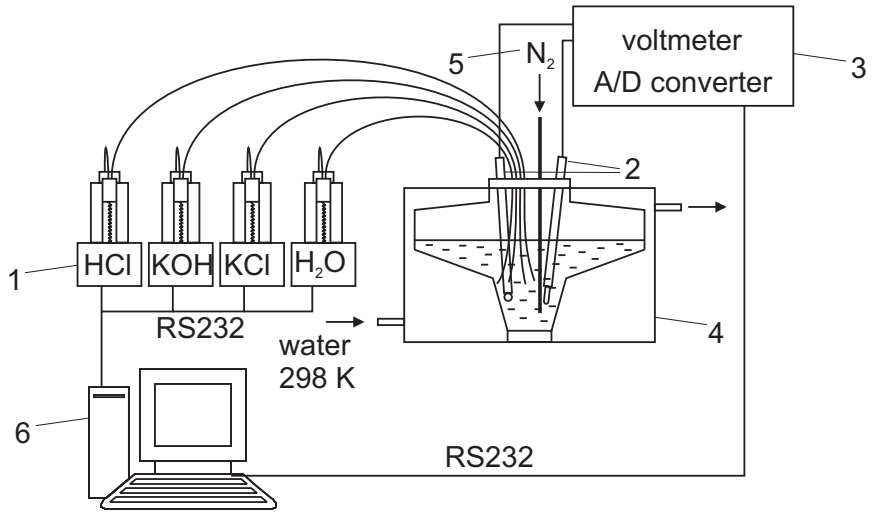

Figure 1.2: Scheme of the Jonction titrator, an automated potentiometric titration setup with four burettes.

These components are connected according to the scheme depicted in figure 1.2. The RS232 standard cables are used for the connections of the burettes and the voltmeter to the PC.

Automatic burettes serve for high-precision dosing of all the solutions to the titration vessel (precision of 1 μL). The additions are defined by the computer. The bottles have to be well sealed to prevent the dissolution of CO_2.

The burette tubing endings were fitted with ca. 15 cm of a narrow teflon tubing (1/16"OD $\times$0.01"ID, see figure 1.3). These tubings were fitted with PEEK fittings 1/16" ID and 1/8" ID (Alltech, cat. # 37172 and 37168, respectively), by using the Easy Flange tool (Alltech , cat. # 35900), and joined with a PEEK union (Alltech, cat. # 20088). Custom teflon caps with five holes were produced in order to introduce these tubing endings into the titration cell. These caps are produced according to the Metrohm standard for the electrode sleeves, so that they could be placed into a standard Metrohm titration cell lid (see below).

The pH-measurement electrode couple used in this work is a separated glass, and an Ag/AgCl reference electrode. The voltmeter and an A/D converter are

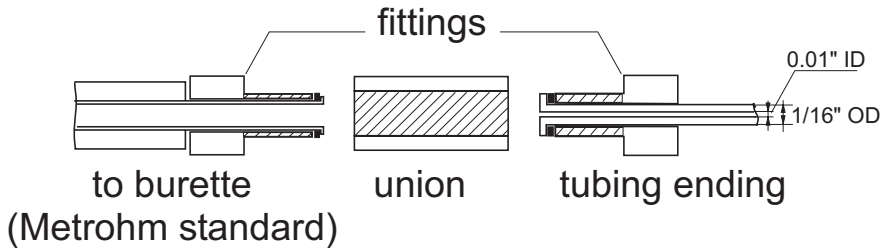

Figure 1.3: Fitting of the burette endings, which prevents leakage or and contact with air.

embedded in one housing (HighImp4 instrument). The communication of the voltmeter unit with the PC is established by means of a Labview-based software.

Jonction titrator can use any kind of standard Metrohm titration cells with double-walls for thermostating. These cells usually have a volume of ca. 200 mL, with a minimum solution volume (for the electrodes to be immersed) of ca. 90 mL. However, a substantial increase in the solution volume may occur during the constant ionic strength titrations. Moreover, one might want to perform several successive titrations at different ionic strengths without changing the sample. In that case, salt additions between the titration runs are necessary, and the total volume of the cell content may vary substantially, depending on the investigated pH range and the ionic strengths. At the same time, the electrodes have to be immersed even into small volumes. Therefore, construction of a custom titration cell is recommended, with a design that allows titrations of small samples, and a big volume increase during the experiment, without overflowing the cell. We have designed a double-wall plexiglas titration cell, which allows a range in volume between 45 and 450 mL (see figure 1.4). The newly designed titration cell is fitted with a standard Metrohm titration cell lid (e.g. 6.1414.010), from which the clamp part has to be cut away.

Degassing of the titration cell with pure nitrogen is necessary to prevent contamination of the titration system with carbon dioxide. Before being introduced

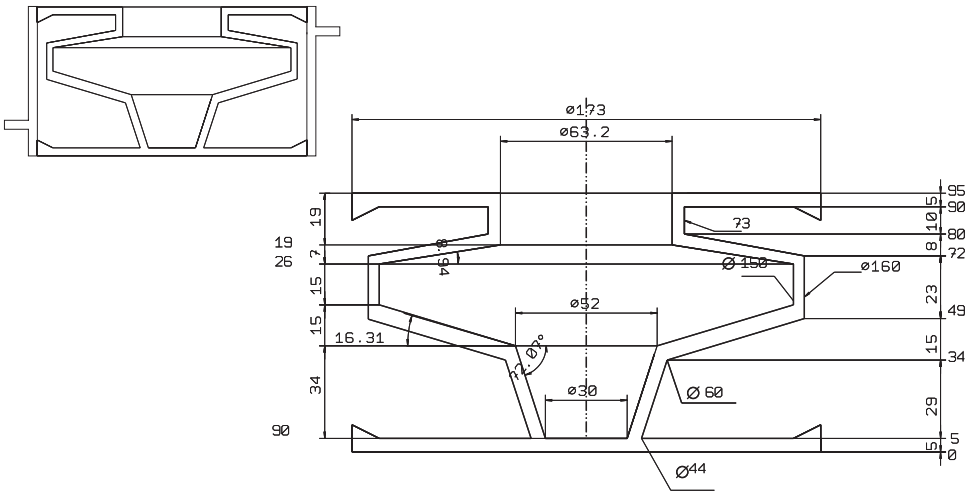

Figure 1.4: The titration cell is composed of the inner part, which is scooped out of one piece of plexiglas, and the outer wall, which is sealed around the cell,. The space between the inner part ant the outer wall serves for thermostating.

into the cell, the gas is washed by passing it through conc. KOH solution, then pure water, and then 0.1 M KCl solution (see figure 1.5). The solutions should be periodically changed, since the KOH solution is loosing it's CO_2 neutralizing capacity upon time. The pH of the KOH solution can be checked with pH-paper, and should be above 13. Although the compositions of the final washing solution and the solution in the titration cell should be as close as possible, during all the described experiments, the final washing solution was always 0.1 M KCl. The degassing tubing can either be kept above the solution surface, or submerged below. The advantage of the latter is that the nitrogen stream can be broken into very small bubbles by the stirrer, which in turn can accelerate the degassing of the solution. In the other hand, this can cause foaming in some suspensions.

All other details and the acquired experience about this hardware are summarized in the Appendix.

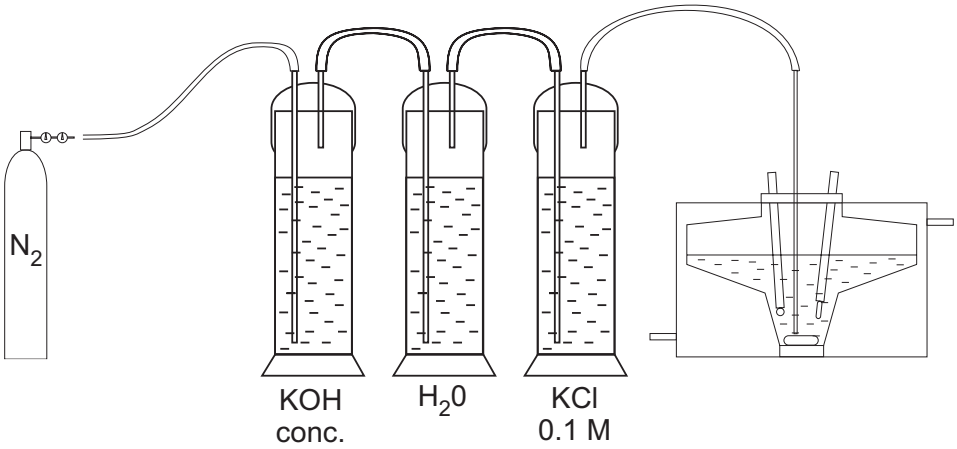

Figure 1.5: The degassing apparatus.

Figure 1.6: A photo of the Jonction titration setup.

1.4 Materials

The burette solutions are: HCl, 0.25 M, prepared form 1 M solution (Merck, Titrisol); KOH 0.25 M, prepared from 1 M solution (J. T. Baker); KCl 3 M, prepared from pure salt (p.a., Acros Organics), and pure decarbonated water. The concentrations of the burette solutions can be varied according to the pH range of interest, ionic strengths range, burette precision or some other preference. The reported concentrations were found to be the most convenient for all the titrations performed during this work. For all the solutions, the Millipore water (from the Millipore A 10 deionization and purification system) was used, from which the CO_2 was removed through boiling. This procedure consists of boiling the water for 5-10 min., and then cooling it under pure nitrogen atmosphere.

1.5 Experimental procedure

The typical experiment is performed in the following manner. First, the analyte is added to the titration cell, which is then closed. The electrodes and all the tubings were flushed with Millipore water, rinsed with soft paper, and mounted to the cell. Then, the titration software is launched. The experiment is fully controlled by the software, and from this point, the manual control over the burettes is disabled.

First, the initial solution is automatically dosed to the titration cell, and the pH is automatically adjusted to the pre-defined initial value. This is necessary only in the case of analyte titrations, otherwise the initial automated dosing will result with a solution where pH equals the initial pH. Then, a sequence of titration steps is repeated until the final pre-defined pH value is achieved. Each step in the titration consists of an acquirement of the reading values, namely the electromotive force (EMF), all the added volumes, the total volume, and additions of the burette solutions. The measurement of the pH is recorded after

the solution has reached thermodynamic equilibrium, which can be seen from the drift of the electrode signal. After the final pH is achieved, the forward run is finished, and the sense of the pH-sweep is reversed. The sequence of titration steps is repeated in the backward-run. These two runs are repeated at all the pre-defined ionic strengths. The experiment is terminated after all the forward and backward titrations were effectuated at all the desired ionic strengths. The details about all the algorithms, EMF measurement, etc. can be found in the Appendix.

1.6 Data treatment

The automatization of the experiment enables accumulation of many data points. Therefore, fast data analysis procedures were programmed, in which the experimental data from different titration runs were separated and analyzed.

The evaluation of the concentration of the proton-binding species at a certain pH, used in the present work, is known for a long time (e.g. [14]). It is based on the electroneutrality condition, and the principle can be described by taking the solution of acetic acid as an example: To calculate the degree of protonation (see definition 1.6), the concentration of the charged species CH_3COO^- has to be evaluated (it is assumed that the total concentration, $[CH_3COOH]_0$, is known from the sample preparation):

$$\theta = \frac{[CH_3COOH]_0 - [CH_3COO^-]}{[CH_3COOH]_0} \tag{1.14}$$

The concentration $[CH_3COO^-]$ can be calculated by subtracting the H-Acidty of the solution which contains acetic acid (the analyte):

$$[\text{H-Acy}]_{\text{HAc}} = [H^+]_{\text{HAc}} - [OH^-]_{\text{HAc}} - [CH_3COO^-] = [Cl^-]_{\text{HAc}} - [K^+]_{\text{HAc}} \tag{1.15}$$

from the H-Acdity of a blank solution:

$$[\text{H-Acy}]_{\text{blank}} = [H^+]_{\text{bl}} - [OH^-]_{\text{bl}} = [Cl^-]_{\text{bl}} - [K^+]_{\text{bl}} \tag{1.16}$$

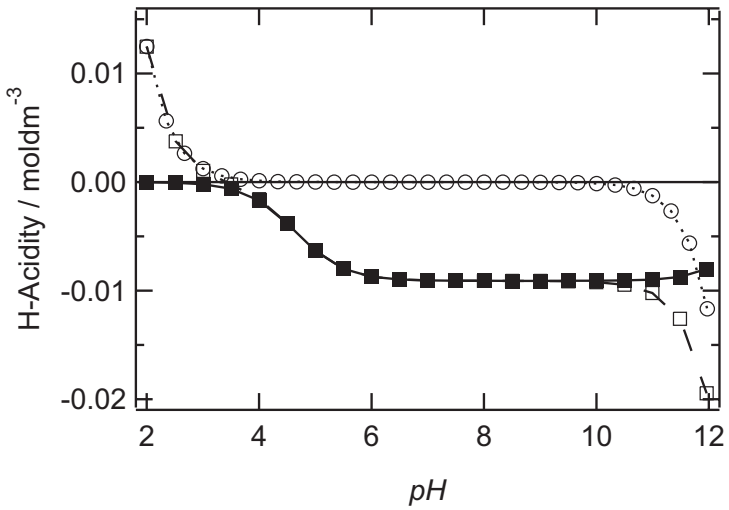

Figure 1.7: Experimental potentiometric titration curves. ∘ blank titration curve; □ Acetic acid titration curve; ■ Acetic acid charging curve.

This subtraction has to be done for all the measured pH values. The H-Acidities are determined by the concentrations of the strong acid and base counterions (Cl^- and K^+, respectively), and thus can be calculated from the experimental concentrations of the added strong acid and base. The charges of the ions coming from highly dissociated salts, like KCl, cancel out in the electroneutrality expression.

The result of a typical potentiometric titration experiment, is presented in figure 1.7. The H-Acidity versus pH curves are called the titration curves, and are calculated from the experimental data. The curve that represents the overall excess charge concentration in the analyte titration, with respect to the blank solution at the same pH, is called the "charge titration curve" or simply the "charging curve". It is the difference between the analyte and the blank titration curves.

In the above figure, the data shown are from a simulated experiment, thus do not include experimental errors. Two features of the presented data are important: First, in contrast to the proton binding isotherm (figure 1.1), the charge

titration curve (closed squares) is not constant at high pH: it shows a slight decrease of the $[CH_3COO^-]$ with an increasing pH. This is due to the fact that the concentrations depend upon the total volume, and the latter varies in the real titration experiment (it increases with increasing pH in the presented figure). To discard this artefact, the concentration $[CH_3COO^-]$ can be either multiplied by the total volume to give an amount in moles, or recalculated into the degree of protonation through division by the total concentration $[CH_3COOH]_0$, which varies with the total volume in the same way as $[CH_3COO^-]$. Second, the experimental points from the blank and the analyte titrations do not coincide on the pH scale. To obtain the interpolated values, analytical function for the blank titration curve was used, which enables computation of the OH-Alkalinities of the blank solution at the experimental pH values from the analyte titration. The blank titration curves were fitted to an analytical function by means of the least squares method (a fast converging Newton method was used, acquired from the NAG library [17]). This has enabled a comparison of the fitted parameters with the literature values, and a cross-check of different experiments. In turn, the literature values of the blank titration curve parameters were used as a calibration of the whole experiment. All the data analysis programming was done in the FORTRAN language.

The volume dependency of the charging isotherms (see figure 1.7) can be discarded by either converting the H-Acidity into the degree of protonation (1.6), or by multiplying the H-Acidity with the total volume. In the latter case, the amount of charge in the units of mols is obtained. As an example, figure 1.8 is showing the raw titration curves and the "charging" curves of acetic acid. The volume dependence is apparent from the difference between the forward and backward titration data. Figure 1.9 is showing the two volume-independent representations (charge in units of mols and the degree of protonation). Here, the forward and backward titration data coincide.

The analytical expression for the electromotive force as a function of the

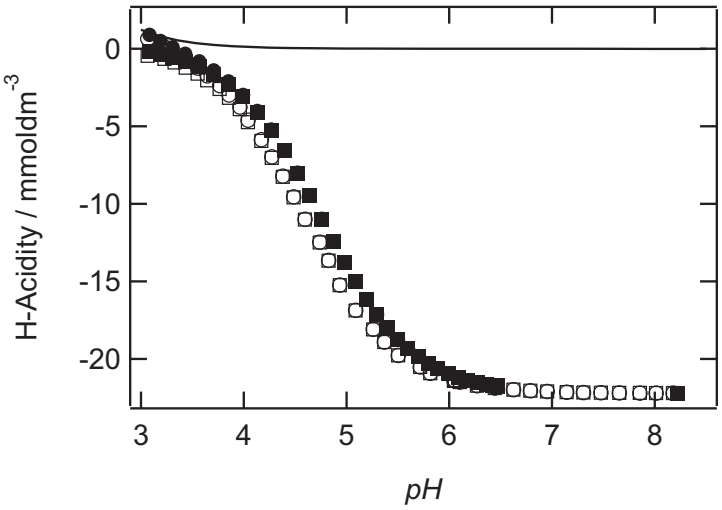

Figure 1.8: Titration curves and charging curves of acetic acid. ○: titration curves; □: charging curves. Open symbols: forward titration runs. Closed symbols: backward titration runs.

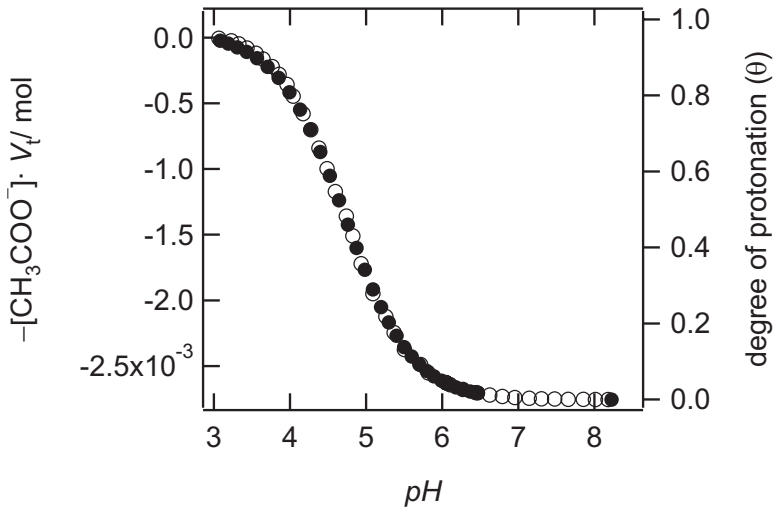

Figure 1.9: The charging curve of acetic acid, multiplied with the total volume of the solution. ○: forward titration run. ●: backward titration run.

titrant volume EMF(V_a or V_b), can be obtained from the electroneutrality condition for the blank solution (1.16). The right hand part can be expressed through the volumes of the added strong acid and base and the total volume of the system (V_a, V_b, V_t), and the burette concentrations of these solutions (c_a, c_b):

$$[\text{H-Acy}]_{\text{blank}} = \frac{c_a V_a - c_b V_b}{V_t} = \frac{10^{-\text{pH}}}{\gamma_H} - \frac{10^{\text{pH}-pK_w}}{\gamma_{OH}} \tag{1.17}$$

Here, the concentrations of the H^+ and OH^- ions are expressed through pH, K_w, and the activity coefficients, according to the definition of pH (1.8) and the ionic product of water (1.9). As an approximation we can use the common activity coefficient ($\gamma_H = \gamma_{OH} = \gamma$), which accounts for the non-ideal behavior of ions [18], and obtain:

$$[\text{H-Acy}]_{\text{blank}} = \frac{c_a V_a - c_b V_b}{V_t} = \frac{1}{\gamma}(10^{-\text{pH}} - 10^{\text{pH}-pK_w}) \tag{1.18}$$

The pH of the solution can be expressed through the experimentally measured EMF, assuming the linear relationship:

$$\text{EMF} = E_0 + \Delta \cdot \text{pH} \tag{1.19}$$

In the above expressions, the experimentally accessible quantities are all the volumes and the electromotive force of the electrode couple. The rest of the quantities are parameters: c_a, c_b, K_w, γ , E_0, and Δ. It could be argued that the concentrations of the burette solutions can be known from the sample preparation, but since the blank titration curve is more sensitive to these concentrations than the accuracy of the preparation, it makes more sense fitting them.

Non-linear least squares fitting, and the cross-correlations between the blank titration curve parameters. As mentioned in the description of the data treatment, non-linear least squares fitting of the blank titration curves is performed in order to obtain the blank titration data at the pH values of the analyte titration curve. The advantage of this approach in front of a simple interpolation procedure, is that in this manner, one can verify the experimental precision by

comparing the values of the fitted parameters with some expected, or literature values. However, in order to obtain unambiguous values from fitting, one has to establish the set of parameters, which can be simultaneously fitted.

In the case of the blank titration curves, the sum-of-the-squares function can be obtained by combining equations 1.18 and 1.19:

$$\text{sum} = \sum_i [\frac{c_\text{a} V_{\text{a,i}} - c_\text{b} V_{\text{b,i}}}{V_{\text{t,i}}} - \frac{1}{\gamma}(10^{(E_0 - \text{EMF}_\text{i})/\Delta} - 10^{(E_0 - \text{EMF}_\text{i})/\Delta - pK_\text{w}})]^2 \quad (1.20)$$

where i is the counter of the experimentally measured data. In the case of functions with a number of parameters that are to be fitted, the least-squares method may not be free of ambiguities. Namely, sets of parameters may occur, which give the same minimum in the sum-of-the-squares function (cross correlations between parameters [19]).

Let's now examine the sets of parameters, which can not be fitted simultaneously. For example, if we vary simultaneously the parameters γ, c_a and c_b (the rest of them we keep fixed), we could find different values which give exactly the same sum-of-the-squares (the change in the left term in equation 1.20 can be compensated by a change in the right term, if we choose an appropriate γ). Thus, we can not fit those parameters simultaneously. In the same manner, we can deduce that combinations [c_a, c_b, pK_w, E_0, Δ], and [pK_w, E_0, Δ, γ] can not be fitted. Furthermore, parameters pK_w and γ could be simultaneously tuned without affecting the sum-of-the-squares function, which means that they can not be fitted in combination with each other.

Equation 1.20 shows that distinguishing of c_a and c_b is possible only if there is a significant difference between the added amounts of strong acid and base ($V_{\text{a,i}}$ and $V_{\text{b,i}}$, respectively). Otherwise, when $V_{\text{a,i}} \approx V_{\text{b,i}}$, the first term becomes $V_{\text{a,i}}(c_\text{a} - c_\text{b})/V_{\text{t,i}}$. In this case, only the difference $(c_\text{a} - c_\text{b})$ can be obtained from fitting, and the two concentrations can not be deduced.

Having in mind the above demonstrations, the most reasonable set of fitted parameters might be [c_a or c_b, γ, E_0 and Δ]. The choice was to fix the acid

burette concentration c_a, since this solution is stable regarding the dissolution of CO_2 so it's analytical concentration is more accurate than that of the KOH. After examining the correlations between the fitted parameters by plotting them against each other (in this manner, the cross-correlations are "visualized"), it was observed that either E_0 or Δ have to be fixed (not fitted, see figures 1.16 and 1.17). The features of the blank titration curve fitting will be discussed in more detail in section 1.8.

1.7 Results

A typical result of a forward and backward blank titration at ionic strength of 0.1 M, obtained through the procedure described in section 1.6 is shown in figure 1.10. The fitted parameters from forward titration curve are: $c(\mathrm{KOH}) = 0.2506\,\mathrm{M}$, $E_0 = 384.14\,\mathrm{mV}$, $\gamma_{\mathrm{H}} = \gamma_{\mathrm{OH}} = 0.82$, and from the backward titration curve: $c(\mathrm{KOH}) = 0.2505\,\mathrm{M}$, $E_0 = 383.5\,\mathrm{mV}$, $\gamma_{\mathrm{H}} = \gamma_{\mathrm{OH}} = 0.80$. Other parameters from function 1.17 were not fitted, but fixed at the following values: $c(\mathrm{HCl}) = 0.2500\,\mathrm{M}$, $\Delta = -59.0\,\mathrm{mV}$, $K_{\mathrm{w}} = 10^{-14}$. Figure 1.11 is showing the residuals calculated from the fitting. To discard the volume-dependency (see section 1.6), the residuals are represented as charge in units of mols. The fitting is usually very good, with a mean residual value (averaged over all the experimental points) of the order of $10^{-6}\,\mathrm{mol}$ see figure 1.11, which is considered as the detection limit. Since the total volume of the system is approximately 100 mL, the detection limit can be expressed in terms of concentration, and it equals $10^{-5}\,\mathrm{M}$. If the solutions are prepared with care, the burettes functioning impeccably, and the CO_2 dissolution is lowered to minimum, the forward and backward curves should coincide. Figure 1.11 nicely shows the influence of the CO_2 dissolution. Here, the fitted H-Acidities were subtracted from the experimental (as shown in the previous figure), and multiplied with the total volume. As explained in section 1.6, the conversion of H-Acidities into amounts in moles is necessary to discard

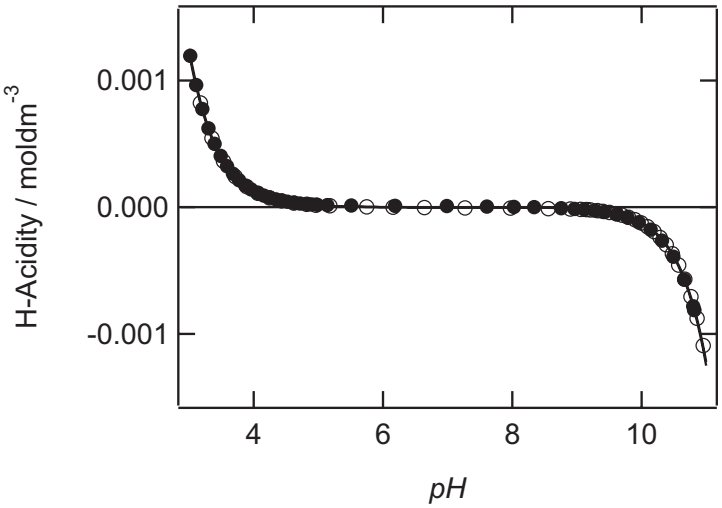

Figure 1.10: Forward and backward blank titrations at $I = 0.1\,\mathrm{M}$. The markers represent the experimental data (○:forward,●:backward), and the lines represent the fitted functions. The burette concentrations are: $c(\mathrm{HCl}) = 0.25\,\mathrm{M}$; $c(\mathrm{KOH}) = 0.25\,\mathrm{M}$; $c(\mathrm{KCl}) = 3.00\,\mathrm{M}$. The aimed pH increment is 0.17 units.

the total volume dependency of the data (without this the subtracted acidities at different pH could not be compared). The experiment was started at pH=3, and the titration was performed up to pH=11. After the solution was exposed to a basic pH, the CO_2 started dissolving, which is apparent from an increase of the residuals in the backward-run. The solution was again freed (to a certain extent) of the CO_2 , due to the degassing in the acidic region. This process repeats at all the examined ionic strengths, and can be tracked in figure 1.11.

In order to test the instrument, the experimental procedures and data processing, titrations of simple acids and bases were performed. In this chapter, the results for ethylene-diamine and acetic acid are presented. The pK-values obtained by non-linear least squares fitting were compared with the literature values [11]. The comparison between the fitted and the literature value serves as an estimation of the precision of the pH-scale [14].

The proton binding isotherms (in terms of charge in mol units, see section

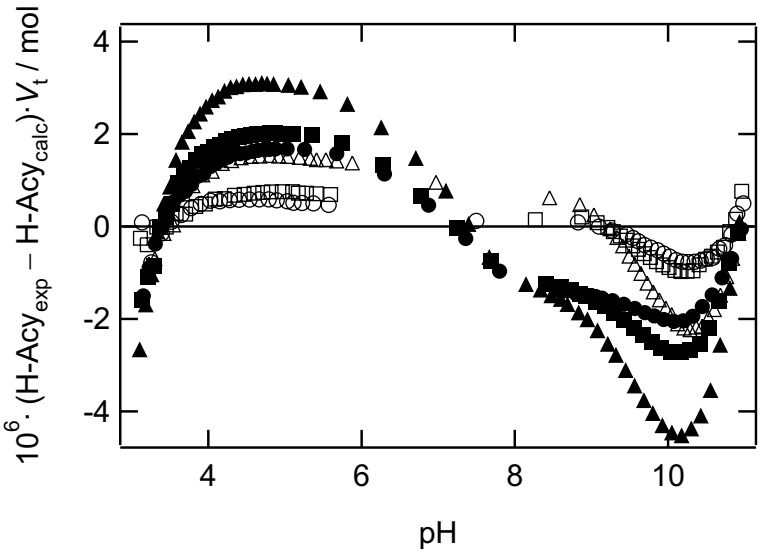

Figure 1.11: The differences between the experimental and the calculated H-Acidities for forward and backward titrations at different ionic strengths. Open symbols denote the forward-runs, and closed symbols the backward-runs. $\circ : I = 0.1\,\text{M}$; $\square : I = 0.5\,\text{M}$; $\triangle$: $I = 1.0\,\text{M}$.

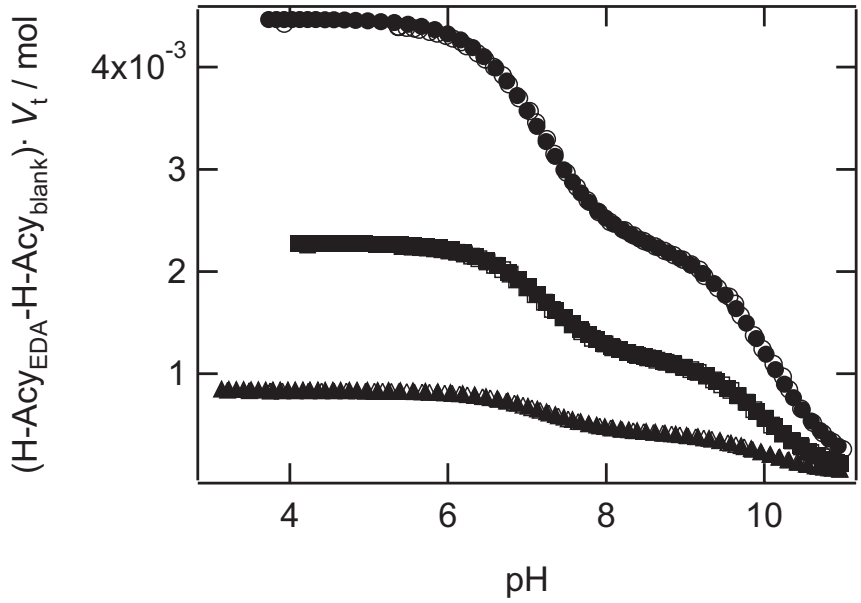

Figure 1.12: Titration curve of ethylene diamine at three different initial concentrations, at $I = 0.1\,\mathrm{M}$. Open symbols denote the forward, and closed the backward titration runs. $\circ$: $[\mathrm{EDA}]_0 = 5.0\,\mathrm{mM}$; $\square$: $[\mathrm{EDA}]_0 = 2.5\,\mathrm{mM}$; $\triangle$: $[\mathrm{EDA}]_0 = 1.0\,\mathrm{mM}$.

1.6) of ethylene diamine at three different initial concentrations are presented in figure 1.12. These experiments were performed in order to verify the precision of the charge calculated from the titration curves. The proton binding isotherms from the same experiments, at the scale of the degree of protonation, coincide very well, as presented in figure 1.13. This result testifies about a very good experimental accuracy (as mentioned before, the detection limit is ca. $10^{-5}\,\mathrm{M}$), even at concentrations of the analyte of 1 mM.

The proton binding isotherms of acetic acid at three different ionic strengths are shown in figure 1.14. The solid lines represent the fitted proton binding isotherms. The only fitted parameter is the mixed $\mathrm{p}K_\mathrm{d}$. The ionic strength dependence of this parameter reflects the variation of the activity coefficient of the charged species. The proton binding isotherm of ethylene diamine exhibits two well distinguished steps, and a plateau value at 1/2, as can be seen in figure

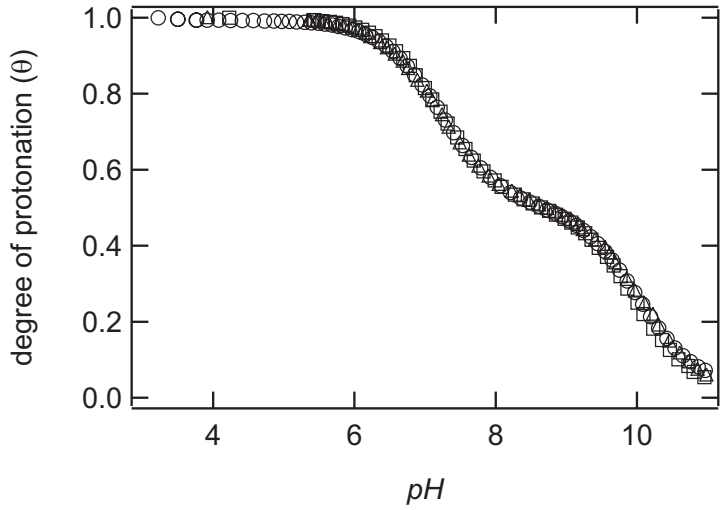

Figure 1.13: Proton binding isotherms of ethylene diamine at different concentrations. ∘ : $[\mathrm{EDA}]_0 = 1.0\,\mathrm{mM}$; □ : $[\mathrm{EDA}]_0 = 2.5\,\mathrm{mM}$; △: $[\mathrm{EDA}]_0 = 5.0\,\mathrm{mM}$.

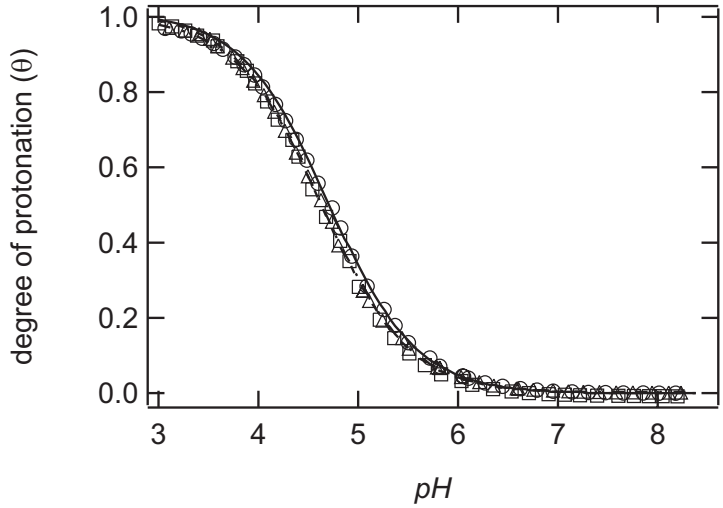

Figure 1.14: Proton binding isotherms of acetic acid at three ionic strengths.∘ : $I = 0.1\,\mathrm{M}$; □ : $I = 0.5\,\mathrm{M}$; △: $I = 1.0\,\mathrm{M}$. Full lines represent the fitted functions.

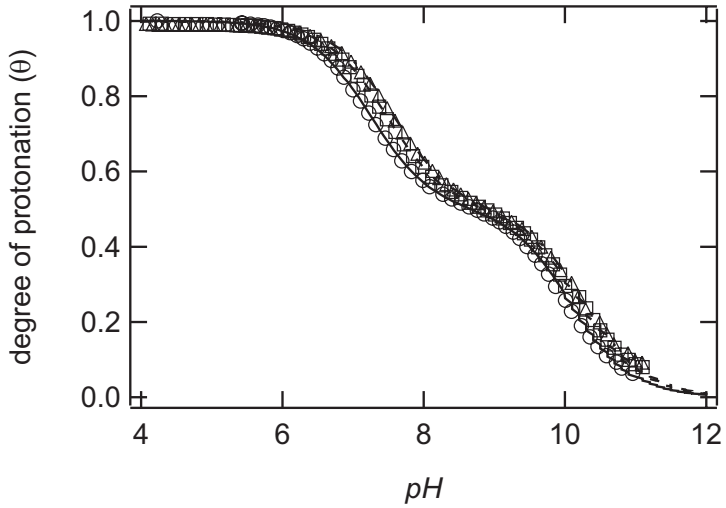

Figure 1.15: Proton binding isotherms of ethylene diamine at three ionic strengths. $\circ$: $I = 0.1\,\mathrm{M}$; $\square$: $I = 0.5\,\mathrm{M}$; $\triangle$: $I = 1.0\,\mathrm{M}$. Full lines represent the fitted functions. The fitted values of $\mathrm{p}K_\mathrm{d}$ are summarized in the table 1.2.

1.15. It can be noticed that the titration steps are somewhat broader than for the acetic acid. The same treatment as for the acetic acid, can be performed for ethylene diamine. The two $\mathrm{p}K_\mathrm{d}$ can be obtained by fitting, and their values depend upon the ionic strengths. The values are summarized in table 1.1, together with the literature values[11]. It should be noticed that the constants reported in Martell and Smith are the concentration constants, defined as:

$$K_\mathrm{conc} = \frac{[\mathrm{H}^+][\mathrm{A}^-]}{[\mathrm{HA}]} \tag{1.21}$$

To compare the fitted mixed deprotonation constants (see the definitions 1.3 and 1.4) with the literature values, a correction of the mixed constants for the activity coefficient of the proton is required. The ionic strength dependence is more pronounced than in the case of acetic acid, which is due to the interactions of the protonated sites, as will be discussed in chapter 2. From table 1.1, it can be verified that the experimentally obtained deprotonation constants fit very well with the literature values. The only exception is in the case of ethylene diamine at

Table 1.1: The fitted mixed deprotonation constants versus the corrected literature values.

		1^{st} step		2^{nd} step	
Substance	I / M	fit	literature [11]	fit	literature [11]
Ethylene diamine	0.1	10.02	10.02	7.21	7.02
	0.5	10.14	10.15	7.44	7.43
	1.0	10.21	10.29	7.54	7.56
Acetic acid	0.1	4.70	4.66		
	0.5	4.62	4.62		
	1.0	4.64	4.67		

1.0 M ionic strength, where the data are less accurate due to the CO_2 dissolution, which is becoming more pronounced in the later stage of the experiment.

1.8 Discussion

The quality of the blank titration fitting is usually very good. However, this does not necessarily mean that the obtained parameters have physical meaning. Namely, the fitting of non-linear functions with several parameters can be ambiguous, due to the cross-correlations between the parameters [19], or the insensitivity of the function value to a parameter in a certain range of the domain.

In order to verify the cross-correlations between the parameters E_0, Δ and γ which, by analytical inspection of the sum-of-the-squares function (see section 1.6), do not appear as correlated, the values obtained from fitting were plotted against each other (figures 1.16 and 1.17). Since the absolute values of E_0 and Δ are not very significant by themselves [20], they are compared to the calibration values E_0' and Δ'. In these representations, the activity coefficients γ are

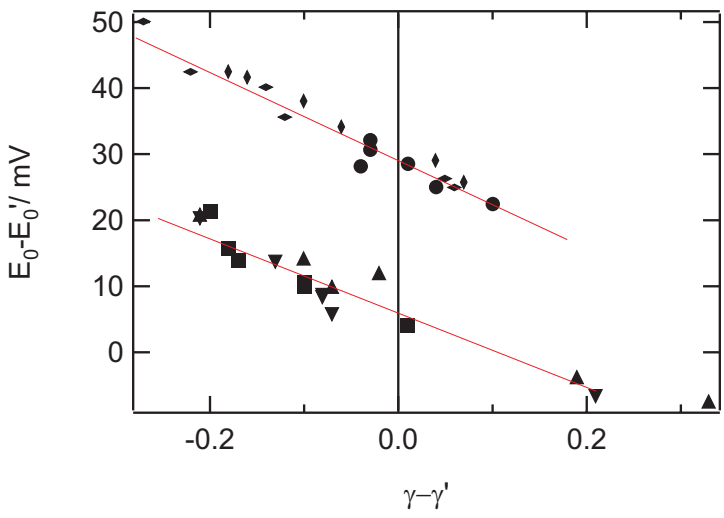

Figure 1.16: The cross-correlations between E_0 and γ from various experiments with two different electrode couples. Parameter E_0 is presented with respect to the value obtained from the calibration of the electrodes with standard buffers E_0', and γ with respect to the Davies value γ'. The parameters E_0 and Δ were obtained by fitting the set [E_0, Δ, γ and c_b].

compared to the values obtained with the Davies formula (1.22). Both figures are showing remarkable correlation between the electrode parameters and the activity coefficient.

The parameters E_0 and Δ depend on the electrodes that are used for the experiment. The electrode response is changing upon time, which is caused by the changes in the electrode solutions, wearing of the glass and the ceramic diaphragm of the reference electrode, etc. This is evident from figures 1.16 and 1.17, where a change of the electrodes has caused a parallel shift of the data.

The fitted activity coefficients are compared with the values calculated from the Debye-Hckel limiting law at $I < 0.002\,\mathrm{M}$, and Davies formula for higher ionic strengths (see figure 1.18):

$$\gamma' = \frac{a \cdot \sqrt{I}}{2 \cdot (1 + \sqrt{I})} + \frac{b}{2} \cdot I \tag{1.22}$$

where I is the ionic strength in M, and a and b are empirical coefficients, $a = 1.022$

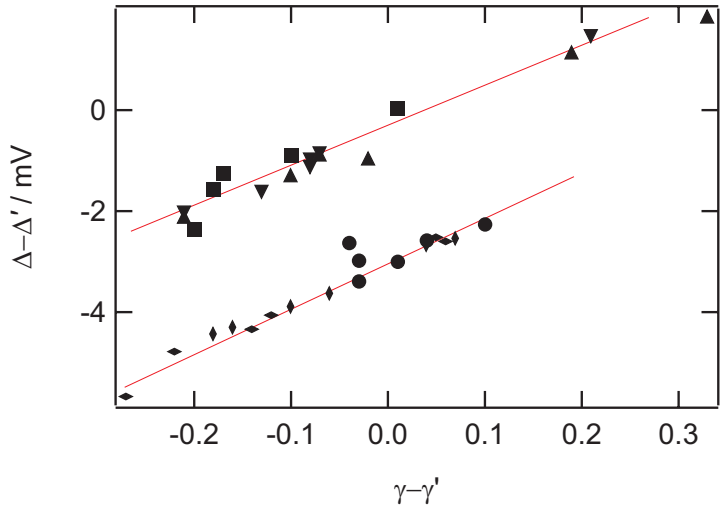

Figure 1.17: The cross-correlations between Δ and γ from various experiments with two different electrode couples. The slope Δ is presented with respect to the value obtained from the calibration of the electrodes with standard buffers Δ', and γ with respect to the Davies value γ'. The parameters E_0 and Δ were obtained by fitting the set [E_0, Δ, γ and c_b].

and b is given in table 1.2. Although the fitted values are significantly scattered, a trend is noticeable, which is similar to the prediction of the Davies equation at low to moderate ionic strengths. At $I = 1.0\,\mathrm{M}$, the discrepancy is significant, which could be due to an experimental error (these points stem from the titrations which were performed as the last in the course of an experiment, at which stage the system contains more dissolved CO_2).

The parameters obtained from fitting are determinant for the experimental pH-scale. Figure 1.19 is showing several modeled blank titration curves, with different parameters. It can be concluded that γ influences the curve at high and low pH. Parameter E_0 shifts the titration curve parallel with the pH-scale, while parameter Δ causes a shift, and broadening of the titration curve. The ionic strength influences the curve through the activity coefficients, shifting it in high and low pH regions. The influence of pK_w is growing with pH, and it is becoming predominant over pH at pH = p$K_\mathrm{w}/2$. At low pH, pK_w does not have

Table 1.2: Parameter b from the Davies formula, and the corresponding activity coefficients.

I / M	b	$\log \gamma'$	γ'
0.1	−0.46	−0.10	0.80
0.5	−0.37	−0.12	0.76
1.0	−0.34	−0.09	0.82

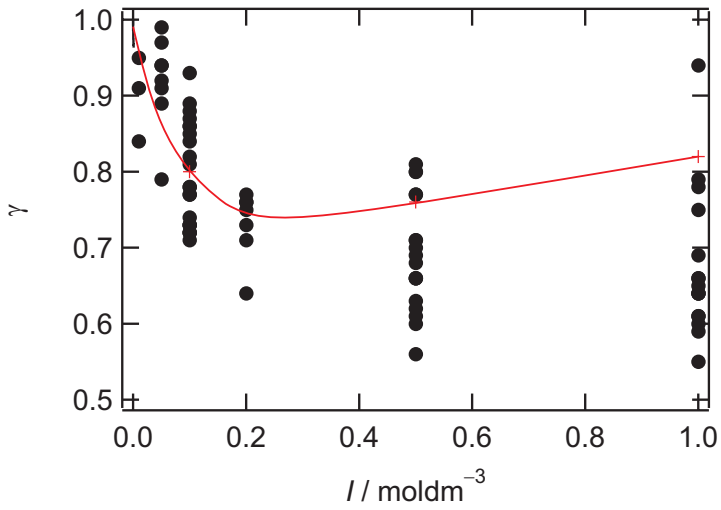

Figure 1.18: The activity coefficients γ obtained from the blank titration curve fittings, versus the ionic strengths. The solid line is calculated by means of the Davies formula.

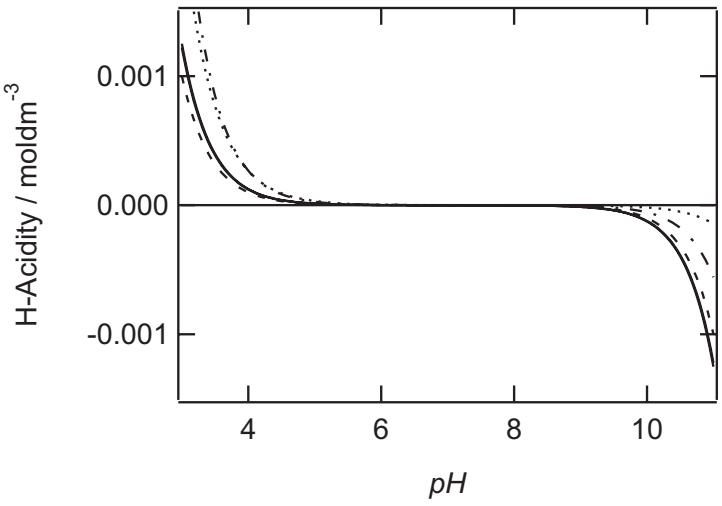

Figure 1.19: Influence of various parameters on the blank titration curve. a) Solid line: curve obtained with parameters $c_{\mathrm{a}} = 0.25\,\mathrm{M}$; $c_{\mathrm{b}} = 0.25\,\mathrm{M}$; $pK_{\mathrm{w}} = 14.00$; $\gamma = 0.90$; $E_0 = 380.00\,\mathrm{mV}$; $\Delta = -59\,\mathrm{mV}$. b) Dashed: parameters the same as in a) except ; $\gamma = 0.70$. c) Dash-dotted: parameters the same as in a) except ; $E_0 = 420.00\,\mathrm{mV}$. d) Dotted line: parameters the same as in a) except ; $\Delta = -45mV$.

an influence on the curve (see 1.18).

Also, it is worth mentioning that if the electrode response is perfectly linear with pH, then an error in the electrode parameters E_0 and Δ will not necessarily cause an error in the whole examined pH-scale. If a reference pH-scale is determined through electrode parameters E_0' and Δ', the two scales will coincide around $pH \approx (E_0' - E_0)/(\Delta - \Delta')$.

The proton binding isotherms are functions which are reflecting the protonation steps. The normalization of the charging curves with respect to the maximum charge of the acidic or basic species (1.6) gives the degree of protnation with versus pH. The degree of protonation can attain values between 0 and 1, and reflects the protonation state of the species. The steps in the proton binding isotherms occur in the pH regions around the pK_{d} values, where the equilibrium is changing in favor of one species, depending on the direction of the change in pH. In

these regions, the solution has a higher buffering capacity [8]. The plateau values reflect the regions in pH where one species predominates over all the others, and the change in pH does not cause a change in speciation. Special are the proton binding isotherms of polyelectrolytes and interfaces, which are broader than the proton binding isotherms of simple acids. These substances have a buffering capacity in a broader pH range.

A very important feature of the proton binding isotherms are the trends with respect to the ionic strength. These trends can be interpreted through the activity coefficients. As a rule of a thumb, at $I < 0.2\,\mathrm{M}$, for acids, the $\mathrm{p}K_\mathrm{d}$ shift to lower values with an increasing ionic strength. The opposite is valid for bases. The activity coefficients actually express the deviation in the behavior of ions with respect to the ideal solutions. This deviation is influenced by the electrostatic potential of the counterion, which is positive in the case of a base, and thus favorable for deprotonation. The acid counterion is negative, thus electrostatically attractive for protons, which is favorable for protonation. The electrostatic potential, experienced by the protons, depends on the ionic strength, and is higher at lower ionic strength. At $I > 0.2\,\mathrm{M}$, the trend in the activity coefficients with respect to the ionic strength is reversed, which reflects hydration layer influence on the deviation from ideality. The hydration layer of an ion is growing with decreasing electrostatic potential [18].

The accuracy of the experimental proton binding isotherms, and the experimental pH window, are important for assessment of the sources of errors. These can be divided in two groups, namely error in the calculated degree of protonation, and the error of the pH scale.

The degree of protonation can be falsely calculated due to the following:

In the low and high pH regions, the H-Acidities have high values, whereas the charge concentration, which obtained by subtracting the blank H-Acidity form the analyte H-Acidity, can have a very a low value. In effect, one subtracts two big numbers to obtain a small one. This is sensitive to errors because a small

relative error in the H-Acidities will cause a big error in the charge concentration. This error is scaling with the initial concentration of the analyte. Thus, the initial concentration is a determining factor for the pH window which can be experimentally studied. This error can be noticed in figure 1.13, from the broadening of the curves at high pH (the curve at $[\mathrm{EDA}]_0 = 1\mathrm{mM}$ is laying slightly above the others at high pH).

An error in the calculation of the initial concentration of the analyte can occur due to a poor dosing control during the preparation of the analyte solution, or e.g. due to a fact that the concentration of the stock solution is not known.

An error in the preparation of the burette solutions, causing an error in e.g. c_a, which is not fitted from the blank. An erratic preparation of the burette solution, which concentration is fitted, will not cause any errors, since the proper fitting will pollute the right value.

All the occurrences, which are affecting the titration curve parameters (equation 1.17 for blank titration), can be sources of errors for the pH scale, because they have to be exactly the same for the blank and the analyte titration. These can be changes in the electrode reading conditions between the analyte and the blank titrations. Then, the parameters E_0 and Δ are changed, and so is the pH scale. The error can as well arise if the experimental temperature is not the same for the blank and the analyte titration (all the titration curve parameters are temperature dependent to a larger or lesser extent). Furthermore, the temperature affects all the pK values, so that the proton binding isotherms at different temperatures are not comparable. Because the literature values for $\mathrm{p}K_\mathrm{d}$ values are reported at 25 °C, this is the standard working temperature.

The measure for the experimental accuracy are the proton binding isotherms of the simple acids and bases, performed at the initial concentrations of interest, and the agreement of the fitted pK_d, with the literature values. Good analyte standards for this are the ethylene diamine and the acetic acid. Their only disadvantage is a rather high volatility in both cases. To give an insight in the

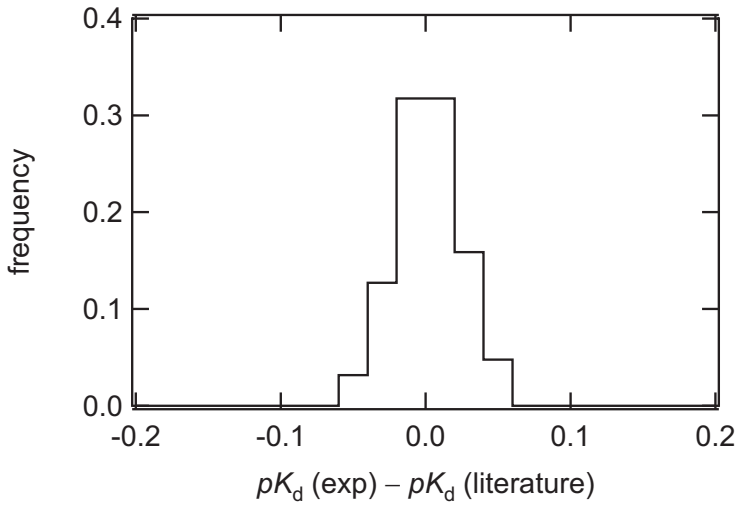

Figure 1.20: Statistics of the fitted pK values for various standard systems (HAc, EDA, Alanine,etc.) with respect to the literature values.

performance of the described method, and the accuracy of the proton binding isotherms and the corresponding pK_d values, figure 1.20 is a statistic of the fitted values, from various experiments (with ethylene diamine, and acetic acid as analytes).

1.9 Conclusion

A high-precision computer-controlled potentiometric titrator with four burettes, and a high-impedance voltmeter was developed. The four-burette setup is very convenient to perform constant ionic strength titrations. The advantage of this system is that it enables the adjustments of the ionic strength in the titration cell, without having to change the analyzed solution nor any of the burette solutions.

The data treatment, which includes fitting of the experimental blank titration curves is advantageous, because it enables an insight in the electrode quality, and gives insight in the possible sources of errors.

High-precision potentiometric titrations appear as a powerful tool for study-

ing the concentrations of the charged species in a solution. If all the sources of errors are under good control, the absolute error of the determined analyte concentration is not higher than 10^{-6} mol. Thus, 100 mL of analyte solution with initial concentration of 10^{-5} M can be easily be analyzed with only 1 % error. The pH scale is defined by the blank titration curve parameters. The accuracy of the pH scale, obtained in this manner, is 0.04 units.

The pH-scale, calculated from the blank titrations, can easily be verified through titrations of substances with known dissociation constants pK_{d}. For this purpose, ethylene diamine and acetic acid have shown to be convenient standards, because their proton binding isotherms exert well-defined protonation steps. Ethylene diamine is turned out to be more convenient, since it protonates in two well defined steps, around pH=10 and pH=7.5, so that the pH scale can be verified in a range of several units. Furthermore, in the case of ethylene diamine, the ionic strength trends of the proton binding isotherms are sufficient to be experimentally distinguished.

Chapter 2

Proton binding isotherms of poly(amidoamine) dendrimers

2.1 Introduction

During the past two decades, dendritic polyamines have invoked great interest of the polyelectrolyte community, due to their unique properties and potential applications as metal complexing agents [21, 22], nanoreactors for particle synthesis [23], light harvesting devices [22], or as gene vectors [24, 25]. Their unusual properties have been studied by numerous authors [26–39]. Their conformation has been investigated in solution mainly by scattering [26–28] and spectroscopic methods [29, 30], while in the adsorbed state on surfaces with AFM [31, 40] and reflectometry [32]. Their charging behavior was studied by electrochemical techniques [33–35], NMR [36, 37], and capillary electrophoresis[38]. The most abundant physico-chemical studies, are those of poly(propylene imine) (PPI) dendrimers [28, 33, 35–37], and poly(amidoamine) (PAMAM) dendrimers (see Fig. 2.1) [26, 27, 29–31, 41]. In both cases, these dendrimers can accumulate positive charge by protonation of the primary amines at the rim and the tertiary amines in the interior. Their charge is thus pH dependent, whereby they are

positively charged at low pH and neutral at high pH.

The charging mechanisms of poly(amidoamine) and poly(propyleneimine) dendrimers will be presented in chapter 3. In the present chapter, the aim is to discuss experimental potentiometric titration data for poly(amidoamine) dendrimers. The interpretation of the proton binding isotherms will be presented in terms of a site binding model, which can be used to infer both the macroscopic, and microscopic protonation mechanisms. After introducing the model, the most important relations for the macroscopic interpretation will be put forward. The overall proton binding isotherms and the protonation macroconstants, calculated by means of the site binding model, will be compared with the experimental proton binding isotherms and the macroscopic protonation constants obtained by direct fitting of the isotherms.

2.2 Macroscopic protonation equilibria in polyelectrolyte solutions

The macroscopic protonation equilibria of polyelectrolytes is equivalent to the protonation equilibria of polyprotic acids, where the macroscopic protonation state, or "macrostate", is defined by the number of the protonated sites, m, and the total number of protonation sites, N [6, 11]. Thus, there are N protonation steps, and to each step, a macroscopic protonation constant is assigned:

$$K_m = \frac{[\mathrm{H}_m\mathrm{A}]}{[\mathrm{H}_{(m-1)}\mathrm{A}]a_{\mathrm{H}}}. \tag{2.1}$$

The degree of protonation, θ, can be calculated from the probabilities of the macrostates, P_m:

$$\theta = \frac{1}{N}\sum_{m=1}^{N} mP_m. \tag{2.2}$$

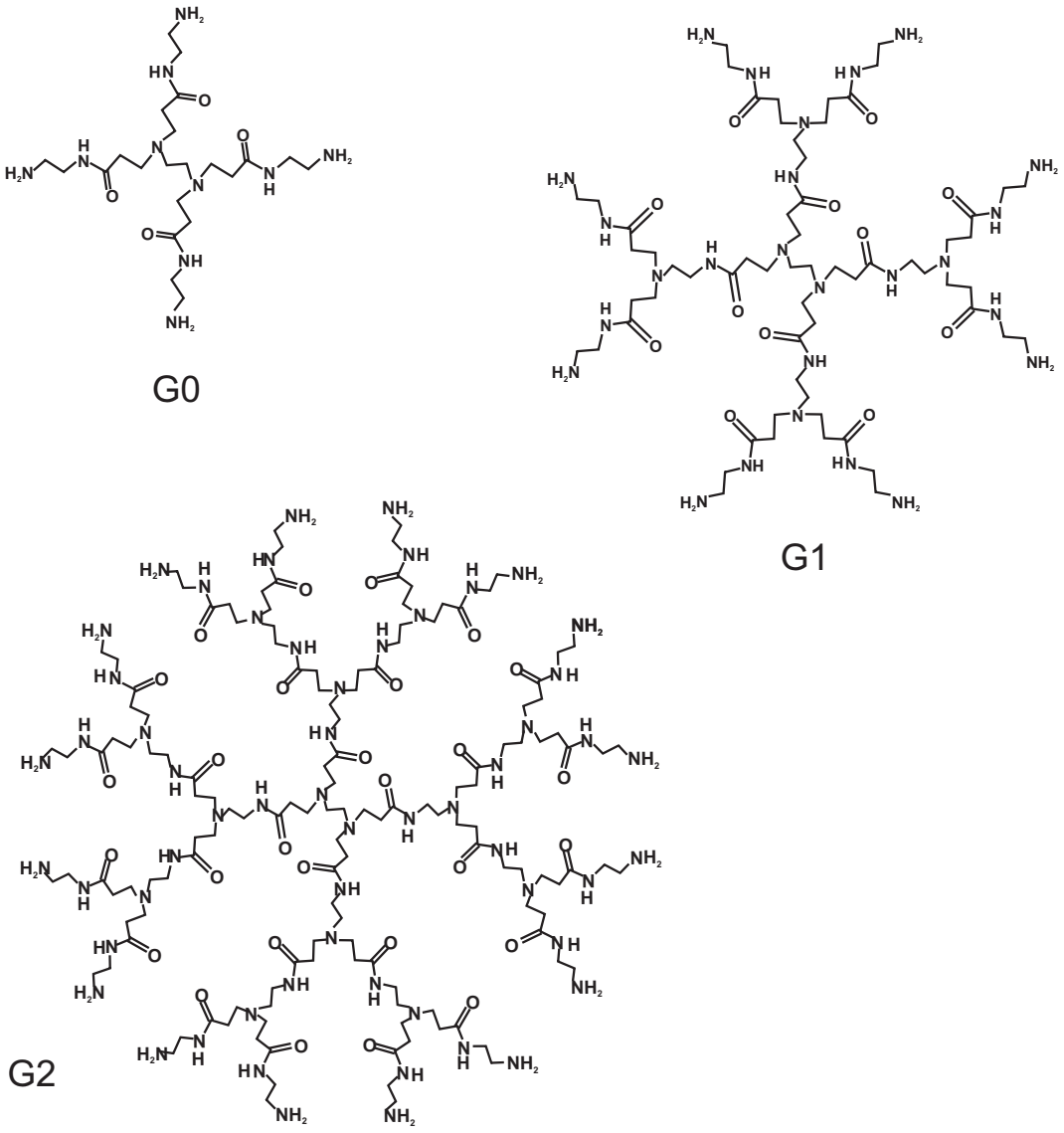

Figure 2.1: Chemical structure of the zeroth, first and second generation of poly(amidoamine) dendrimers.

The probability of a macrostate can be expressed through the macroscopic protonation constants:

$$P_m = \frac{a_{\mathrm{H}}^m \prod_{i=1}^m K_i}{1 + \sum_{m=1}^N a_{\mathrm{H}}^m \prod_{i=1}^m K_i} \tag{2.3}$$

Equations 2.2 and 2.3 define the proton binding isotherm, $\theta(\mathrm{pH})$. However, the macroscopic picture of protonation equilibria does not give information about the distribution of bound protons among the different protonation sites. For the convenience of the following discussions, it is also useful defining the cumulative protonation constant for a macroscopic protonation state m:

$$\bar{K}_m = \prod_{i=1}^m K_i. \tag{2.4}$$

Thus, from eq. 2.3 and eq. 2.4, the macrostate probability can equivalently be expressed as

$$P_m = \frac{a_{\mathrm{H}}^m \bar{K}_m}{1 + \sum_{m=1}^N a_{\mathrm{H}}^m \bar{K}_m}. \tag{2.5}$$

Protonation equilibria of polyprotic acids or bases can be described with a site binding model, which is analogous to the classical Ising model [6, 33, 36, 37, 42]. To each protonation site i, a state variable s_i $(i = 1, 2, ..., N)$ is assigned, such that $s_i = 1$ if the site is protonated and $s_i = 0$ if the site is deprotonated. The protonation microstate is then specified by the set of state variables $\{s_1, s_2, ..., s_N\}$, abbreviated as $\{s_i\}$. Neglecting the intermolecular interactions in a dilute solution, the free energy of a particular microstate relative to the fully deprotonated state and for unit activity of protons can be written as an expansion

$$\frac{\beta F(\{s_i\})}{\ln 10} = -\sum_i \mathrm{p}\hat{K}_i s_i + \frac{1}{2!}\sum_{i,j} \epsilon_{ij} s_i s_j + ... \tag{2.6}$$

where the sums run over all the sites, $\mathrm{p}\hat{K}_i$ is the microscopic protonation constant of the site i given all other sites are deprotonated, ϵ_{ij} are pair interaction parameters, and $\beta = 1/kT$ [6, 42, 43]. The parameters ϵ_{ij} can be related to the

free energy of the electrostatic repulsion between the protonated sites, E_{ij}:

$$\epsilon_{ij} = \frac{\beta E_{ij}}{\ln 10}. \tag{2.7}$$

The symmetry relation $\epsilon_{ij} = \epsilon_{ji}$ is obeyed, and $\epsilon_{ii} = 0$. The multiplication of ϵ_{ij} with s_i and s_j in equation 2.6 ensures that only the interactions between the protonated sites are taken into account. It is essential to realize that within the present model, the pair interactions act through the molecular backbone, and their magnitude is supposed to decrease quickly with increasing distance between the ionizable groups [44]. Thus, in the first approximation, we can consider only the nearest-neighbor interactions, in which case the presented model is equivalent to the Ising model [9]. Triplet, and other interactions, which in principle could play a role, will be omitted in the present approach. The parameters $\mathrm{p}\hat{K}_i$ and ϵ_{ij} are also called the *cluster parameters*. The model, which is defined through eq. 2.6 (also called the Ising Hamiltonian [42]) allows us to calculate all the quantities related to both macroscopic, and the microscopic equilibria, from the cluster parameters and the pH.

The total number of bound protons can be calculated for each microstate, by

$$m = \sum_{i=1}^{N} s_i \ , . \tag{2.8}$$

The probability of a particular macrostate is given by [42]:

$$P_m(a_{\mathrm{H}}) = \Xi^{-1} \bar{K}_m a_{\mathrm{H}}^m \tag{2.9}$$

where the normalization constant can be interpreted as a partition function

$$\Xi = \sum_{\{s_i\}} a_{\mathrm{H}}^n e^{-\beta F(\{s_i\})}. \tag{2.10}$$

and the $\bar{K}_m$ are the cumulative protonation constants, which can be expanded as [42]:

$$\bar{K}_m = \sum_{\{s_i\}} e^{-\beta F(\{s_i\})} \ \delta_{m,\sum_j s_j}. \tag{2.11}$$

The Kronecker symbol is denoted as δ_{ij}, with $\delta_{i=j} = 1$ and vanishes otherwise. The commonly used macroscopic step-wise dissociation constants (eq. 2.1) can be expressed in terms of the cumulative constants as $\mathrm{p}K_m = \log_{10} K_m = \log_{10}(\bar{K}_m/\bar{K}_{m-1})$. Eq. 2.11 is also being referred to as the *binding polynomial*. It becomes clear, that the site binding model can be used to express the overall degree of protonation θ by introducing eq. 2.11 into eq. 2.5 and 2.2:

$$\theta = \frac{1}{N} \frac{\sum_{n=0}^{N} n\bar{K}_n a_{\mathrm{H}}^n}{\sum_{n=0}^{N} \bar{K}_n a_{\mathrm{H}}^n} \tag{2.12}$$

Alternatively, the degree of protonation can be expressed as [42]:

$$\theta = \frac{a_{\mathrm{H}}}{N} \frac{\partial \log \Xi}{\partial a_{\mathrm{H}}} \tag{2.13}$$

The cluster parameters can be determined by fitting the macroscopic titration curves based on the site binding model. In contrast to the macroconstants, the number of cluster parameters remains the same for all dendrimer generations. For moderately sized molecules ($N \leq 30$) the model was evaluated numerically by direct enumeration of all states. For larger molecules, the model was also solved exactly employing a transfer matrix technique. A detailed description of this technique is given elsewhere [43].

2.3 Experimental

In this stage of the thesis, the Wallingford titrator was used to perform the potentiometric titration experiments (for details, see appendix). The burettes containined 0.25 M HCl (Merck Titrisol), 0.25 M CO_2-free KOH (Baker Dilut-It), 3.0 M KCl (Merck, p.a.), and pure water. All solutions were prepared with water from a MiliQ A10 UV/UF (Milipore) system, from which the residual CO_2 was eliminated through boiling. The double-wall potentiometric plexiglass cell was thermostatized to 25°C, and continuously flushed with moist CO_2-free nitrogen. The potential between a separate glass electrode and an Ag/AgCl

reference electrode was measured with an high-impedance voltmeter (Microlink PH4-S) after the drift criterion of less than 0.1 mV/min has been achieved.

A typical run started with the titration of acidified solution with KOH, and was then back-titrated with HCl. The instrument maintains a constant ionic strength during such a titration. The acid-base, and base-acid titrations were repeated at ionic strengths of 0.1 M, 0.5 M, and 1.0 M. The whole sequence of acid-base titrations at different ionic strengths was carried out automatically within a single titration experiment.

Blank titrations were used to calibrate the glass electrode in a pH-range between 3 and 11 at ionic strengths in the range of 0.1–1.0 M. The exact base concentration and the activity coefficients were determined by a least squares fit. Starburst polyamidoamine (PAMAM) dendrimers (Dendritech Corporation, Midland, USA) were titrated at total concentrations of amine groups of 10 and 20 mM. By taking the difference between the titration curves between the sample and the blank, the charging curve of the dendrimers is obtained. The titration curves were normalized with the known concentration of the dendrimers, and are reported as the overall degree of protonation θ as a function of pH. The estimated errors are ± 0.04 for θ and ± 0.02 for pH, respectively. The overall performance of the system was checked with titrations of ethylenediamine and acetic acid. The resulting ionization constants were in accord with literature values [11] within the expected error. The dendrimer concentrations were determined from the titration curves, and were within 2% of the values expected from the sample dosage.

2.4 Results

Potentiometric titration curves of PAMAM dendrimers at ionic strengths 0.1, 0.5 and 1.0 M in KCl for the different generations G0, G1, G2, G3, G4 and G6 are presented in Fig. 2.2. The solid lines are model calculations to be discussed below. The titration (or charging) curves show the characteristic dependence with the

Table 2.1: Cluster parameters of the site binding model of the poly(amidoamine) dendrimers. Δ has to be recalculated into the next-nearest neighbor parameter, by using formula 2.14.

I (M)	p$K^{(I)}$	p$K^{(III)}$	p$K^{(III')}$	ϵ	ϵ'	Δ
0.1	9.00	6.00	6.70	0.15	2.85	0.14
0.5	9.20	6.50	7.00	0.15	2.85	0.07
1.0	9.30	6.70	7.30	0.15	2.85	0.06

ionic strength for a polybase, which is becoming more acidic with decreasing ionic strength [6, 33]. It was further verified that the titration curves were fully reversible and independent of the dendrimer concentration within experimental error, indicating that dendrimer-dendrimer interactions are negligible.

The titration curves undergo a characteristic transition with increasing generation number. This transition is more clearly illustrated in Fig. 2.3, where the titration curves for the different generations at fixed ionic strength of 0.5 M are plotted. The smallest dendrimer G0 has 6 ionizable sites (4 primary and 2 tertiary amine groups, see Fig. 2.3 and Tab. 2.4) and shows three protonation steps and two intermediate plateaus at $\theta = 4/6$ and $5/6$. On the other hand, the largest dendrimer G6 with 510 ionizable sites shows two protonation steps, and an intermediate plateau at $\theta = 1/2$. The differences between titration curves of the smaller dendrimers are substantial, while the titration curves of the dendrimers G4 and above are minor, and reflect the large molecule limit. This limit, where the titration curves becomes independent of molecular weight, is characteristic for polyelectrolytes.

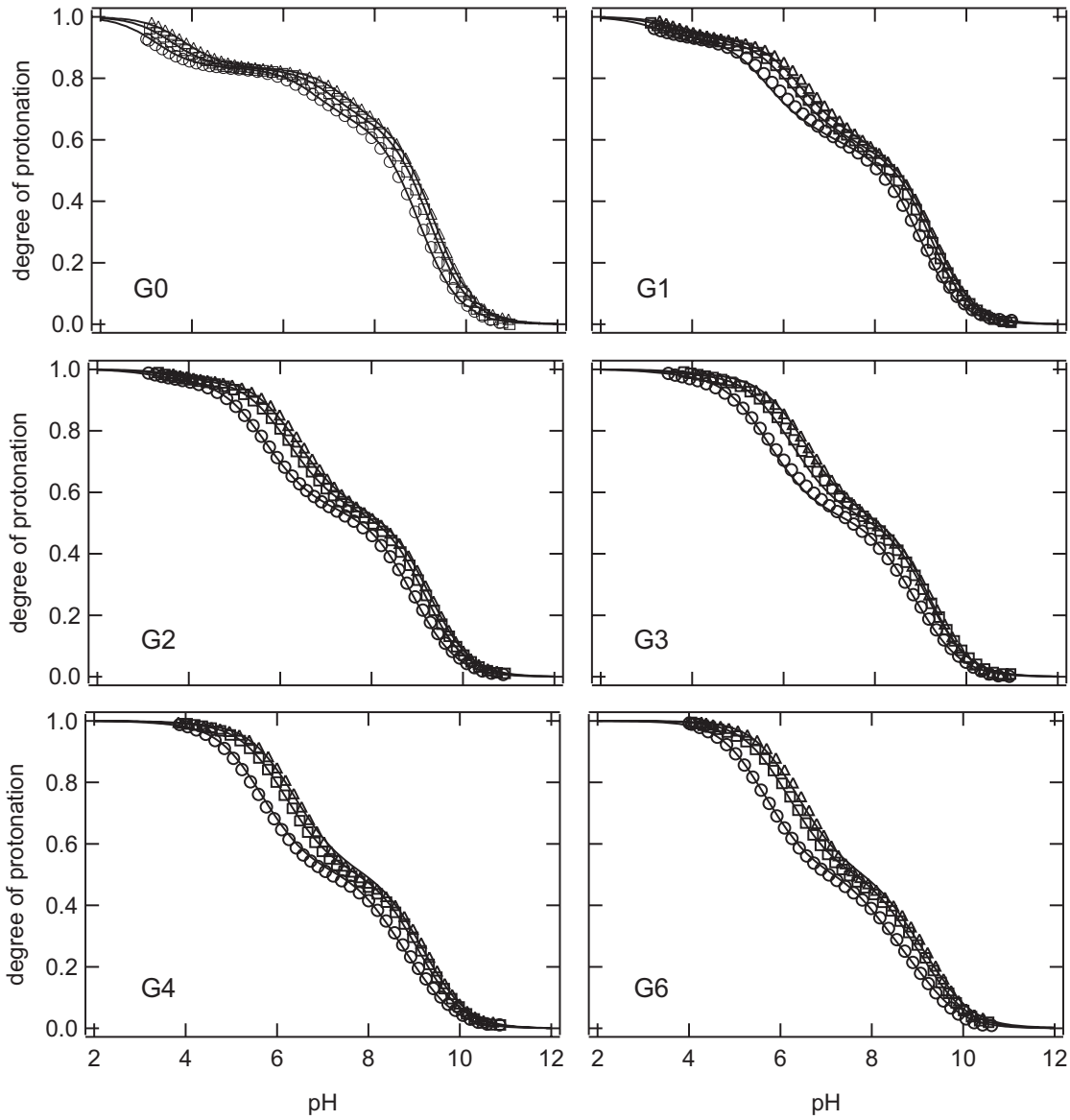

Figure 2.2: Potentiometric titration curves at different ionic strengths in KCl of PAMAM dendrimers of generations G0, G1, G2, G3, G4, and G6. Solid lines are calculations with the site binding model.

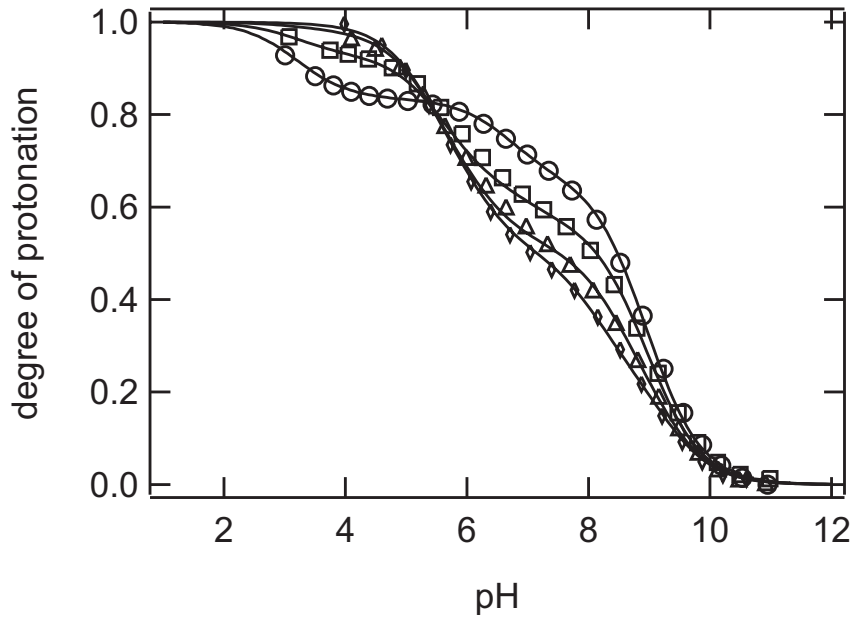

Figure 2.3: Potentiometric titration curves of PAMAM dendrimers of generations G0, G1, G2, G3, G4, and G6 at at ionic strength 0.1 M in KCl. Solid lines are calculations with the site binding model.

2.5 Modelling and Interpretation

The macroscopic equilibria of G0 and G1 poly(amidoamine) dendrimers is described in classical terms, by fitting the pK values directly from the proton binding isotherms, and by calculating them according to the site binding model by using the relations presented in sect. 2.2. The proton binding isotherms are interpreted in terms of the site binding model, where the degree of protonation was calculated from the site binding model.

The macroscopic ionization constants have been determined by a least-squares fit of the experimental titration curve (cf. eq. 2.12). The resulting macroscopic protonation constants $\mathrm{p}K_n$ are summarized in Tabs. 2.5 and 2.5. Six macroconstants can be determined for G0, and fourteen for G1, with reasonable confidence. A disadvantage of this classical picture is that it is becoming impractical with increasing generation number, as the number of macroconstants increases quickly. Furthermore, as will be discussed in chapter 3, it does not lead to insight into the microscopic protonation mechanism of the molecule. Both disadvantages can be overcome with the site binding model discussed now.

The cluster parameters, are illustrated in Fig. 2.4. Since the ionizable amine groups are relatively far apart, we assume pair interactions only. Nearest neighbor interactions act along bonds, namely one containing the amide bond with an interaction parameter ϵ, and the ethyl chain in the center of the dendrimer with an interaction parameter ϵ'. As we shall see, a nonzero next nearest neighbor interaction parameter ϵ'' between the primary amine groups must be introduced, similarly as in the description of the charging behavior of carboxylated dendrimers [34].

The microconstant of the primary amine groups is denoted by $\mathrm{p}\hat{K}^{(\mathrm{I})}$. For the tertiary groups, two different microconstants must be distinguished due to different chemical environments. The microconstant of the innermost tertiary amines is denoted by $\mathrm{p}\hat{K}^{(\mathrm{III}')}$, while for all others the same value of $\mathrm{p}\hat{K}^{(\mathrm{III})}$ will

Table 2.2: Comparison of macroscopic ionization constants pK_m of the PAMAM dendrimer G0 from direct fit of the titration curves and calculated from the site binding model at different ionic strengths. The error of the presented values is ≤ 0.03 units.

	0.1 M		0.5 M		1.0 M	
m	fit	model	fit	model	fit	model
1	9.70	9.59	9.83	9.78	9.98	9.87
2	9.26	9.17	9.47	9.36	9.55	9.45
3	8.74	8.82	8.99	9.01	9.10	9.10
4	8.31	8.39	8.61	8.59	8.73	8.68
5	6.68	6.67	7.13	7.03	7.34	7.32
6	3.15	3.21	3.65	3.57	3.91	3.87

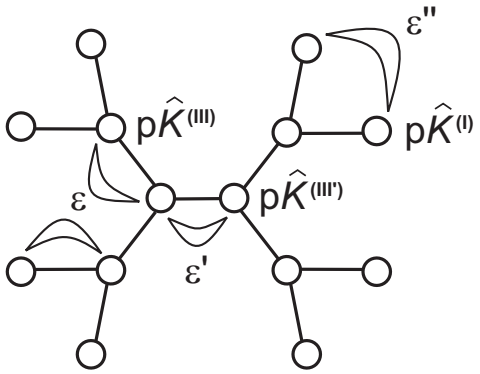

Figure 2.4: Cluster parameter assignment for the poly(amidoamine) dendrimer.

Table 2.3: Comparison of macroscopic ionization constants pK_m of the PAMAM dendrimer G1 from direct fit of the titration curves and calculated from the site binding model at different ionic strengths. The error of the presented values is ≤ 0.03 units.

	0.1 M		0.5 M		1.0 M	
m	fit	model	fit	model	fit	model
1	9.95	9.85	10.02	10.78	10.16	10.15
2	9.70	9.50	9.87	9.72	9.76	9.79
3	9.25	9.25	9.47	9.47	9.76	9.54
4	9.19	9.05	9.34	9.27	9.28	9.34
5	8.78	8.86	9.08	9.08	9.21	9.15
6	8.68	8.65	8.92	8.88	9.07	8.95
7	8.30	8.41	8.57	8.64	8.60	8.72
8	7.96	8.07	8.29	8.30	8.47	8.39
9	7.10	7.06	7.43	7.44	7.50	7.68
10	6.36	6.35	6.91	6.81	7.21	7.00
11	5.95	5.96	6.33	6.43	6.39	6.61
12	5.55	5.61	6.17	6.08	6.56	6.27
13	5.10	5.18	5.52	5.66	5.59	5.84
14	3.07	3.20	3.51	3.57	3.66	3.86

be used.

While these parameters cannot be uniquely determined from a single titration curve, they can be obtained by a simultaneous fit of G0 and G1 data. The interaction parameters are $\epsilon = 0.15$ and $\epsilon' = 2.85$. At this point we have set $\epsilon'' = 0$. The ionization constants increase with the ionic strength and the values are given in Tab. 1. While a slight decrease of the interaction parameters with increasing ionic strength could be found, the data can be equally well described by assuming these parameters to be ionic strength independent. This approach was adopted here for simplicity.

For the dendrimers G2, G3, G4, and G6 it was observed that a good fit cannot be obtained without introducing an interaction between the primary amines ϵ''. While the data for all dendrimer generations can be obtained with the same cluster parameters, one further observes that ϵ'' increases with increasing generation number. It was found that this dependence can be modelled as

$$\epsilon'' = \Delta(k-1) \tag{2.14}$$

where k is the generation number ($k > 1$) and Δ is ionic strength dependent and is given in Tab. 1. For G0 and G1 ($k = 0, 1$), it was found that the interaction parameter ϵ'' is negligible ($\epsilon'' = 0$). From Figs. 2.2 and 2.3 it can be inferred that this five-parameter model describes all experimental data at a given ionic strength to good accuracy.

The interaction parameters for the amide bond, $\epsilon \simeq 0.15$, has not been reported in the literature before, but this value is well comparable with the corresponding value of 0.18 for an alkyl chain with the corresponding number of carbon atoms, as in hexamethyleneamine [6]. The interaction parameter $\epsilon' \simeq 2.87$ is somewhat larger than the value of 2.13 reported for ethylenediamine [6]. This increase is probably caused by the presence of the amido side chains coordinating the nitrogen atoms. Note that ϵ'' decreases within increasing ionic strength, while ϵ and ϵ' are virtually ionic strength independent. This difference can be

understood by realizing that the nearest neighbor interactions parameterized by ϵ and ϵ' act mainly along the hydrocarbon backbone, while the interactions between the primary amines parameterized by ϵ'' act through the solution, and is thus more influenced by the ionic strength due to effects of screening [6, 39]. The trend in the increase of ϵ'' with the generation number is similar to the sequence of conformations observed by small angle scattering [27]. The negligible interaction between the primary amine groups for G0 and G1 reflects the open structure of these dendrimers, while its increase for higher generations is in line with the increasingly compact structure of the larger dendrimers.

The microscopic ionization constants of the amine groups are generally lower than the corresponding values for aliphatic amines, but show the same trends otherwise. For primary amine groups, $\mathrm{p}\hat{K}^{(\mathrm{I})}$ in the range 9.4–9.7 have been reported, while for tertiary amine groups $\mathrm{p}\hat{K}^{(\mathrm{III})}$ lies around 7.5 [6].

As shown in Tabs. 2 and 3, the site binding model can equally well predict the fitted macroconstants $\mathrm{p}K_n$ obtained from eq. 2.11. This feature illustrates that the classical description in terms of the macroscopic equilibria is inherent to the site binding model. In contrast to the classical picture, however, the site binding model is capable of quantifying the protonation behavior within an entire homologous series with a limited number of parameters.

With the site binding model one can further address the microscopic protonation mechanism in detail, as will be discussed in chapter 3.

2.6 Conclusion

Poly(aminido amine) (PAMAM) dendrimers of generations G0, G1, G2, G3, G4, and G6 were investigated by potentiometric titrations, and the data analyzed in terms of classical macroscopic protonation equilibria and a site binding model. While both descriptions are equivalent, the site binding model offers further the possibility to model the titration curves of the higher generation dendrimers,

and to describe all dendrimers within a common set of parameters. These parameters involve the microscopic ionization constants for each group in the fully deprotonated state, and nearest neighbor pair interaction parameters.

Chapter 3

Microscopic protonation mechanisms of dendritic polyamines

3.1 Introduction

In the microscopic picture of protonation, the species are distinguished by both the number of bound protons m, and their distribution among the protonation sites [6, 45]. The studies of the protonation species at the molecular level, were first become feasible with the development of the NMR techniques [46, 47]. This approach has substantially become important for the studies of biologically important molecules, like oligophosphates [48, 49] or aminoacids [50]. As well, the insight into the protonation of specific proton-binding sites within a molecule, is important in the case of metal complexation [21, 51], or incorporation of small molecules [52].

The microscopic charging mechanism of the dendritic polyamine molecules is not immediately obvious, and has prompted quite some discussion in the literature [29, 31, 33, 35–37, 53]. The charging behavior of poly(propyleneimine)

dendrimers has been studied in substantial detail by potentiometric titrations [33] and ^{15}N-NMR [36], and it was shown that these dendrimers protonate in two steps with an intermediate plateau at a degree of protonation of 2/3. Briefly, during the first step occurring around pH 10, the primary amine sites, and the sites in each second shell counting from the rim, protonate. In the second step around pH $\approx$ 5, the rest of the sites protonate. However, it was as well suggested that in the poly(propyleneimine) dendrimers the primary and tertiary amines protonate almost independently, leading to two distinct protonation steps [35]. Since in a larger dendrimer the number of primary and tertiary amine groups is almost the same, this model would incorrectly predict an intermediate plateau at 1/2, and not at 2/3 as observed experimentally.

The charging mechanism of poly(amidoamine) dendrimers was suggested to involve two independent protonation steps of the primary and tertiary amine groups [53], while others have surmised that poly(propyleneimine) and poly(amidoamine) dendrimers should protonate similarly [31]. In this chapter, it will be demonstrated that the protonation mechanism of poly(amidoamine) dendrimers is very different from the poly(propyleneimine) dendrimers, and for higher generations indeed involves the almost independent protonation of primary and tertiary groups, which is consistent with the observed intermediate plateau at 1/2. However, this picture is only partially correct for lower generations, since the two innermost tertiary groups interact strongly, and protonate in two distinct steps. Furthermore, it will be demonstrated that the protonation mechanisms of poly(propyleneimine) and poly(amidoamine) dendrimers can be combined in the case of a dendrimer, with a structure similar to poly(propyleneimine) dendrimer, but with a short core carbon chain, which will be referred to as (2,3) dendrimer.

The microscopic protonation mechanisms, presented hereby, have been obtained by applying the same microscopic site binding model which was introduced in chapter 2. The cluster expansion of the free energy of protonation [6, 33, 36, 37, 42] is used in the same manner as presented there, with a set of

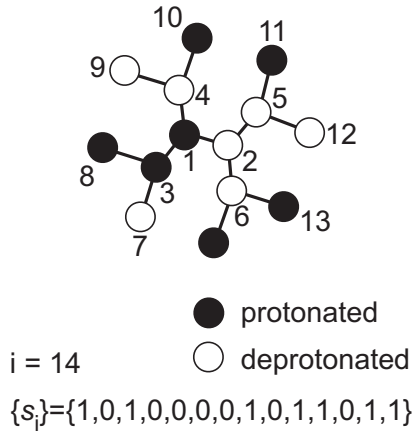

Figure 3.1: One of the possible protonation microstates, for the macrostate defined with $N = 14$, and $m = 6$. The state vector s_i defines the microstate.

statistical-mechanical experssions, which enable the assesment of the microscopic protonation constants, microstate probabilities, and other microscopic properties. Again, the basis for these calculations are the cluster parameters, which in the case of poly(amidoamine) dendrimers, are the same as presented in chapter 2.

3.2 Microscopic protonation equilibria

To define all the possible distributions of the bound protons among the protonation sites, the sites are enumerated with i, and a two-valued "state" variable, $s_\mathrm{i} = 0\,\mathrm{or}\,1$ (0 for deprotonated, 1 for protonated) is assigned to each site. The microscopic protonation state (alternatively, microstate or microspecies) is defined by a state vector $\{s_\mathrm{i}\}$, as demonstrated for the first generation dendrimer molecule in figure 3.1. The microscopic protonation constant, $\hat{K}_j(\{s_i\})$ is attributed to an unprotonated site j when the molecule attains a microstate $\{s_i\}$.

The site binding model is defined in the previous chapter, through equation 2.6. However, the probability of a given microstate depends on the proton activ-

ity, a_{H} [6, 43]:

$$p(\{s_i\}) = \Xi^{-1} a_{\mathrm{H}}^m e^{-\beta F(\{s_i\})} \tag{3.1}$$

The normalization constant Ξ can be interpreted as the partition function of the polyelectrolyte, with respect to different states of protonation:

$$\Xi = \sum_{\{s_i\}} a_{\mathrm{H}}^m e^{-\beta F(\{s_i\})} \ . \tag{3.2}$$

As mentioned earlier, the fully unprotonated molecule is taken as the reference state. The number of microstates for a macrostate m grows with the number of sites, as $\binom{N}{m}$ [6]. The probability of a microstate, can be expressed as a product:

$$p(\{s_i\}) \ = \ \pi(\{s_i\}) P_m(a_{\mathrm{H}}) \tag{3.3}$$

where $\pi(\{s_i\})$ denotes the conditional probability of the microstate $\{s_i\}$ within the macrostate m. This probability is given by

$$\pi(\{s_i\}) \ = \ \bar{K}_m^{-1} e^{-\beta F(\{s_i\})} \tag{3.4}$$

It should be noted that the probability $\pi(\{s_i\})$ does not depend on pH, and can be easily interpreted as the mole fraction of the microspecies within a macrospecies m.

Once all cluster parameters are known, the microscopic protonation constants, for all the unprotonated sites within all the microstates can be calculated in a straightforward fashion. If we label the unprotonated site with j, the association equilibrium can be written as

$$\mathrm{A}\{s_i\} + \mathrm{H} \rightleftharpoons \mathrm{A}\{s_i'\} \tag{3.5}$$

where $s_i = s_i'$ for all $i \neq j$, but $s_j = 0$ and $s_j' = 1$. Using expansion for the free energy (eq. 2.6), the microscopic pK value for the reaction given by eq. 3.5 follows as [42]

$$\mathrm{p}\hat{K}_{\mathrm{A}\{s_i\}} = \mathrm{p}\hat{K}_i - \sum_j \epsilon_{ij} s_j - ... \tag{3.6}$$

This relation defines the change in the microscopic protonation constant of a group, in the presence of another protonated group, and reflects the group additivity concept for the estimation of protonation constants [54]. In the present approach, the microconstants from eq. 3.6 represent secondary parameters, which can be easily evaluated once the primary cluster parameters are known.

3.3 Protonation behavior of hyperbranched polyamines

The concepts presented in the introduction to this chapter will be demonstrated on several examples of branched polyamines. These will include the zeroth and the first generation of the poly(amidoamine) and poly(propyleneimine) dendrimers, and a dendrimer, with a structure similar to the poly(propyleneimine) dendrimer, but with a shorter core unit. To the best knowledge of the author of this text, the latter molecule was not yet synthesized, but could exert some interesting protonation properties to be discussed. It will be referred to as (2,3) dendrimer. The structures of poly(propyleneimine) and (2,3) dendrimers are shown in figure 3.2, and of poly(amidoamine) dendrimer in figure 2.1. The microscopic mechanisms estimated for the lowest two generations, will be applied to predict the microscopic picture of protonation for the higher generations. The number of sites for different generations can be calculated according to the formula

$$N = 2^{G+3} - 2 \tag{3.7}$$

where G denotes the generation number, which is zero for the smallest molecule.

The assessment of the microscopic protonation mechanism refers to prediction of the probabilities of the microspecies with respect to pH: The macroscopic mechanism gives the probabilities of the macrospecies. The microscopic mechanism gives the probabilities of the microspecies, and the microscopic protonation

constants, which can be assigned to each unprotonated site within a certain macrostate. The probabilities of the protonation species can be interpreted in terms of abundances in the solution. The presence of the microspecies can be experimentally confirmed by means of spectroscopic methods, in particular NMR [6, 36, 37], and UV-VIS and IR techniques [6]. The microstates will be presented schematically as shown in fig. 3.1, and the macrostates will be simply denoted with m, which is the number of bound protons to the molecule. The microscopic mechanisms will be presented as schemes of the most prominent microspecies for a certain macrostate, together with the according probabilities and all the microconstants. The macroscopic protonation mechanisms, will be presented in terms of the speciation diagrams P_m(pH) (e.g. fig. 3.7), which are directly reflected in the proton binding isotherms, as can be concluded from the eq. 2.2. In this manner, a comprehensive picture of protonation can be gained for all the molecules studied.

The protonation mechanism can be deduced once all the cluster parameters are assessed. The conditional probabilities of the microspecies within a certain macrospecies can be calculated according to formula 3.4, and the microconstants according to eq. 3.6. The difference in the microstate probabilities reflects the difference in the free energies of microspecies, which can be calculated according to eq. 2.6. In other words, the microstate probability is weighted by the free energy. The proton binding isotherms can be obtained from the cluster parameters in the following manner; The energy spectrum of the molecule is calculated according to eq. 2.6, and the cumulative macroscopic constants can then be calculated from eq. 2.11. The degree of protonation can be obtained from the cumulative protonation constants in a straightforward fashion, by introducng the macrostate probabilities from eq. 2.5 into eq. 2.2.

The number of cluster parameters in the case of studied molecules is small: a very good fitting of the proton binding isotherms of the high-generation poly(amidoamine) dendrimers was achieved by using effectively only five differ-

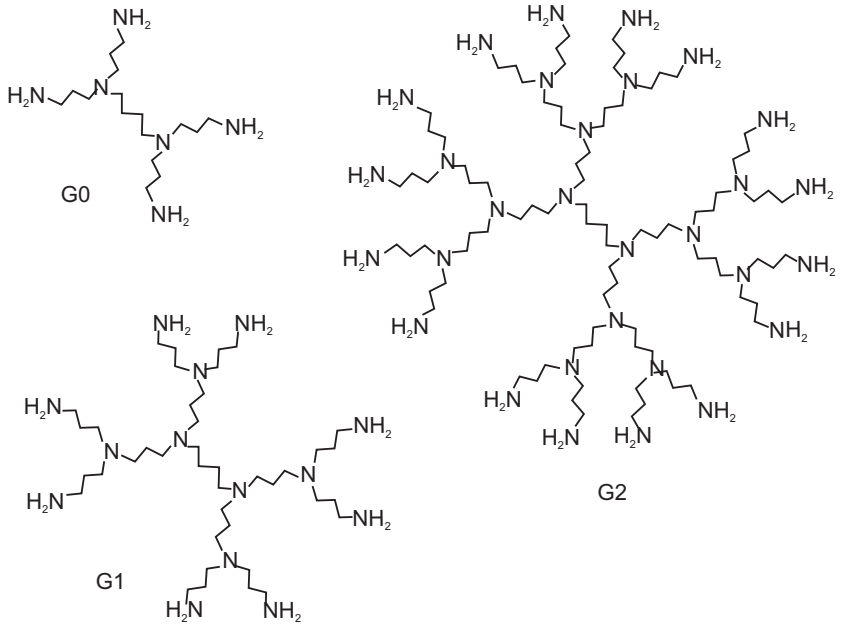

poly(propyleneimine) dendrimers

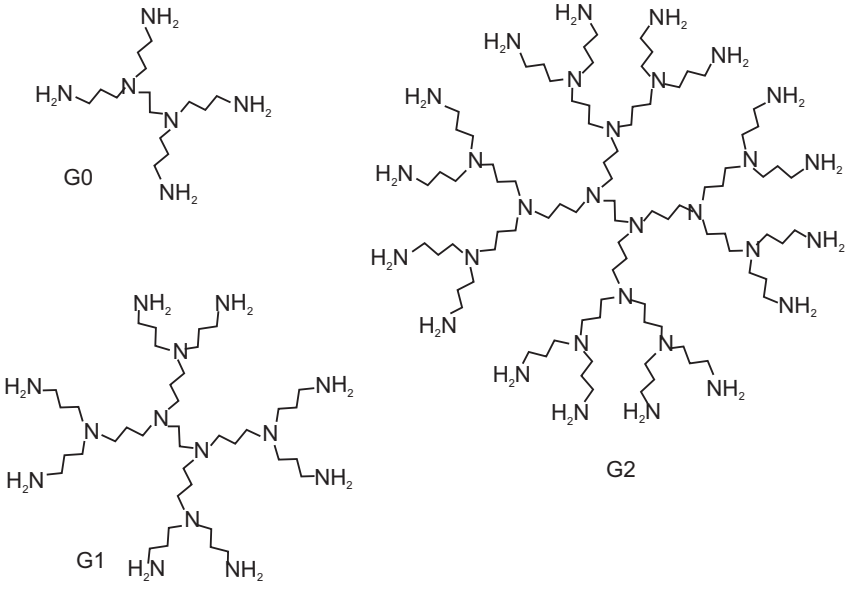

(2,3) dendrimers

Figure 3.2: Chemical structures of the studied molecules.

Table 3.1: Cluster parameters of the site binding model for the poly(propyleneimine) dendrimers for $I = 0.1$M [33].

generation	p$K^{(\mathrm{III}')}$	p$K^{(\mathrm{III})}$	p$K^{(\mathrm{III}'')}$	p$K^{(\mathrm{I})}$	ϵ	ϵ'	ϵ''
0	9.02	-	-	9.97	0.61	1.05	-
1	8.19	-	9.66	9.85	0.61	1.05	1.57
2	8.19	7.99	9.72	9.79	0.61	1.05	1.57
3	8.19	8.02	9.71	9.70	0.61	1.05	1.57
4	8.19	7.95	9.66	9.56	0.61	1.05	1.57

ent cluster parameters (see chapter 2), and only three parameters in the case of the zeroth generation. In the case of poly(propyleneimine) dendrimers, according to [33], seven parameters are needed to fit the proton binding isotherms of the second and higher generations, four for the zeroth, and six for the first generation (see table 3.4). The procedure to obtain the cluster parameters from the experimental proton binding isotherms for poly(amidoamine) dendrimers was described in chapter 2. For poly(propyleneimine) dendrimers, the cluster parameters were obtained in a similar manner [33]. For (2,3) dendrimers, the cluster parameters for the zeroth generation were taken from [44].

3.4 Poly(amidoamine) vs. poly(propyleneimine) dendrimers

The cluster parameters, obtained by fitting the proton binding isotherms of poly(amidoamine) dendrimers are shown in table 2.4 in chapter 2. For the poly(propyleneimine) dendrimers, the cluster parameters were used, as reported in [33], and the values at $I = 0.1$M are presented in table 3.4. For the explanation of the seven different parameters, see figure 3.3.

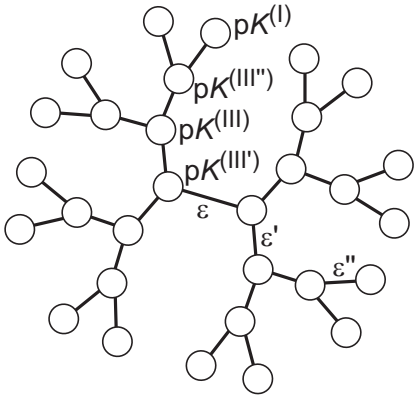

Figure 3.3: The assignment of the cluster parameters for the poly(propyleneimine) dendrimers.

The proton binding isotherms of poly(amidoamine) and poly(propyleneimine) dendrimers, calculated from the cluster parameters, are presented in fig. 3.4. In both cases, the isotherms for higher generations all follow the same curve, and a deviation from this curve can be observed for the lowest two generations. Since the site binding model is inherent to the type of the protonation groups and the pair interactions, and is insensitive to the number of the protonation sites, the appearance of the common proton binding isotherm at high generations can be explained by the fixed respective amounts of different types of sites. For example, for high generations of poly(amidoamine) dendrimer, there are only two types of sites that play an important role with two distinct $\mathrm{p}\hat{K}_i$ values, namely the primary amine groups and the tertiary amine groups; there is only one significant pair interaction parameter, namely ϵ'. In the case of high generations, the innermost sites are greatly outnumbered by the rest, and the ratio of the primary amine groups to the total number of sites N is approaching 1/2. Consequently, the proton binding isotherm exerts a plateau at $\theta = 1/2$. The proton binding isotherms of high generations of poly(propyleneimine) dendrimers are showing a plateau at $\theta = 1/3$. The source of the plateau in these curves can be rationalized

by inspecting the most prominent microspecies, presented in fig. 3.10, as will be discussed later.

The microscopic protonation mechanisms for the zeroth generation of poly(amidoamine) and poly(propyleneimine) dendrimers, are shown in figures 3.5 and 3.6, respectively. In the lower part of these figures, the macroscoopic speciation diagrams, and the overall proton binding isotherm are presented. The proton binding isotherm shows a pronounced protonation step, at $8 < \mathrm{pH} < 10$ for poly(amidoamine), and at $9 < \mathrm{pH} < 11$ for poly(propyleneimine), where two thirds of the sites are protonated. The microscopic mechanisms show that the peripheral sites are protonated in the first step, due to four symmetrically equivalent outermost groups. A common feature of the G0 mechanism for both dendrimers is that the macrostate with four bound protons exerts three distinct microspecies, out of which the one with the protonated primary amine groups is largely predominant over the two with one deprotonated primary group. In principle, another microspecies, with two unprotonated primary amine sites can be imagined, but it turns out that the probability of that one is lower than one per thousand. A difference in these mechanisms can be noticed regarding the last protonation step: In the case of poly(propyleneimine) G0 dendrimer, the inner two sites are protonated in a single step, at $5 < \mathrm{pH} < 7$. In the case of poly(amidoamine) G0 dendrimer, the protonation of the inner two sites occurs in two separate steps, around $\mathrm{pH} \approx 6$ and around $\mathrm{pH} \approx 3.5$. This difference can be explained by the dependence of the pair interaction parameter on the distance between the sites [6, 44]. For poly(propyleneimine) dendrimers, where there are four carbon atoms in between the inner two sites, the pair interaction parameter is lower than for the poly(amidoamine) dendrimers. These sites are separated by only two carbon atoms.

The macrostate probability diagrams of the first generation poly(amidoamine) and poly(propyleneimine) dendrimers are shown in fig. 3.7. The main difference is in the probabilities of the most pronounced intermediate macrostates,

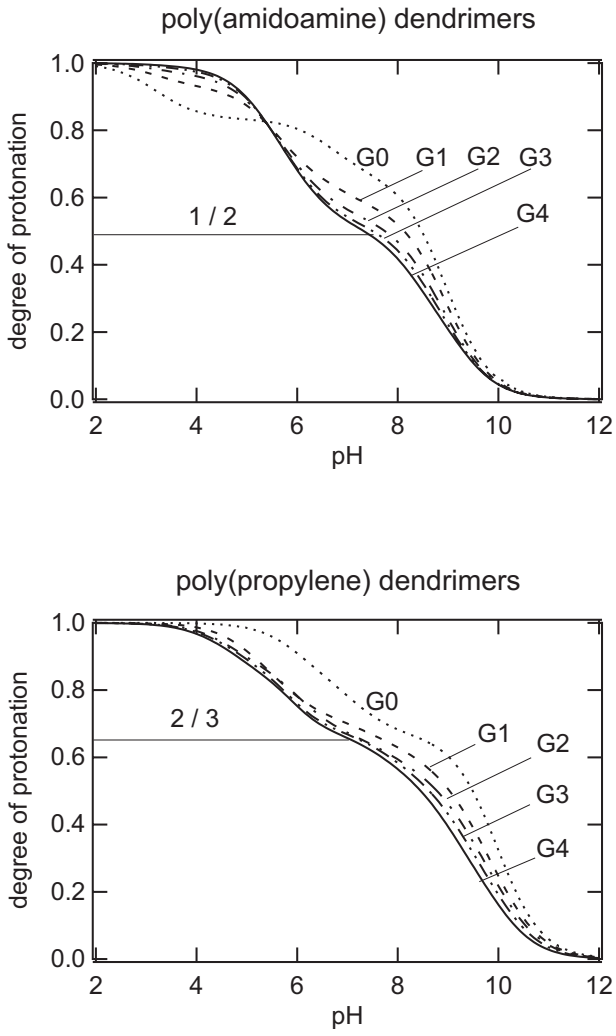

Figure 3.4: Proton binding isotherms of the first five generations of the poly(amidoamine) (top) and poly(propyleneimine) (bottom) dendrimers. The proton binding mastercurve for poly(amidoamine) dendrimers exerts a plateau value of $\theta = 1/2$ at pH ≈ 7.5

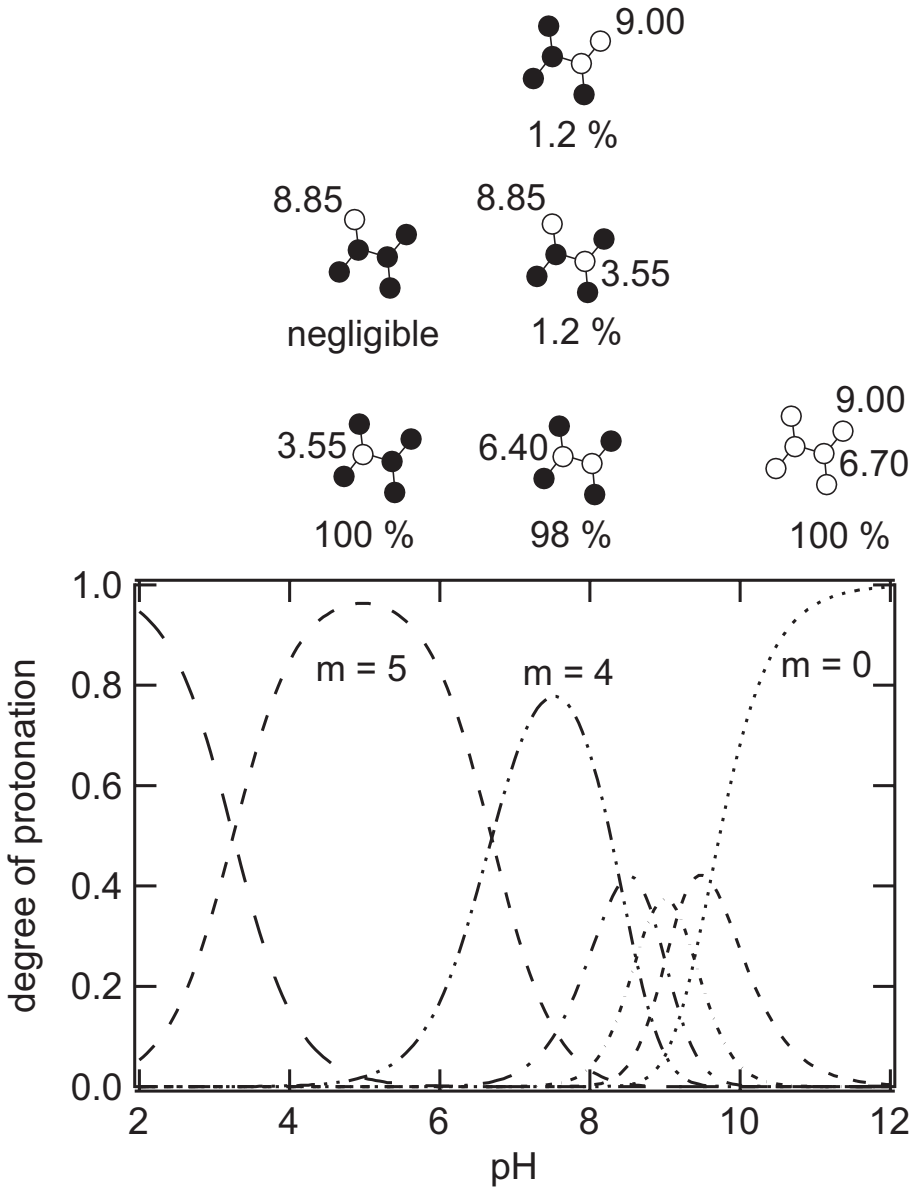

Figure 3.5: Bottom: macrospeciation diagram of the zeroth generation poly(amidoamine) dendrimer as a function of pH (broken lines), where m denotes the number of protons bound to the molecule (macrospecies). The overall titration curve is represented with a full line. Top: the most prominent microspecies for a certain protonation step, where the micro pK values are assigned to the unprotonated sites.

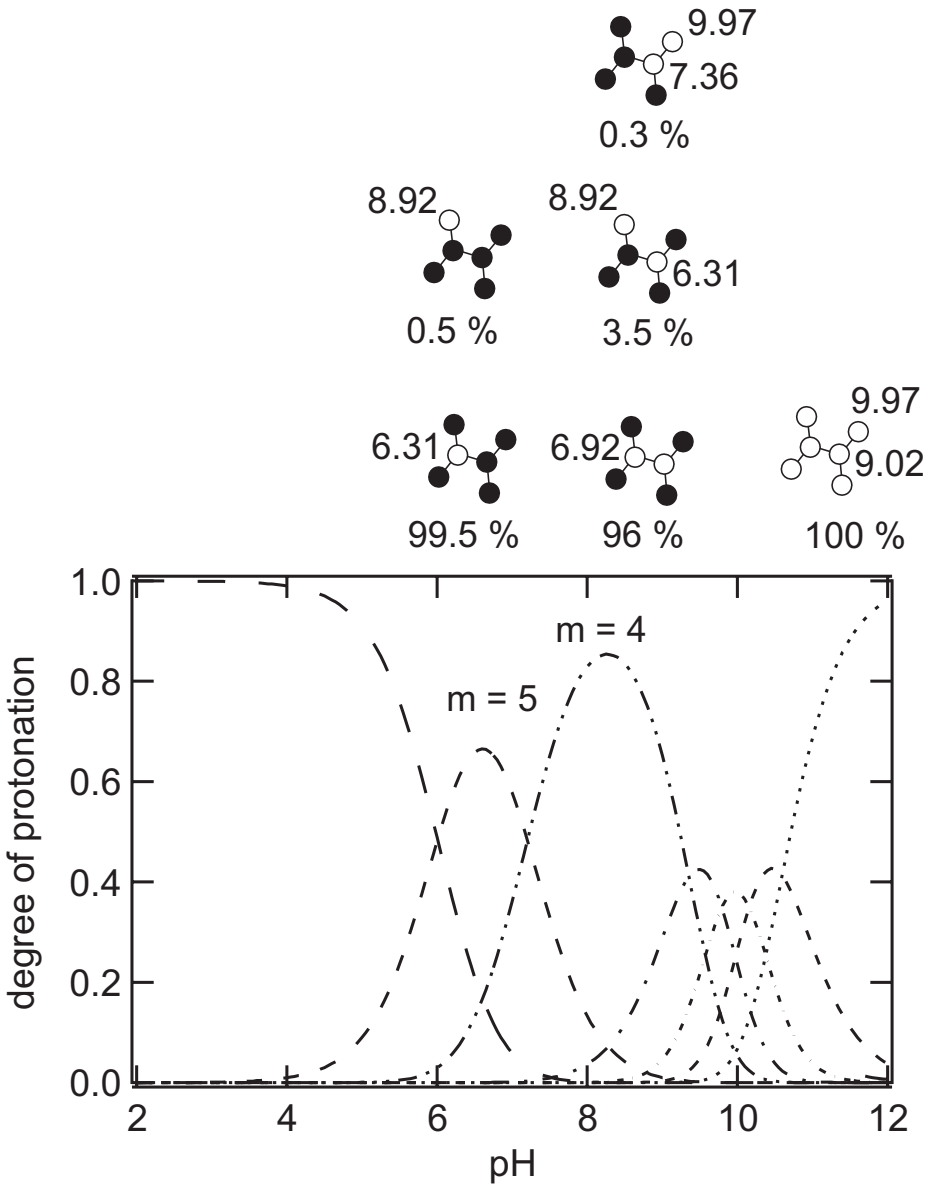

Figure 3.6: Bottom: macrospeciation diagram of the zeroth generation poly(propyleneimine) dendrimer as a function of pH (broken lines), where m denotes the number of protons bound to the molecule (macrospecies). The overall titration curve is represented with a full line. Top: the most prominent microspecies for a certain protonation step, where the micro pK values are assigned to the unprotonated sites.

which are causing a plateau in the proton binding isotherm: In the case of poly(amidoamine) dendrimer, it is the species with $m = 8$, while in the case of poly(propyleneimine) dendrimer, it is the one with $m = 10$. The microscopic mechanisms will be used to establish the most probable microstates for these two macrostates, which play an important role for the overall proton binding isotherms.

The microscopic protonation mechanism for the first generation poly(amidoamine) dendrimer is presented in fig. 3.8. The most prominent microspecies are shown with the according probabilities, and the microconstants are presented for each unprotonated site. The increased complexity of the microscopic protonation picture for the first generation, as compared to the zeroth generation, is not surprising, having in mind that the number of microstates for a certain macrostate grows as $\binom{N}{m}$. The most prominent microspecies can be spotted by inspecting the probabilities of the microstates. In the case of poly(amidoamine) dendrimer, these are the microspecies at $m = 8$, with the protonated primary amine sites, and at $m = 9$, with the protonated primary, and one of the core tertiary amine sites. These microspecies have significantly higher probabilities than the others. For $m > 9$, there is one more significant microspecies, with the protonated primary, and one of the outermost tertiary amine sites, which is a consequence of the long chains, thus almost negligible pair interactions, between the primary and the outermost tertiary sites.

In the case of the first generation poly(propyleneimine) dendrimer, the most interesting microspecies is for $m = 10$, with protonated primary, and the innermost tertiary amine sites, as can be seen by inspecting figure 3.9. Another difference with respect to the mechanism of the poly(amidoamine) dendrimer, is that the difference in the probabilities of the two microspecies at $m = 13$, is less pronounced, which is a consequence of a smaller difference between $\mathrm{p}K^{(\mathrm{III})}$ and the $\mathrm{p}K^{(\mathrm{III}')}$ in the case of poly(propyleneimine) dendrimer. Apart from the above differences, the microscopic mechanisms of the G1 poly(amidoamine) and

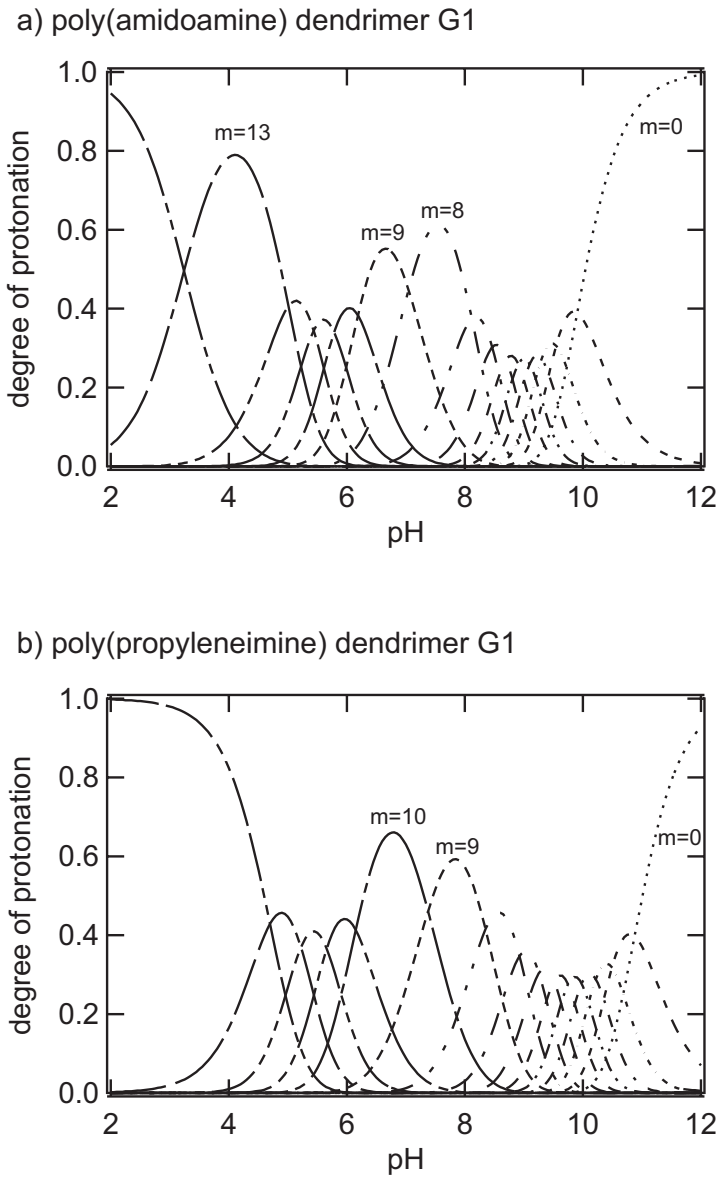

Figure 3.7: The macrospeciation diagrams for the first generation poly(amidoamine) and poly(propyleneimine) dendrimers. The most important macrospecies are denoted with m (the number of bound protons per molecule).

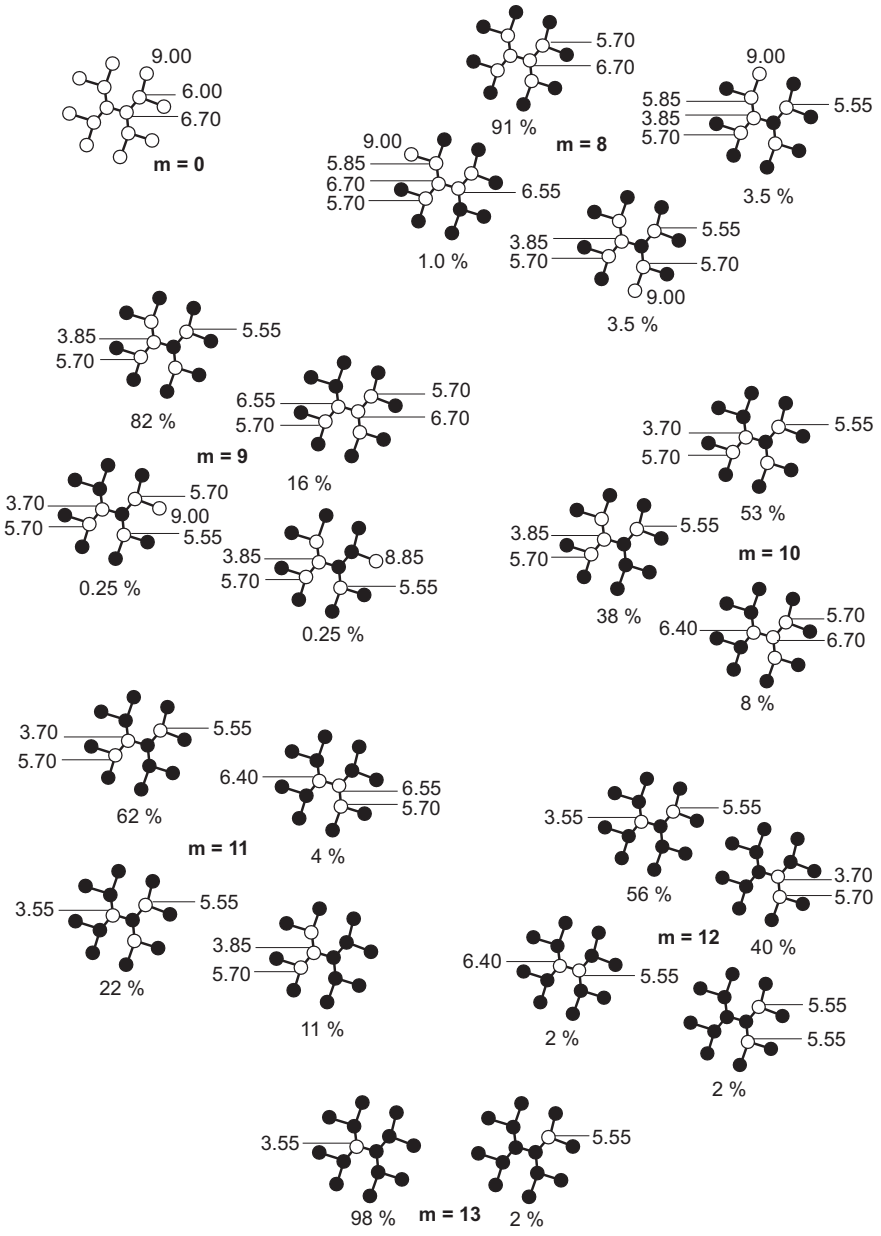

Figure 3.8: The microscopic mechanism of the first generation poly(amidoamine) dendrimer. The most important microspecies are presented for several distinguished macrospecies, denoted with m (see figure 3.7). A probability is assigned to each microspecies, and the micro pK values are assigned to the unprotonated sites.

poly(propyleneimine) dendrimers are similar. For example, at $m = 9$, there is the same most probable microspecies, with the primary, and one innermost tertiary groups protonated. Another similarity is that at $m > 9$, neither of the two mechanisms does exert clearly predominant species.

As the number of the possible microstates grows as 2^N, the computation of the detailed microscopic mechanisms, which requires calculation of the free energy for all the microstates, is becoming increasingly consuming in terms of computation time with an increasing generation number. In fact, for generations higher than the second, this computation was not possible with the 1.7 GHz CPU and 512 MB RAM PC. However, the proton binding isotherm can be predicted by using a recursive approach [43]. The sites are divided into repeating blocks, for which the model can be solved explicitly. The protonation patterns for the blocks are assumed to be conserved when considering the whole molecule. In spite of the fact, that detailed mechanisms for the higher generations of dendrimers were not calculated, the prediction of the most prominent species can be done by extending the mechanism for the first generation. The most prominent species for the fourth generation poly(amidoamine) and poly(propyleneimine) dendrimers are presented in fig. 3.10.

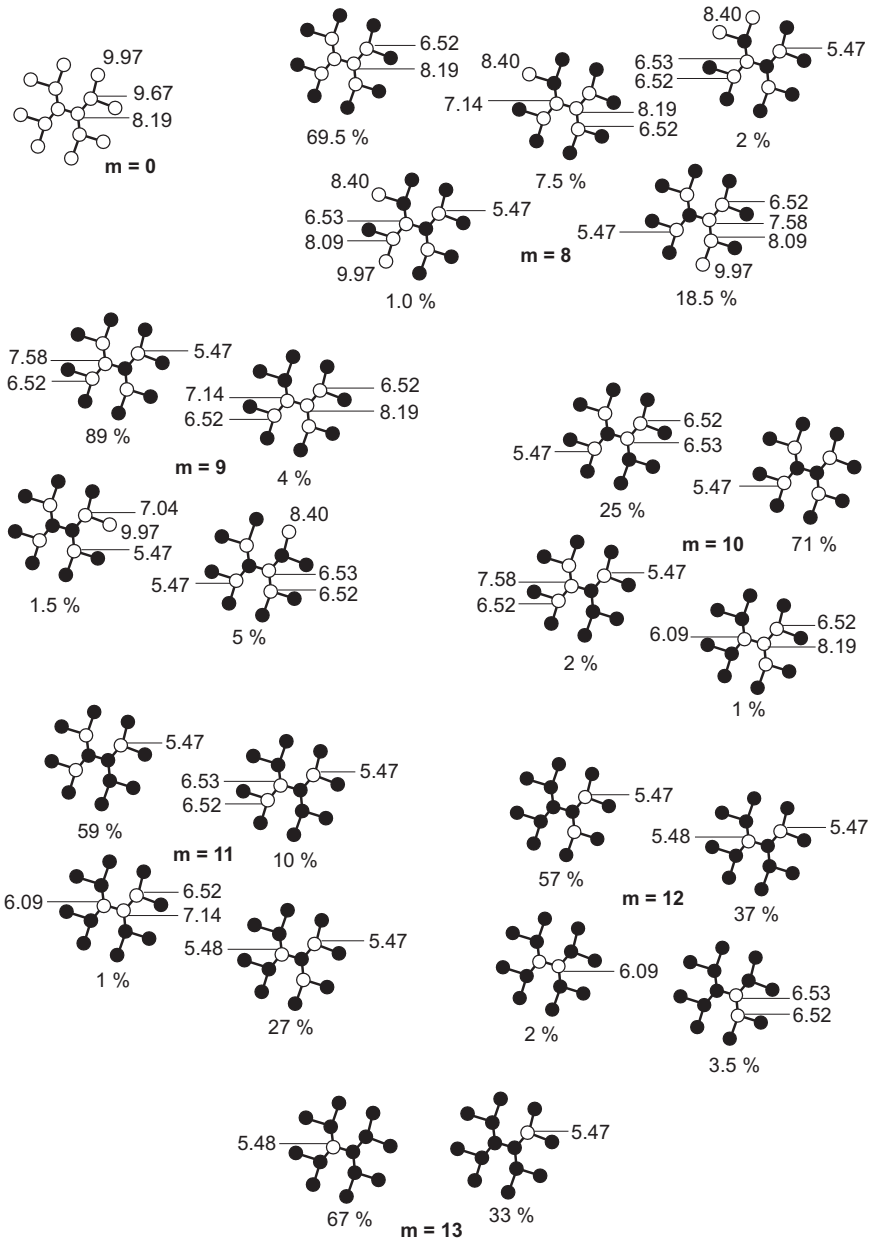

Figure 3.9: The microscopic mechanism of the first generation poly(propyleneimine) dendrimer. The most important microspecies are presented for several distinguished macrospecies, denoted with m (see figure 3.7). A probability is assigned each microspecies, and the micro pK values are assigned to the unprotonated sites.

A difference in the microscopic protonation mechanisms of the higher generations of the two types of dendrimers is evident from the proton binding isotherms for high generations. As discussed in the previous chapter, in the case of poly(amidoamine) dendrimer, the outermost primary amine groups protonate almost randomly in the first step, at $7.5 < \mathrm{pH} < 10$. One of the innermost sites protonates around $\mathrm{pH} \approx 7$, but for higher generations, this does not contribute significantly to the overall degree of protonation. In the second step, at $4 < \mathrm{pH} < 7$, the rest of the sites protonate almost randomly, with an exception of one of the core sites, which protonates last, around $\mathrm{pH} \approx 3.5$. The intermediate protonation microstate with the protonated outermost primary amine sites is prominent for the plateau value in the overall proton binding isotherm at $\theta = 1/2$.

In the case of the poly(propyleneimine) dendrimers, the plateau value at $\theta = 1/3$ is a consequence of the existence of an intermediate microspecies with alternating protonated and deprotonated shells, which is depicted in fig. 3.10. The primary amine groups protonate at $8.5 < \mathrm{pH} < 11$. As can be inferred from $\mathrm{p}K^{(\mathrm{III}')}$ and the proton binding isotherm (see fig. 3.4), the rest of the sites, leading to the shell-like intermediate structure, protonate around pH=8. This occurs in a step which is not clearly distinguished from the protonation of the primary amine sites. Thus, in the proton binding isotherm, this appears as a less steep continuation of the steep part at high pH. One of the innermost tertiary amine sites protonates next, but this contribute significantly to the overall degree of protonation for higher generation poly(propyleneimine) dendrimers. As can be inferred from the microconstants within the intermediate microstate, the second step, at $3 < \mathrm{pH} < 6$, can be divided in two sub-steps, which are not distinguishable from the proton binding isotherm. In the first of these two sub-steps, around $\mathrm{pH} \approx 5.5$, protonate the outermost tertiary amine sites, and the second core site, while the other tertiary amine sites stay unprotonated. In the case of the fourth generation, the latter unprotonated sites contribute only with around

6 % to the total number of sites. For high generations, this number is found to converge to 8.3 %. All of these unprotonated sites protonate around pH $\approx$ 4.8, which leads to the fully protonated molecule. A peculiarity of the intermediate microspecies of the poly(propyleneimine) dendrimer, is that the protonation state of the alternately protonated shells changes if the generation number is increased by one.

3.5 Poly(propyleneimine) dendrimer with ethylenediamine core - (2,3) dendrimer

The protonation of the poly(propyleneimine) dendrimer with ethylenediamine core, which will be addressed to as (2,3) dendrimer, is interesting due to the structure featured with a short ethane carbon chain in the middle of the molecule, as shown in figure 3.2. The three carbon atom chains in the branched part are the same as in the poly(propyleneimine) dendrimer. Therefore, this molecule has structural features of both poly(propyleneimine) and poly(amidoamine) dendrimers. The hyperbranched part is the same as in poly(propyleneimine), and the core as in poly(amidoamine) dendrimer. Therefore, if the site binding model, presented for the poly(amidoamine) and poly(propyleneimine) dendrimers is correct, the microscopic protonation mechanism of the (2,3) dendrimers should exert features of both poly(propyleneimine) and poly(amidoamine) dendrimers. For the low (zeroth) generation, the protonation mechanism should be more similar to the poly(amidoamine) dendrimer, and for the higher genereations, where the branched part dominates the structure, the mechanism should be similar to the poly(propyleneimine) dendrimer.

The cluster parameters, used to infer the protonation mechanism for the (2,3) dendrimer from the site binding model, were used as reported in [44]. They are listed in table 3.5 and presented in fig. 3.14 (the scheme refers to the fully

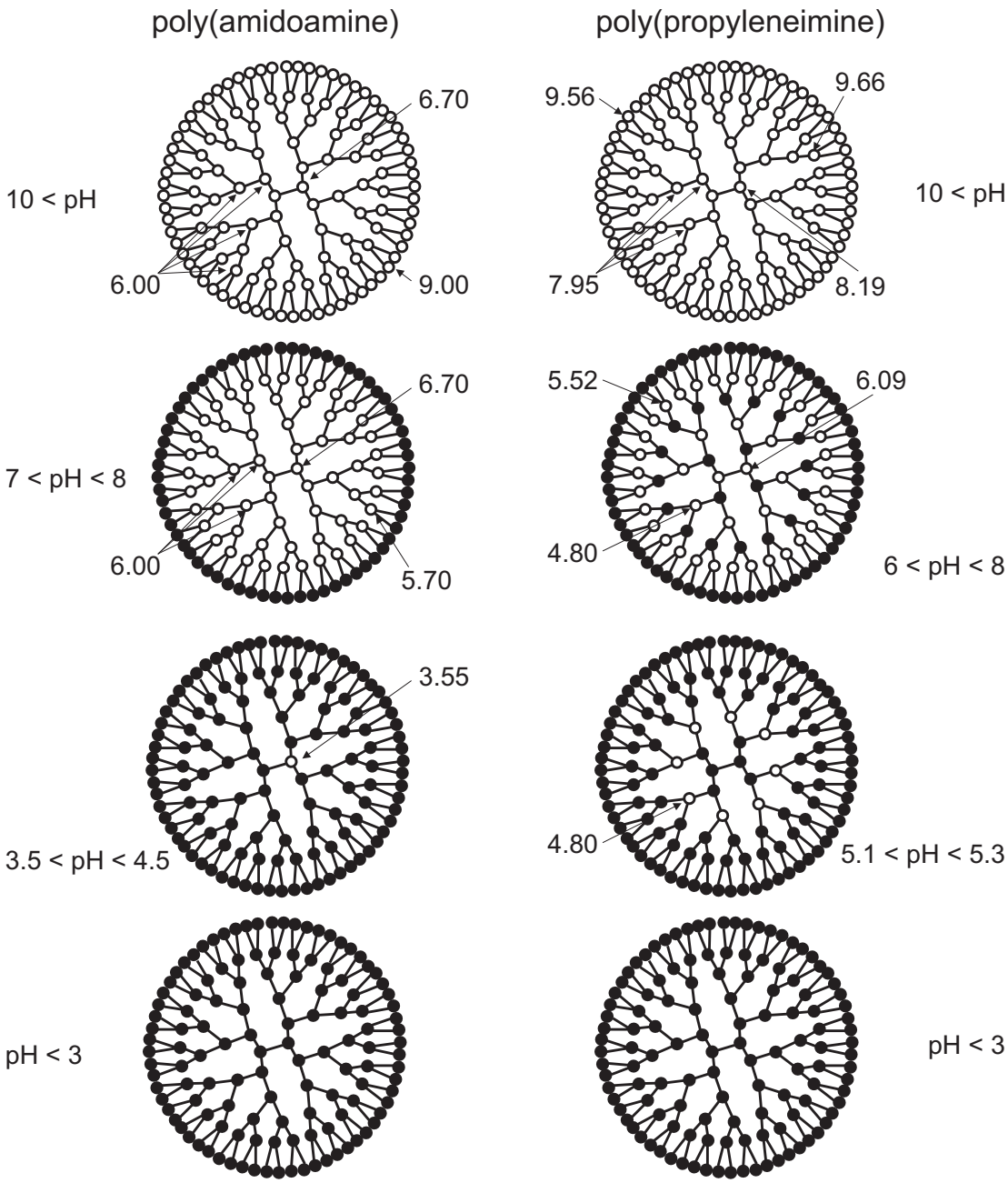

Figure 3.10: The most important microspecies of the fourth generation poly(amidoamine) (left) and the poly(propylene) (right) dendrimers, indicating the protonation mechanism. The pH ranges in which these microspecies occur, and the microconstants for particular protonation sites are indicated.

Table 3.2: Cluster parameters of the site binding model for the (2,3) dendrimer.

$pK^{(III)}$	$pK^{(I)}$	ϵ	ϵ'
7.50	9.40	2.20	1.00

unprotonated molecule). It was assumed that one $p\hat{K}_i$ value is satisfactory for all the tertiary amine sites. As well, the pair interaction parameters were assumed to depend purely on the spacer length between the sites. In this manner, the parameters, which were estimated for the zeroth generation in [44], were used for all the higher generations.

The proton binding isotherms of the first five generations of the (2,3) dendrimer are presented in fig. 3.11. Some of the features, which were established for poly(amidoamine) and poly(propyleneimine) dendrimers, can be noticed here as well. The proton binding isotherm of the zeroth generation is distinguished from the other curves, which are becoming more similar to a common curve, as the generation number is growing. The proton binding isotherm of the zeroth generation shows three distinguished titration steps, while for the higher generations, two well distinguished steps are noticeable.

In fig. 3.12, the macroscopic speciation diagrams, and the according most probable microspecies, are presented for the zeroth and the first generation (2,3) dendrimer. In the case of the zeroth generation, two intermediate macrostates are determinant for the overall proton binding isotherm, and the microscopic protonation mechanism is very similar to that of the poly(amidoamine) dendrimer (see fig 3.5).

The macroscopeciation diagram for the first generation (2,3) (fig. 3.12), shows pronounced species at $m = 8$, $m = 9$ and $m = 13$. As a reminder, this is similar to the macroscopic speciation of the poly(amidoamine) dendrimer. However, the macrospecies at $m = 8$ is less dominant than the species at $m = 9$, which is

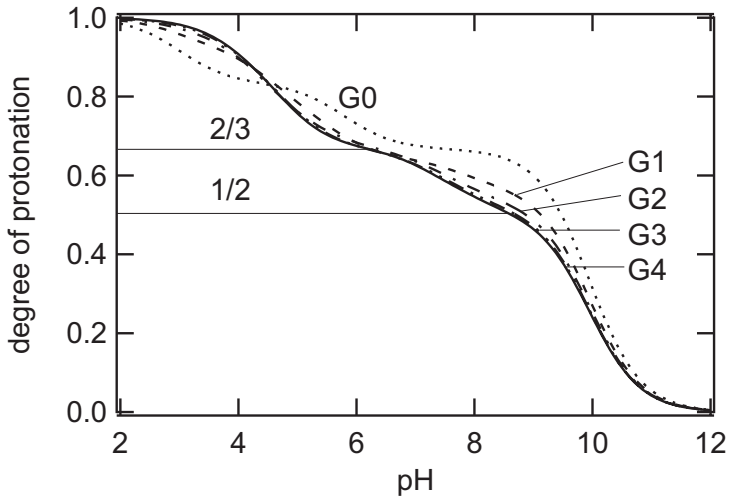

Figure 3.11: The proton binding isotherms of the first five generations of (2,3) dendrimers, calculated from the cluster parameters for the zeroth generation [44]. In the proton binding mastercurve, a plateau at $\theta = 2/3$ is pronounced, another one can as well be noticed at $\theta = 1/2$.

similar as in the case of the poly(propyleneimine) dendrimer. But, contrary to the poly(propyleneimine) dendrimer macrospeciation, the species at $m = 10$ is not pronounced. The above considerations already point out, that the mechanism for the (2,3) dendrimer may show combined characteristics of both poly(amidoamine) and poly(propyleneimine) dendrimes.

Figure 3.13 is showing the detailed microspeciation for the (2,3) dendrimer. As a consequence of a distinction between the $\mathrm{p}\hat{K}_i$ values for the primary and tertiary amine sites ($\mathrm{p}K^{(\mathrm{I})} - \mathrm{p}K^{(\mathrm{III}')} = 1.90$), and significant pair interactions, the number of the significant microspecies is lower, than in the case of poly(amidoamine) and poly(propyleneimine) dendrimers. For example, for $m = 9$, there are only two significant microspecies, while in the case of poly(amidoamine) and poly(propyleneimine) dendrimers, there are four of them. Similarly, for $m = 8$, there are only three significant microspecies, while there are four and five, for poly(amidoamine) and poly(propyleneimine), respectively.

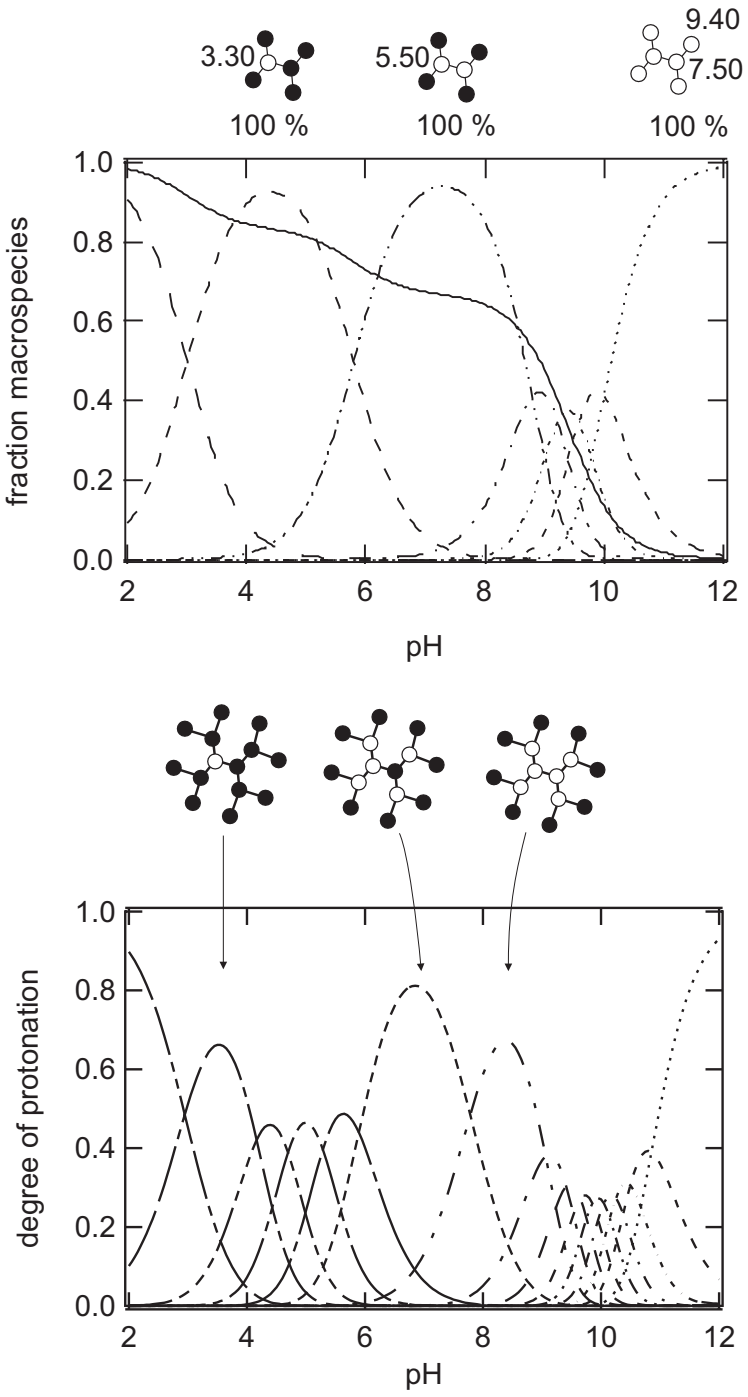

Figure 3.12: The macroscopic speciation diagrams, with the according most probable microspecies, for the zeroth (top) and first (bottom) generation of (2,3) dendrimer.

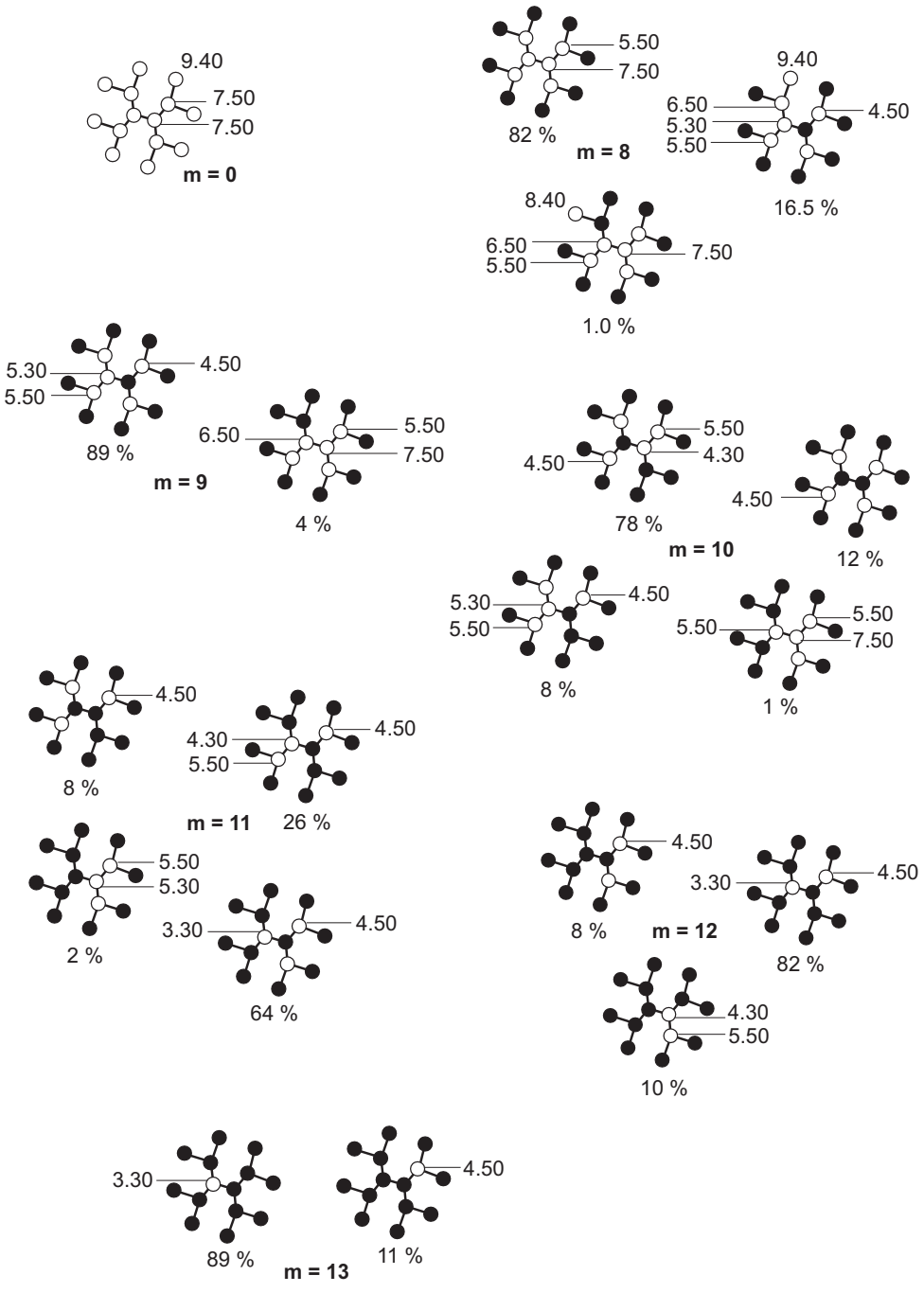

Figure 3.13: The microscopic mechanism of the first generation (2,3) dendrimer. The most important microspecies are presented for several distinguished macrospecies, denoted with m (see figure 3.7). A probability is assigned each microspecies, and the micro pK values are assigned to the unprotonated sites.

The most convincing evidence that the protonation mechanism of the (2,3) dendrimer would exert intermediate microspecies, characteristic for both poly(amidoamine) and poly(propyleneimine) dendrimer, is demonstrated in figure 3.14. The prominent microspecies at pH ≈ 8.5 has the outermost primary amine sites protonated, as in the case of poly(amidoamine) dendrimer. At $5 < \mathrm{pH} < 7$, the prominent microspecies is featured with alternated protonated and deprotonated shells, as in the case of the poly(propyleneimine) dendrimer. Therefore, the proton binding isotherm of the fourth generation of the (2,3) dendrimer (presented in fig. 3.11) is featured with a clear plateau at $\theta = 2/3$, as in the case of poly(propyleneimine) dendrimer. However, a less pronounced plateau at $\theta = 1/2$ can be noticed, which is characteristic for the poly(amidoamine) dendrimers. For the generations higher than the first, the proton binding isotherm is mostly affected by the protonation of the hyperbranched part of the molecule, which is similar (same) as in the poly(propyleneimine) dendrimer. This is the reason why the protonation mastercurve resembles the poly(propyleneimine) mastercurve, with a pronounced plateau at $\theta = 2/3$.

3.6 Conclusion

The presented site binding model is very useful for prediction of the protonation mechanisms. Precise microscopic protonation mechanisms, which include the probabilities of all the microstates, can be obtained for polyprotic molecules with a very large number of sites. For this, a symmetric arrangement of the sites is necessary, as is the case for dendrimers. However, for molecules with less than thirty sites, the symmetric arrangement is not essential.

The microscopic protonation mechanism can be fully inferred from the cluster parameters, which include microscopic pK values for the unprotonated molecule, and the nearest neighbor pair interaction parameters. The $\mathrm{p}\hat{K}_i$ values are inherent to a particular site, and the pair interaction parameters depend on the distance

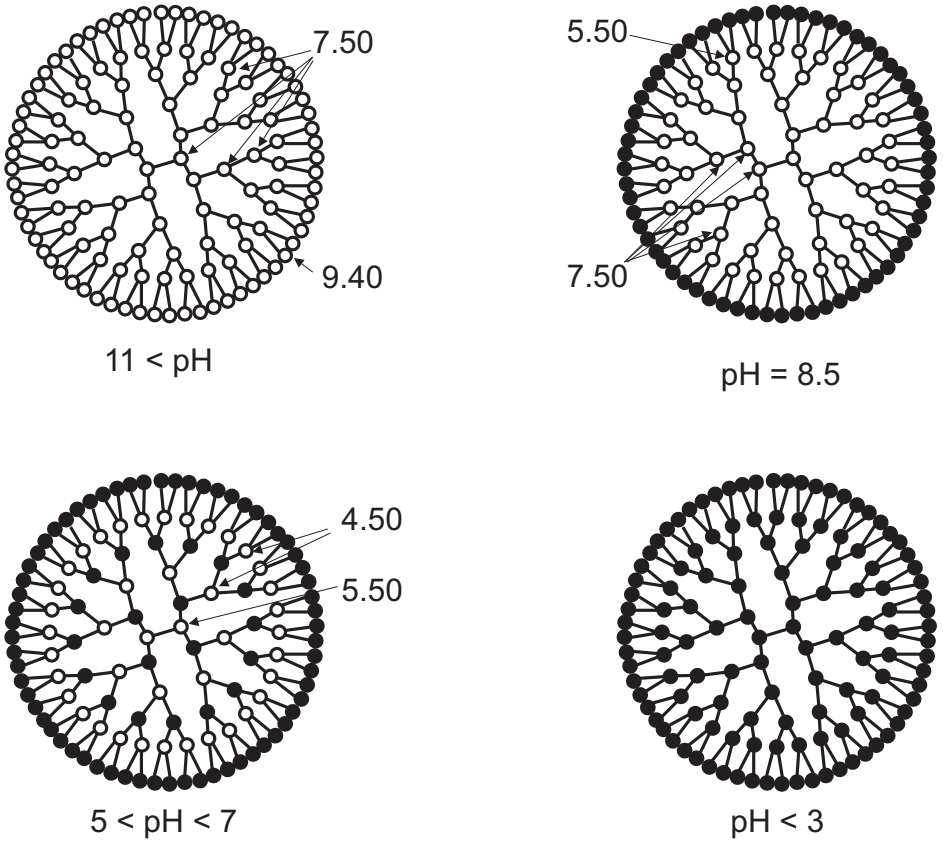

Figure 3.14: The most prominent microspecies of the (2,3) dendrimer, at pH-values which correspond to a plateau in the overall titration curve. The micro-constants of particular protonation sites are indicated.

between the protonated sites. Due to the symmetry of the molecule, only a limited number of cluster parameters is necessary for an assessment of the protonation mechanism for even very large molecules.

The poly(amidoamine) and poly(propyleneimine) dendrimers exert different microscopic protonation mechanisms, due to a difference in the structure of the two molecules. In the case of poly(amidoamine) dendrimers, the core carbon-chain is short, while the "arms" of the hyperbranched part are long, and vice versa for the poly(propyleneimine) dendrimer. For poly(amidoamine) dendrimers, this causes the mechanism to be mainly sensitive to the $p\hat{K}_i$ parameters; the pair interaction parameter is playing a role only for the protonation of the last core site, at low pH. In the case of poly(propyleneimine) dendrimer, both the $p\hat{K}_i$, and the pair interaction parameters play an important role.

The difference in the microscopic protnation mechanisms of the poly(amidoamine) and poly(propyleneimine) dendrimers affects the overall proton binding isotherm. In the case of poly(amidoamine) dendrimer, the intermediate microspecies is present at $7 < \text{pH} < 8$, where the outer rim sites are protonated, and the tertiary amine sites deprotonated. This is reflected in a plateau in the proton binding isotherm at $\theta = 1/2$. The protonation mechanism of the poly(propyleneimine) dendrimers is featured with an intermediate microspecies around $\text{pH} \approx 7$, where the primary amine sites, and the sites in each second shell, counting from the outermost, are protonated. Consequently, a plateau in the proton binding isotherm is present at $\theta = 2/3$.

The imaginary dendrimer, which is also discussed, is built from a short inner core unit with two carbon atoms (as in poly(amidoamine) dendrimer), and the hyperbranched part with "arms" of three carbon atom chains (as in poly(propyleneimine) dendrimer). The microscopic protonation mechanism shows features characteristic for both poly(amidoamine) and poly(propyleneimine) dendrimers. At $5 < \text{pH} < 7$, a microspecies with alternated protonated and deprotonated shells is present, which is the same as the one

observed in the poly(propyleneimine) dendrimer mechanism. A less pronounced microspecies, present at pH $\approx$ 8.5, with protonated primary amine sites, is the same as the one observed in the mechanism of the poly(amidoamine) dendrimer. The latter microspecies is becoming more important for low generations, due to the fact, that for higher generations, the structure of this dendrimer is dominated by the hyperbranched part.

Chapter 4

Charging of carboxylated latex particles in the presence of pDADMAC

4.1 Introduction

Adsorption of polyelectrolytes at solid surfaces is widely used to control the colloidal stability and the hydrodynamic properties in colloidal suspensions, which is of great interest in, for example, food and paper industry, or purification of waste water. The colloidal stability is greatly affected by the charge carried by particles in suspensions [55]. Furthermore, the surface charge, as well as the polyelectrolyte charge, and the concentrations of ionic species within the adsorption layer are playing an important role for the conformation and structure of the adsorbed or grafted polyelectrolyte layers. While the scaling theory, set forward by de Gennes [56], led to a breakthrough in understanding the conformations of the adsorbed polyelectrolyte layers [57, 58]. However, the ionic distributions in the adsorbed layers still require explicit computations by means of Monte-Carlo simulations [59].

An insight into the charging processes at interfaces can be gained through the shear (or ζ-) plane potential, which can be experimentally determined from the electrophoretic mobility or streaming potential measurements. By applying the theory of Derjaguin, Landau, Vervey and Overbeck (DLVO) [60], an insight about the shear plane potential may be gained from the measurements of the aggregation rates, in the initial stages of the particle aggregation, where dimers are formed from monomers [61]. In these studies, the aggregation rates are usually compared with the electrophoretic mobilities, and the fast aggregation regime typically coincides with the isoelectric point [62, 63]. As well, an evidence of the charge distributions at solid surfaces with adsorbed polyelectrolytes can be gained indirectly, by measuring the thickness and conformation of the adsorbed polyelectrolyte layers [64, 65].

Potentiometric titrations provide a direct measurement of the surface charge. In this case, the excess charge present in the solution, compensated by the protons or OH^- ions, is attributed to the surface, which is acting as a conjugated acid or base [8]. Several potentiometric titration studies of the systems consisting of strong [66–68], and weak [69] polyelectrolytes, adsorbed on oppositely charged surfaces, are available. In these studies, the measured amounts of adsorbed polyelectrolytes, and the net surface charge have been interpreted in terms of the self-consistent mean field model [57]. The same approach was found appropriate in interpretation of the layer thickness [70], the effects of the polyelectrolyte polydispersity [64], and some other effects, like the influence of the surface curvature on the adsorption [71]. In the self-consistent mean field approach, the interactions between the ionic species, polylectrolyte segments, the solvent, and the surface sites are treated explicitly. The relation between the surface charge and the potential within the adsorbed layer can be solved by applying a site binding model, which is acting as a boundary condition for solving the Poisson-Boltzmann equation [66]. The minimum free energy, and the corresponding spatial distributions of the ions and the polyelectrolyte segments, are found by means of

Monte Carlo algorithms. The self-consistent mean field model invokes a number of Flory-Huggins coefficients, which describe the interactions between different constituents of the system (poleyelectrolyte segments, surface groups, inert electrolyte ions, solvent molecules) [72].

In this chapter, the primary aim is to present the potentiometric titration data of the strong cationic polyelectrolyte poly(dimethyl-diallylammonium chloride) (pDADMAC), adsorbed onto carboxyl latex particles (see figure 4.1). The fraction of the total added pDADMAC charge, which influences the surface potential (at the point of zero charge) will be evaluated from the proton binding isotherms, and compared to the adsorbed amount of pDADMAC sites.

The experimental proton binding isotherms will be interpreted with the Stern model [6], which is extended for a specific adsorption of oppositely charged ions [8, 73]. The model is treating the dissociation of the surface sites through a discrete site-binding model, similar to those which were developed for the metal-oxides [74–77], with a difference that it accounts only for negative carboxylate sites. In the case of adsorbed polyelectrolytes, the model is able to reproduce the point of zero charge, by considering the presence of positively charged ions at the surface, which do not undergo dissociation. The ratio of the positive polyelectrolyte sites to the negative carboxylate sites depends on the adsorbed amount. So far, interpretation of the proton binding isotherms of the charged surfaces with adsorbed oppositely charged polyelectrolytes has not been reported in terms of the Stern model, which presents a mean-field approach. Our aim is to explore the advantages and limitations of such an approach, when applied to adsorbed polyelectrolytes. The basic Stern model was first developed for the interpretation of the ionic distributions and the corresponding electrostatic potentials near homogeneous charged surface (namely that of a mercury drop in water). Some decades ago it became widely used for inorganic surfaces with discrete charging sites, like metal oxides [75], and surfaces with organic acidic or basic surface moieties [74]. The applicability of the Stern model is increased through extensions, such as to

include the specific adsorption of ions [73, 78], or different proton binding sites [79].

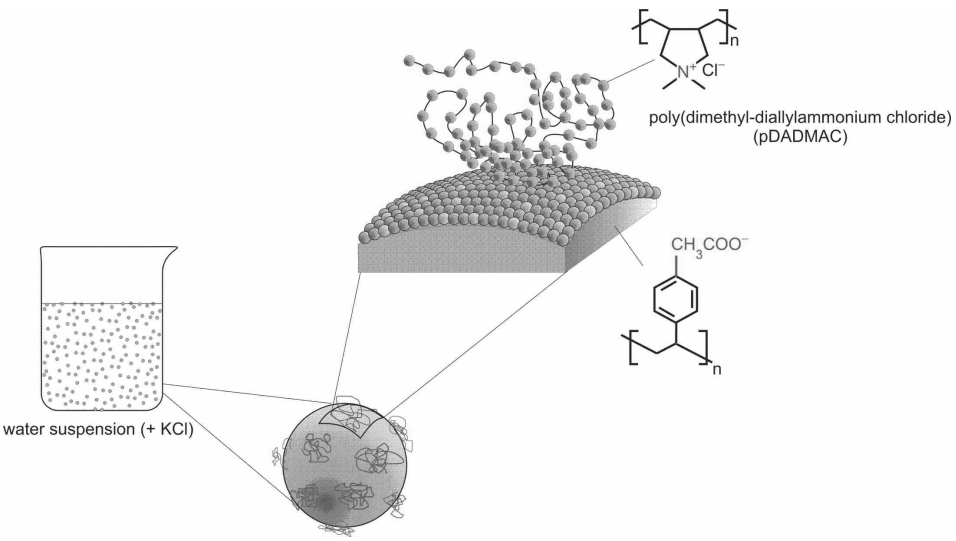

Figure 4.1: The system under investigation is composed of poly(dimethyldiallylammonium chloride) which is adsorbed on the surface of the carboxylate latex particles. The particles are suspended in water, which contains KCl.

4.2 Extension of the Basic Stern model

The pDADMAC sites can be considered to be situated in the 0-plane, or displaced towards the solution. In the first case, the system can be described by means of the basic Stern model. If the fixed positive charge is considered as displaced from the surface origin, the first step towards modeling could be to place this charge at the origin of the diffuse layer, as depicted in fig. 4.2. The latter approach will be referred to as the modified Stern model, where the negative electrostatic potential in the 0-plane has a higher magnitude, due to a smaller influence of the positive pDADMAC sites. This modification is equivalent to the model which includes the specific adsorption of the counterions, with an infinite binding constant [73] for the cations.

The basic Stern model is a classical approach for solving the charging equilibria at homogeneous surfaces [6, 8, 74], where the interface is divided into two compartments, namely the surface and the diffuse layer. As a consequence of the electroneutrality condition, the charge in the diffuse layer, σ_{d} has to neutralize the surface charge, σ_0:

$$\sigma_{\mathrm{d}} = -\sigma_0 \tag{4.1}$$

The Gouy-Chapman equation can be invoked to calculate the potential in the diffuse layer:

$$\psi_{\mathrm{d}} = (2kT/e)\mathrm{arcsinh}[e\sigma_{\mathrm{d}}/(2kT\epsilon_0\epsilon_{\mathrm{r}}\kappa)] \tag{4.2}$$

where e is the elementary charge, σ_{d} is the charge per surface area at the origin of the diffuse layer, $\epsilon_0\epsilon_{\mathrm{r}}$ is the permittivity of the medium, kT the thermal energy, and κ the inverse Debye-length:

$$\kappa = (\frac{2e^2I}{\epsilon_0\epsilon_{\mathrm{r}}kT})^{1/2} \tag{4.3}$$

where, I is the ionic strength in units of number of ions per m^3. On the other

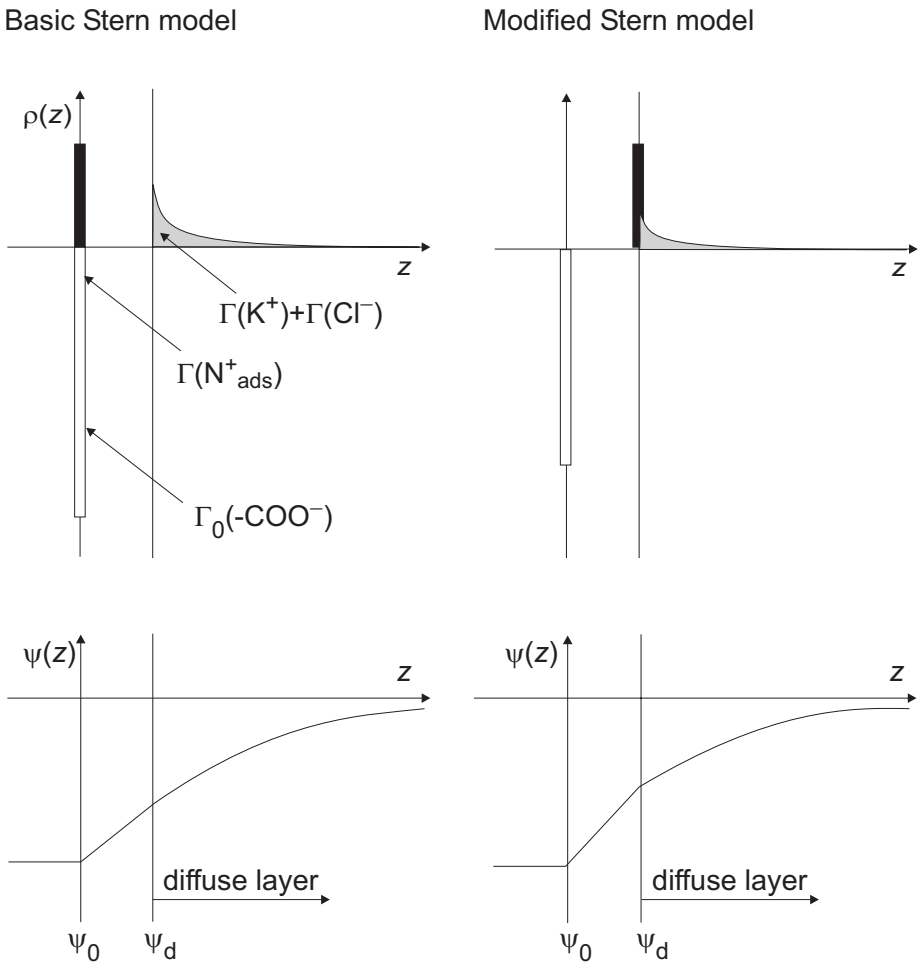

Figure 4.2: Basic Stern model (left), and the extension of that model for the specifically adsorbed ions (right). Presented are the charge density distributions (top), and the corresponding electrostatic potentials (bottom), with respect to the axis normal to the surface.

hand, the surface charge is governed by the surface protonation equilibria:

$$-\mathrm{COOH} \rightleftharpoons \mathrm{H^+} + -\mathrm{COO^-}\ ; \tag{4.4}$$

The corresponding deprotonation constant is

$$K_\mathrm{d} = \frac{a_{\mathrm{H^+}} \cdot \Gamma(-\mathrm{COO^-})}{\Gamma(-\mathrm{COOH})} \exp(q\psi_0/kT), \tag{4.5}$$

where ψ_0 is the potential at the surface (in the plane of the surface-bound protons). Adsorbed pDADMAC sites are considered as completely dissociated, so that pDADMAC sites are carrying a pH-independent positive charge. In the Stern model, a potential drop between the 0-plane, and the d-plane is allowed, such that:

$$C_\mathrm{S} = \frac{\sigma_0}{\psi_0 - \psi_\mathrm{d}} \tag{4.6}$$

where C_S is the Stern layer capacitance, which can be related to the distance between the surface and the diffuse layer plane:

$$d = \frac{C_\mathrm{S}}{\epsilon_0 \epsilon_\mathrm{r}} \tag{4.7}$$

The surface potential and the surface charge can be found numerically, by solving equations 4.1-4.6

4.3 Experimental

Poly(dimethyl-diallylammonium chloride) (pDADMAC), of molecular weight $100 - 200\,\mathrm{kDa}$, was purchased from Aldrich (Cat. No. 26062-79-3). The carbon and nitrogen content, and the mass percentage of the purchased solution have been verified by the total carbon and nitrogen analysis, and were found to agree with the formula. The solution was used without any further purification, and was diluted to give the necessary concentration.

The sample of carboxyl-sulfate latex particles was kindly supplied by the BASF company. The diameter of the particles and the polydispersity, measured with atomic force microscopy (AFM) are 190 nm and 25.3 %, respectively. Static and dynamic light scattering measurements of the particle diameter resulted in a value of 250 nm. The difference between the values measured with AFM and light scattering, is due to the fact that the diameter measured by light scattering is intensity-weighted [80]. The surface area of the pure particles, calculated from the AFM measurement, and taking the polydispersity into account, is $27.3\,m^2\,g^{-1}$. Prior to the experiments, the particles were dialyzed against the Milli-Q water, which was daily exchanged, until the conductivity of the outer batch water was below $\sim 1.1\,\mu Scm^{-1}$. For this, dialysis membranes (Spectra-pore, pore size of 500 kDa) have been used. The water, from which the CO_2 was removed by boiling, was used for the preparation of all the solutions. The burette solutions for the potentiometric titrations, were prepared from CO_2-free KOH (Baker, Dilut-it), HCl (Merck Titrisol) and KCl (Merck, p.a.). For the pH measurements during the sample preparations, a combined glass electrode (purchased from Metrohm AG) and a standard pH-meter (Metrohm 691) were used.

The potentiometric titration experiments were performed with pDADMAC-latex mixtures, at five different pDADMAC loadings (see table 4.3). The final concentration of the latex was 10 g/L in all experiments. About 20 g of a 47 g/L latex stock solution was first mixed with pDADMAC stock solution, and the mixture was adjusted to pH = 10. The total amount of titrated latex particles is determinant for the accuracy of the charge determination from the potentiometric titration (see chapter 1). The total titratable charge calculated from the latex loading is 0.16 mmol, which means that the error of the charge determination is lower than 2 %. The mixture was then shaken head-over-head for cca 2 minutes, and the pH was adjusted again. Samples prepared in this way were then subjected to potentiometric titration experiments.

Potentiometric titrations were performed with the Wallingford Titrator[16]

Table 4.1: Sample preparation for the titration experiments. Additions of the pDADMAC stock solution (750 mg / L) to 20 g of 47 g/L latex suspension.

pDADMAC loading (mgm^{-2})	0.15	0.40	0.65	0.85	1.00
additions pDADMAC stock solution (g)	5.0	13.9	21.5	29.0	34.4

(for a description of the automated titrators, see appendix). The experimental set-up consists of four burettes (Metrohm Dosimat 765, cylinder volume 5 mL), containing KOH and HCl at 0.25 M, KCl at 3 M, and water. The electromotive force is measured with a high impedance voltmeter (Microlink PH4-S), which is embedded in a computer interface (Microlink 3000) for the communication with external units (burettes, stirrer). For that task, separate glass and Ag/AgCl reference electrodes (both purchased from Metrohm AG) were used. The home-made plexiglass reaction vessel (minimum and maximum volume of the titrated system is 45 mL, and 450 mL, respectively) was thermostatized at 25 °C by an external thermostat (Haake DC 10), and the solution was constantly degassed with nitrogen, previously washed with concentrated KOH, water, and 0.1 M KCl solution.

The potentiometric titration experiments are fully controlled by the computer. First blank titrations were performed, where the electrode readings were recorded after a drift criterion of 0.1 mV/min was satisfied, which is usually achieved in less than 3 minutes (except in the region around pH = 7, where up to 5 minutes were needed). Then,the samples of the composite pDADMAC-carboxylate latex suspensions were transferred to the titration cell. The experiment begins with an addition of HCl, KCl, and water, in order to reach the initial conditions (pH = 3, the ionic strength of 10 mM, and total volume of 100 mL). At the beginning, the pH is corrected in a rapid step-wise manner, through acid and base additions, followed by the adjustment of the ionic strength to the pre-defined initial value.

After that, the initial conditions are achieved (pH = 3, and I = 10 mM). Then, titration to pH = 11 is performed with a pH step of 0.4 units, which is kept constant (see see fig. A.5 in the appendix). This is followed by a backward titration to pH = 3 with constant dosages of 0.2 mL of HCl. In the dynamic titration mode, the consecutive additions of acid or base are being calculated according to the pre-defined step in pH.

The titrations of the mixture were performed in a "rapid" manner, in order to avoid the slow processes that were observed through long equilibration times and high drifts (up to 1 mV/min after three minutes) of the electrode signal. These processes could possibly be desorption, or conformational changes of the adsorbed pDADMAC. "Rapid" means that the maximum waiting time between the readings was 3 minutes, in the case that the drift criterion of 0.1 mV/min was not achieved sooner. Still, for high pDADMAC loadings and in a narrow pH region, the drifts after 3 minutes were observed to be in the order of 5 mV/min. The pH region of such high drifts seems to be reproducible for a certain loading. Each addition of acid or base is followed by the ionic strength adjustment through an addition of KCl buret solution or water. After such a forth and back titration cycle, the ionic strength is increased. The above procedure has been repeated until all titrations have been performed at all the pre-defined ionic strengths.

For the electrophoretic mobility measurements, the sample preparation (adsorption of pDADMAC) for the electrophoretic mobility measurements was done in a similar way as for the potentiometric titrations. The total amount of pDADMAC per surface area was the same as for the titration samples, as given in table 4.3. The final latex concentration in the samples was 5 mg / L. In order to achieve approximately the same additions of the pDADMAC and the latex, the stock solutions were diluted to 20 mg / L and 0.32 mg / L, for latex and pDADMAC, respectively. The final pH was varied in a range of several pH units, such as to include an anticipated isoelectric point (assumption was that the isoelectric point will coincide with the point of zero charge). The pH

was measured with a standard Metrohm 691 pH-meter, equipped with a combined pH electrode (Metrohm 6.0234.110). The values were acquired after there was no pH-drift registered by the instrument, but for a maximum time of five minutes. In this manner, the pH measurement conditions in the electrophoretic mobility measurements, resemble as much as possible to these conditions in the titrations. Electrophoretic mobilities were measured with a doppler-velocimeter setup (Malvern Zetasizer 2000). The cell potential was set to 75 V for the measurements at $I = 0.1\,\mathrm{M}$, and to 100 V for the measurements at $I = 0.01\,\mathrm{M}$, in order to optimize the current. The modulator frequency was set to 1 kHz. Each data point was measured six times. For each measurement, the count rates of the scattered photons were accumulated for 30 seconds.

The sample preparation for the batch experiments were performed in the following manner. The latex suspension (stock solution at $0.160\,\mathrm{mg\,/\,L}$) was dialyzed against the Milli-Q water, which was daily exchanged until a constant conductivity of cca $1\,\mu\mathrm{Scm}^{-1}$ in the surrounding water. The pDADMAC was used as purchased, and several stock solutions were prepared, in order to cover a wide range of the final sample concentrations. 14.17 g of latex suspension was mixed with a comparable volume of the pDADMAC stock solution. Then the pH and the ionic strength were adjusted by using 0.1 M HCl and KOH solutions, and a 1 M KCl solution. Thus, the resulting mixture has a particle concentration of $800\,\mathrm{mg\,/\,L}$. After mixing, the samples were gently stirred for 24 hours. Then, the majority of the particles was sedimented by centrifugation for 4 hours at 24000 rpm (103864 G), at $25\,^{\circ}\mathrm{C}$ (Ultra-centrifuge Beckman Coulter Avanti J30-I). The rest of the particles were separated from the supernatant by filtration (Millex, hydrophilic PVDF filters, pore size $0.1\,\mu\mathrm{m}$). The supernatant was analyzed by the total carbon and nitrogen analysis. For this, the calibration was done by using potassuim-hydrogenphtalate and KNO_3 as standards.

4.4 Data treatment

This section contains an important explanation of two corrections that are being performed on the raw proton binding isotherms of the composite system pDADMAC-carboxylate latex. The first correction has to be carried out in order to subtract the charge of the free ions, added during the sample preparation. These include K^+ ions which were added to the sample as KOH in order to adjust the pH to the adsorption value, and Cl^- ions which were added with pDADMAC. The net excess charge which stems from these strong electrolyte ions causes a shift in the proton binding isotherms parallel with the y-axis. Therefore, the difference between these two concentrations was subtracted from the raw proton binding isotherms. The corrected proton binding isotherms are presented in the figure 4.3 (left).

In the second correction, the charge of the quaternary amine sites, which does not influence the surface potential in the point of zero charge, is subtracted from the proton binding isotherms. These sites will be referred to as not adsorbed and their charge denoted $[N^+_{diss}]$. It has to be mentioned that $[N^+_{diss}]$ includes the charge of adsorbed pDADMAC sites which are displaced from the surface, wherefore their charge is compensated by the the bulk solution ions. Their influence on the surface potential is mitigated, and they can not be distinguished from the dissolved sites in the proton binding isotherms. Thus, the total charge of the added pDADMAC is split into two terms, namely adsorbed ($[N^+_{ads}]$) and dissolved ($[N^+_{diss}]$), so that the electroneutrality condition reads as:

$$[K^+] + [H^+] + [N^+_{ads}] + [N^+_{diss}] = [Cl^-] + [OH^-] + [\sim COO^-] \tag{4.8}$$

The point of zero charge, where the surface potential equals zero, corresponds to the common intersection point of the proton binding isotherms at different ionic strength [78], [6]. This enables estimation of the dissolved pDADMAC charge $[N^+_{diss}]$, from the proton binding isotherms.

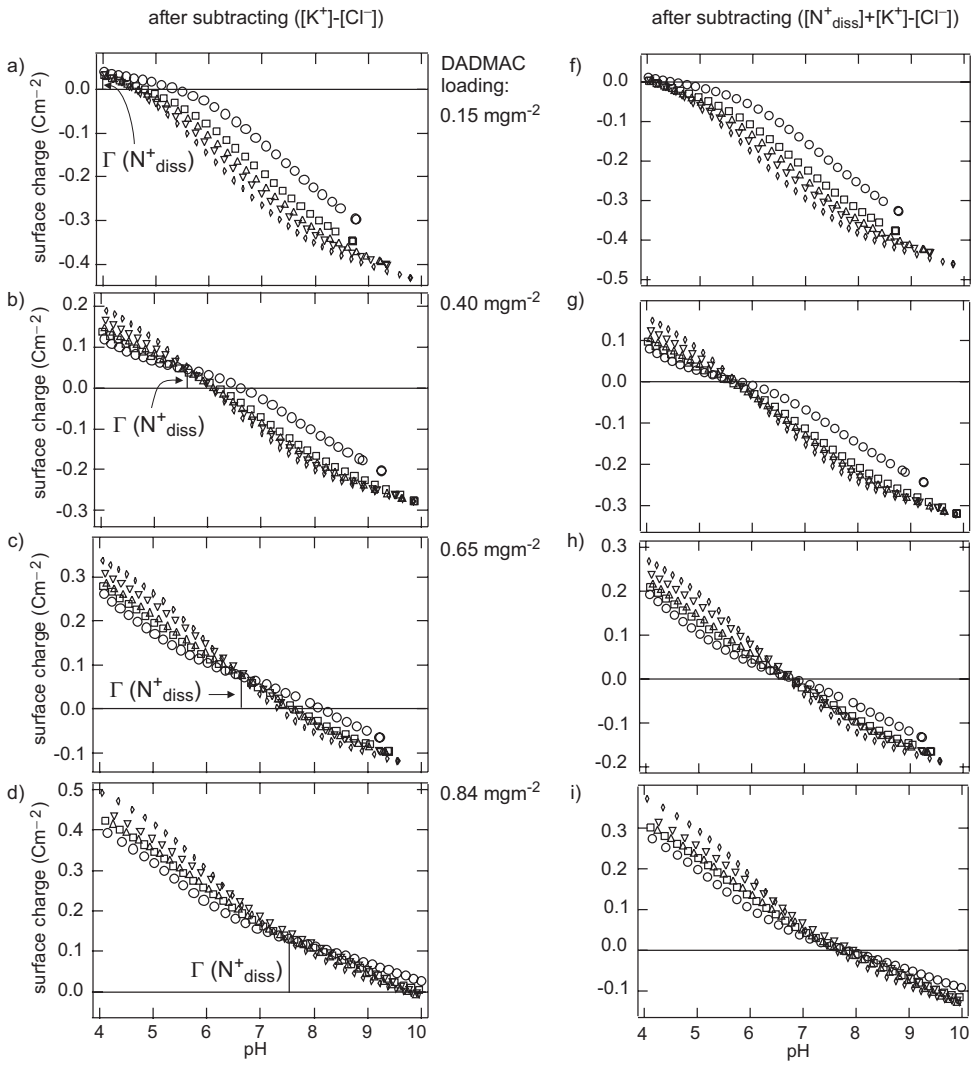

Figure 4.3: Experimental proton binding isotherms of the pDADMAC-carboxylate latex mixture at four different loadings of pDADMAC. Left: proton binding isotherms corrected for the Cl^- from pDADMAC, and K^+ from the sample preparation. Right: after subtracting the excess charge present at the common intersection point, $\Gamma(N^+_{diss})$. Ionic strengths: $\circ$ 0.01 M, $\square$ 0.05 M, $\triangle$ 0.10 M, $\triangledown$ 0.50 M, $\Diamond$ 1.00 M.

The outcome of the second correction is shown in the figure 4.3 (right). After the correction, at the common intersection point (point of zero charge), the surface charge equals zero. Assuming that $[N^+_{diss}]$ corresponds to the charge of dissolved pDADMAC, it makes sense subtracting this quantity from the total added pDADMAC charge, and comparing with the adsorption isotherm, which is shown in fig. 4.6.

Both of the above corrections were performed only in the case of the composite pDADMAC-carboxylate latex system data. The proton binding isotherms of the pure latex are presented as obtained by the standard data treatment, as explained in chapter 1. In the case of pure pDADMAC titrations, the charge of the Cl^- ions, added with pDADMAC, was subtracted.

4.5 Results

The proton binding isotherms of pure carboxylate latex suspension are presented in figure 4.4. The total amount of the titrated sites in this experiment is 0.1 mmol. For this total amount of titratable sites, the accuracy of the calculated surface charge equals $\pm 2\,\%$, within the experimental window $4 < \mathrm{pH} < 10$. Open symbols represent experiments in which the initial pH in the titration was set to 3.0, and the final pH to 11.0 (forward titration runs). The closed symbols represent the opposite direction titration run. The data are showing a monotonic dependence of the surface charge upon pH, which is typical for weakly acidic particles [6, 61]. The maximum charge, which is achieved above $\mathrm{pH} = 10$, equals $600 \pm 20\,\mathrm{mCm^{-2}}$, which corresponds to 3.74 elementary charge units per nm^2. At low pH, typically below $\mathrm{pH} = 4$, the surface charge approaches zero.

The lines in figure 4.4 represent the best fit of the basic Stern model to the experimental data. The model parameters are presented in table 4.5. Better fitting could not be achieved by a lower value for the Stern capacitance. The basic Stern model in which the Stern capacitance equals infinity is equivalent to

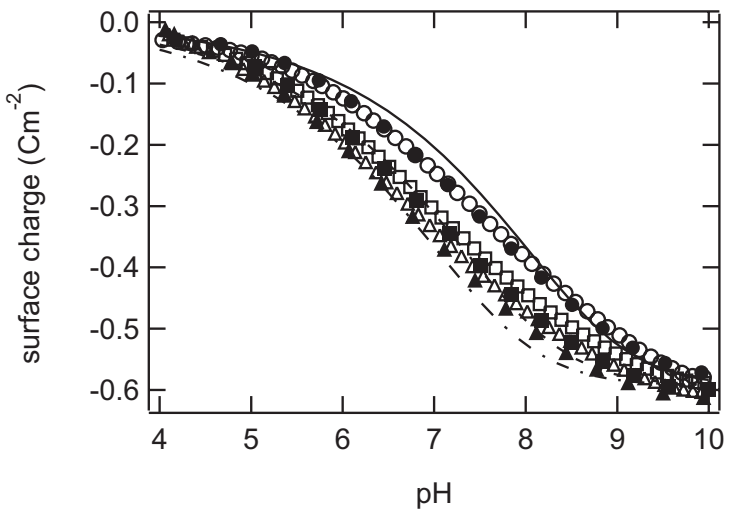

Figure 4.4: The proton binding isotherm of carboxylated latex suspension at three ionic strengths: ○ ● 0.01 M, □ ■ 0.05 M, △ ▲ 0.10 M. The maximum surface charge equals 600 mC m^{-2}. Open and closed symbols represent the forward, and the backward titration runs, respectively. The lines represent the Basic Stern model predictions, the parameters are presented in table 4.5.

the simple double layer model which does not include a capacitor [74, 78].

The proton binding isotherms of the pure pDADMAC solution are shown in figure 4.5. In this case, 0.0161 g of the pure pDADMAC was titrated, which corresponds to 0.1 mol of nitrogen (quaternary amine sites). The amount of pDADMAC monomer units corresponds to cca 600 mC g^{-1} by considering every monomer unit as one elementary charge (100 % quaternization). The curves are showing a constant charge in the whole experimental pH range.

The results of the adsorption measurements, in the range of the loadings which were used for the titration experiments, are presented in figure 4.6. It can be noted that at pH = 10, all the added pDADMAC is adsorbed. The adsorption data calculated from the proton binding isotherms are in a reasonably good agrement with the results obtained from the batch experiemnts. Thus, it is likely that [N^+_{diss}] corresponds to the pDADMAC in the solution (at least at the point of zero charge). In the batch experiments, the adsorption of pDADMAC to

Table 4.2: The parameters of the basic Stern model for the pure carboxylate latex.

Γ_0 (sites nm^{-2})	pK_d	C_S (Fm^{-2})
3.74	4.20	∞

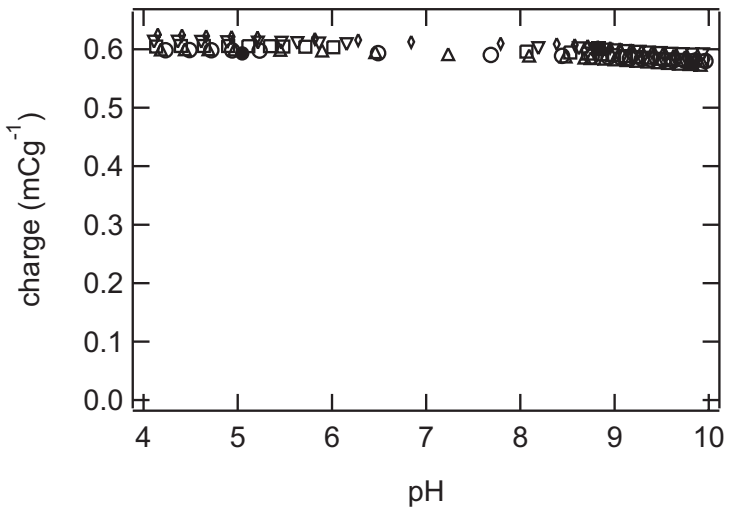

Figure 4.5: Proton binding isotherms of pDADMAC at five different ionic strengths: ∘ 0.01 M, □ 0.05 M, △ 0.10 M, ▽ 0.0.50 M, ◊ 1.00 M.

the carboxylate latex particles was measured at pH = 4 and pH = 10, and at ionic strength 0.1 M, and in the concentration range of pDADMAC as studied in the titration experiments. The pDADMAC surface concentration of 1.0 mgm^{-2} corresponds to 1:1 binding of pDADMAC sites to the latex surface sites. Figure 4.6 is showing that the adsorption is higher at pH = 10 than at pH = 4.

It has to be stressed that the sample preparation for the adsorption experiments is somewhat different than for the titration experiments, which may be a reason for the discrepancies between the measured adsorbed amounts. The adsorbed amounts obtained from the proton binding isotherms may not be the equilibrium amounts, since these experiments were not performed in conditions of equilibrium adsorption. Generally, the adsorbed amounts may depend on pH and the ionic strength, thus may vary during the titration experiments. However, from the agreement between the titration and the batch experiment data at low loadings, it may be assumed that the adsorption of pDADMAC does not substantially change during the titration. The fact that the charge reversal occurs in a narrow pH range, i.e. the common intersection point, points out in the same direction. For all the model calculations which will be presented further, the adsorbed amounts were used, as obtained from the titration experiments (the values are listed in table 4.5). This is reasonable, because neither the charge of the pDADMAC in the solution, nor the quaternary amine sites in the surface vicinity that are compensated with Cl^- ions, affect the protonation behavior of latex.

The proton binding isotherms for all the studied mixtures, at several different ionic strengths, and corrected only for the amount of chloride ions added through pDADMAC, and potassium ions added during the sample preparation, are presented at the left side in figure 4.3. As discussed in the data treatment section, the positive charge present at the common intersection point, $[N^+_{diss}]$ could be used to calculate the adsorbed amount of pDADMAC, by subtracting it from the loaded pDADMAC. The proton binding isotherms to the right in figure 4.3,

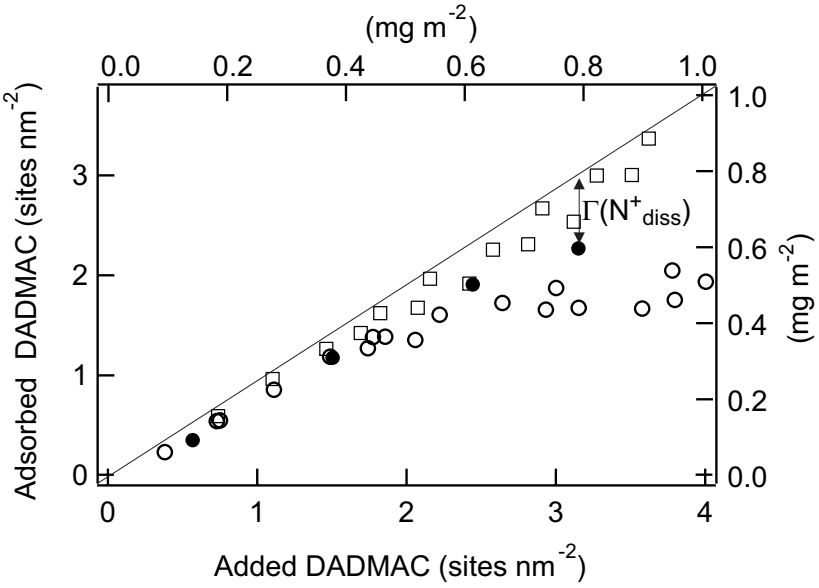

Figure 4.6: Adsorbed amounts, calculated from the potentiometric titration experiments (•), compared to the adsorbed amounts measured in the batch experiments at $I = 0.1$M (∘ : pH = 4, □ : pH = 10). The solid line represents the high-affinity adsorption (straight line with unit slope and zero intercept), where all added pDADMAC is adsorbed. The dissolved amount of pDADMAC sites is indicated for the highest loading.

which are corrected for charge [N^+_{diss}], will be used to test the models. In the case of the highest loading (1.00 mg m^{-2}), the common intersection point is not clearly detectable. Therefore, [N^+_{diss}] could not be estimated, and calculation of the model curves was not possible.

A comparison of the proton binding isotherms of the mixture, with the proton binding isotherms of all the components (pure latex suspension and pure pDADMAC solution), is presented in figure 4.7. The charge of the components (these experiments are described in figures 4.4 and 4.5), is normalized to the concentrations actually present in the mixture. The lines represent the sum of the component charges. For this summation, the charges of pDADMAC at the pH values of the pure latex isotherms, were computed by interpolation. A significant disagreement between this sum, and the experimental proton binding isotherms of the actual mixture becomes apparent.

Modeling of the proton binding isotherms of the carboxylate latex particles in the presence of the adsorbed pDADMAC was attempted with two models, namely the basic Stern model and the modified Stern model for the specific adsorption of counterions. The basic Stern model, with a pK_d value for the carboxylate sites of 4.9 is not able to reproduce the curves, as can be seen in the figure 4.8 (left column). The Stern capacitance influences the slope of the curves (the lower the capacitance, the lower the slope), but does not affect the position of the point of zero charge, which can in this case not be correctly reproduced in the modeled curves.

Much better descritpion was achieved with the modified Stern model, which was described in the introduction to this chapter. The parameters that resulted in the best fitting are presented in the table 4.3. The fitting was also attempted with a protonation constant value of 4.2 (as obtained from the fitting of the proton binding isotherms of the pure latex suspension, see figure 4.4 and table 4.2), but resulted with worse fits.

The proton binding isotherms, as compared to the pH-dependencies of the

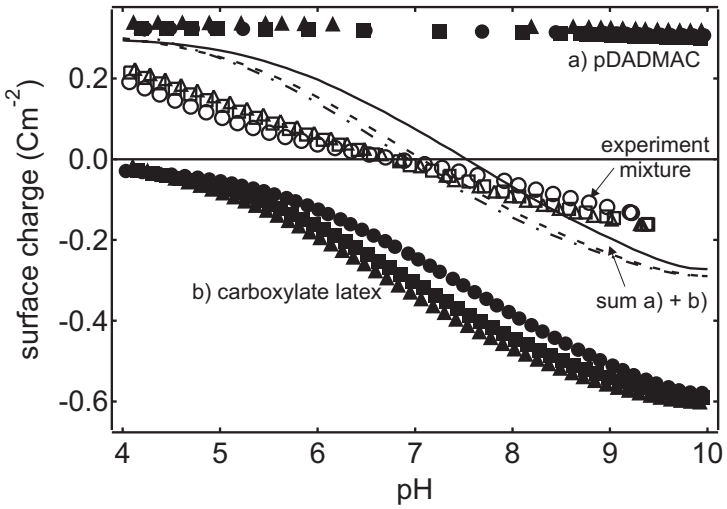

Figure 4.7: Proton binding isotherms of carboxylated latex suspension in the presence of pDADAMAC, at a loading of 0.65 mgm^{-2}, at five different ionic strengths. Closed symbols represent the isotherms of pure components (pure pDADMAC solution in the upper part, and the pure latex suspension in the lower part of the graph), recalculated to the concentrations present in the mixture. The lines represent the sum of the (interpolated) isotherms of the pure components. Open symbols represent the experimental proton binding isotherm of the mixture. Ionic strengths: ○ ● 0.01 M, □ ■ 0.05 M, △ ▲ 0.10 M.

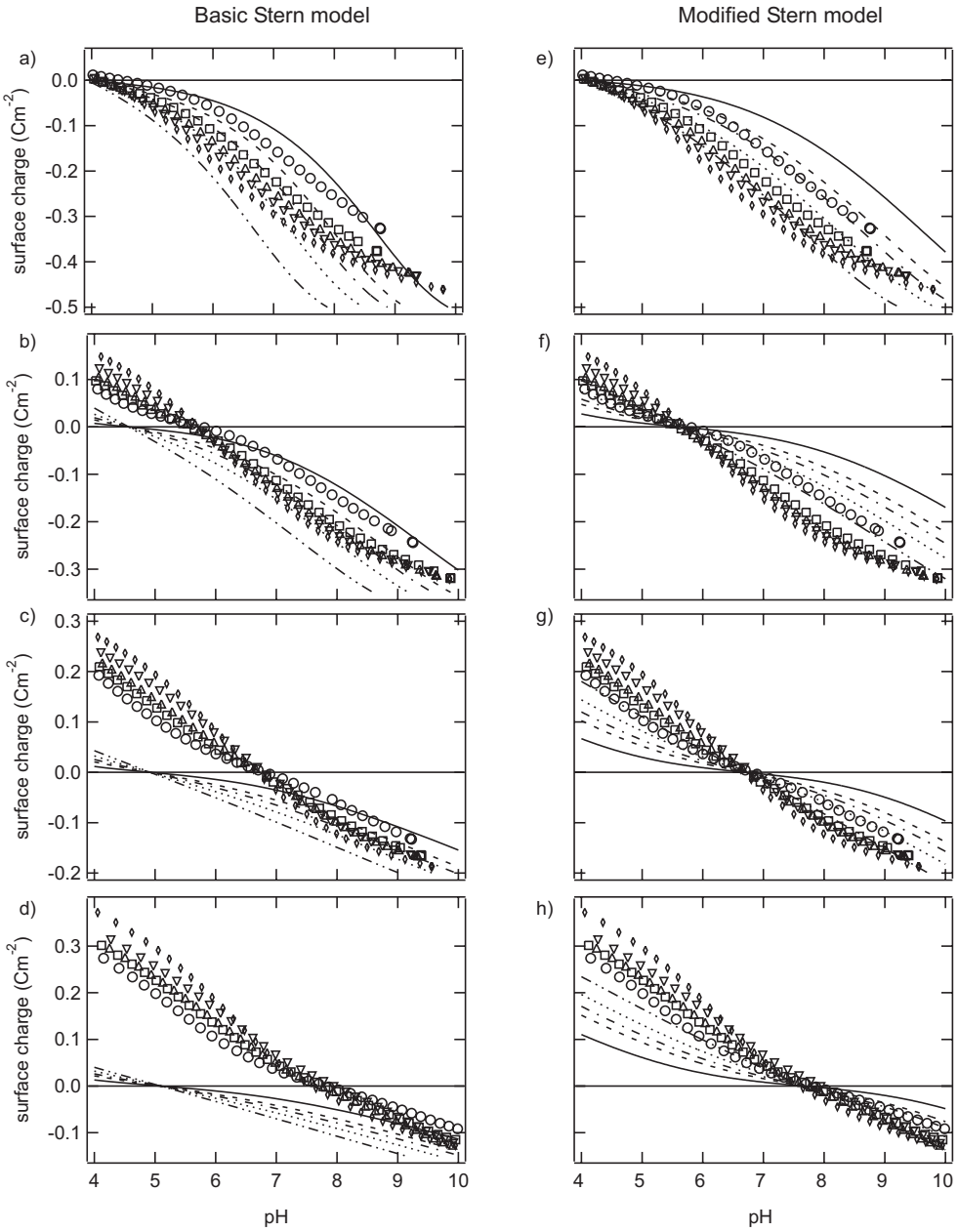

Figure 4.8: A comparison between the predictions of the proton binding isotherms (lines), for four different surface compositions (as indicated in table 4.5), of the basic Stern model (left), and the modified Stern model (right). The parameters used for the basic Stern model calculations are the same as for the modified Stern model (listed in table 4.5), except for the Stern capacitances (given in Fm^{-2}): a) ∞, b) 5.00, c)1.50, d) 1.00. Ionic strengths: $\circ$, full line: 0.01 M; $\square$, dashed: 0.05 M; $\triangle$, dash-dot: 0.10 M; $\triangledown$, dot: 0.50 M; $\Diamond$, dash-dot-dot: 1.00 M.

Table 4.3: The parameters used to calculate the modified Stern model predictions of the proton binding isotherms for different pDADMAC-latex mixture compositions. The adsorbed and dissolved amounts were calculated from the charge at point of zero charge. Stern capacitance is denoted C_S.

pDADMAC loading (sites nm^{-2})	$\Gamma(N^+_{ads})$ (sites nm^{-2})	$\Gamma(N^+_{diss})$ (sites nm^{-2})	C_S (Fm^{-2})	pH_{pzc}
0.56	0.35	0.21	6.95	4.00
1.50	1.18	0.32	3.02	5.82
2.44	1.91	0.53	2.90	6.84
3.15	2.27	0.88	2.40	7.76
1.00	-	-	-	> 9.0

electrophoretic mobilities, are presented in figure 4.9. The lines in the top figures were calculated by means of the modified Stern model, as described in the introduction to this chapter, and using the parameters listed in table 4.3. The coincidence between the point of zero charge, as obtained from the proton binding isotherms, and the isoelectric points, as obtained from the electrophoretic mobility measurements, is obvious. The lines in the bottom figures represent the predictions of the O'Brien [81] and White theory for the electrophoretic mobilities. For this, the shear-plane potential was calculated from the surface potential (ψ_0) by means of the Gouy-Chapman theory (the fitted shear-plane distances are given in table 4.4). The calculation of the electrophoretic mobilities from the shear-plane potential is described in the paper of O'Brien and White. In the present work, the mobilities have been obtained by interpolation, from databases which contain mobilities for various values of the shear-plane potential.

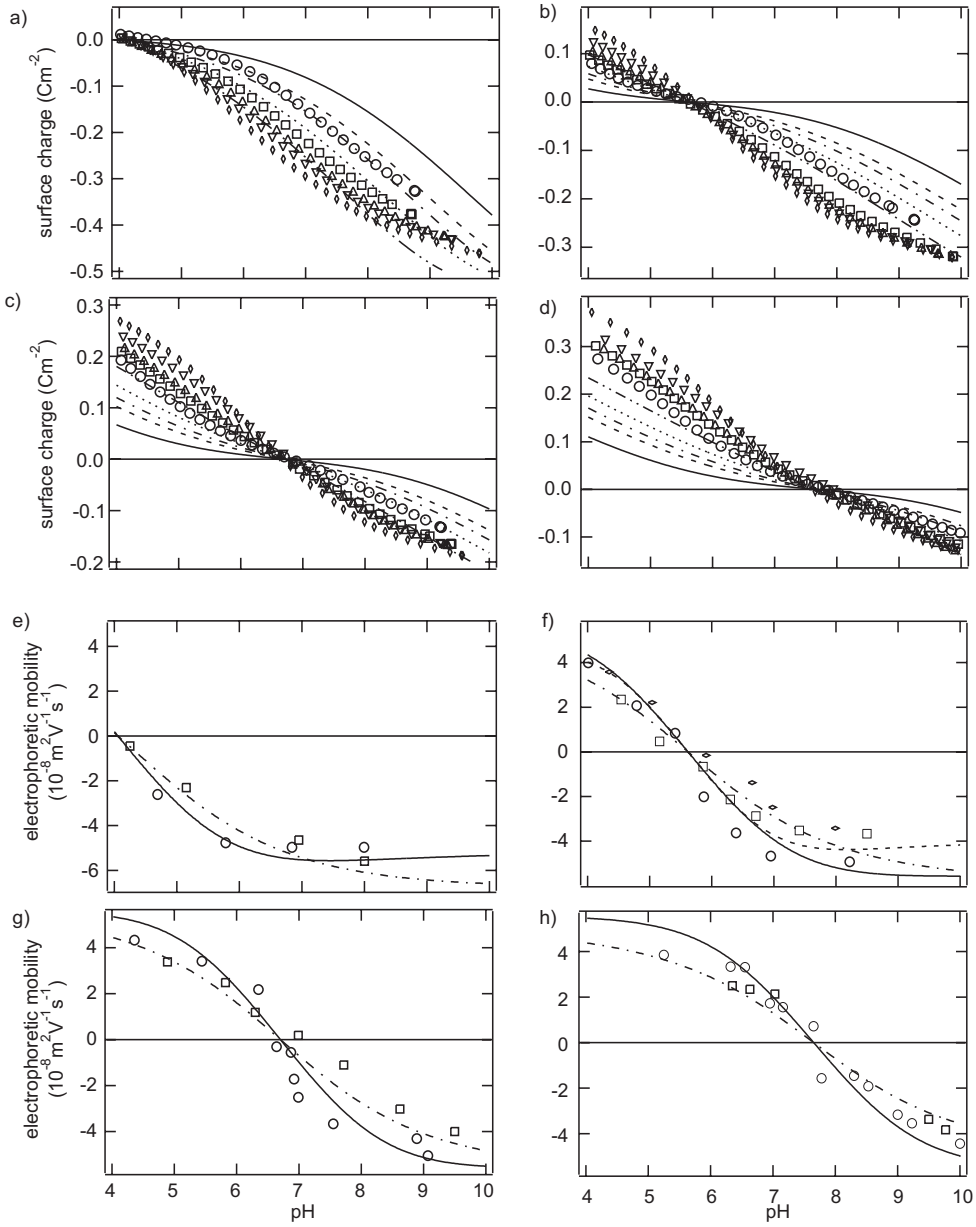

Figure 4.9: Proton binding isotherms (a-d) and pH-dependence of the electrophoretic mobility (e-h) of carboxylated latex suspension in the presence of pDADAMAC. pDADMAC loadings: 0.15 mg / m^2 (a,e); 0.40 mg / m^2 (b,f); 0.65 mg / m^2 (c,g); 0.84 mg / m^2 (d,h). Ionic strengths: ∘ 0.01 M, □ 0.05 M, △ 0.10 M, ▽ 0.25 M, ◊ 1.00 M. The lines in the figures (e-d) represent the the modified Stern model predictions (parameters listed in table 4.5). The lines in figures (e-h) represent the O'Brien and White model prediction (shear plane distance listed in table 4.5).

Table 4.4: The shear plane distances obtained by fitting the experimental electrophoretic mobilities according to the O'Brien and White theory [81].

pDADMAC loading (mgm^{-2})	0.15	0.40	0.65	0.84
shear plane distance (nm)	0.20	0.30	0.32	0.40

4.6 Discussion

The adsorption isotherms from the batch experiments (figure 4.6) at pH = 10 are showing a high-affinity equilibrium adsorption behavior of pDADMAC at the carboxylate latex surface. Small deviations from this behavior are possibly due to a fact that the equilibrium was not reached. High-affinity adsorption is a regime, where the adsorption is quantitative up to a saturation limit, after which the adsorbed amount can not be further increased, but remains constant upon further additions. In the present case, when the adsorption is carried out at pH = 10, the saturation limit is not reached in the range of loadings examined.

The presence of the adsorbed oppositely charged polyelectrolyte is promoting the development of the negative charge at the latex surface, which is in turn promoting the adsorption [69, 82, 83]. However, at pH = 4, lower adsorption was observed, and in this case the adsorption is not of the high-affinity type. The increased adsorption at higher pH is not surprising, having in mind that the charge, present at the surface of the carboxylate latex particles is increasing with an increasing pH. This points out that in the studied (low) range of loading, adsorption of pDADMAC to the carboxylate latex surface can be regarded as an example of the screening-reduced regime, according to de Keizer et al. [84].

The proton binding isotherms of the pure latex suspension (fig. 4.4) are showing typical protonation behavior for weakly acidic particles [6, 8]. The experimental data could be reasonably well fitted with the simple double layer model. The value of 4.2, obtained for the microscopic pK_{d} of a carboxylic surface site,

seems a bit too low (the reported values are usually around 4.9 [61], [85] and for comparison, the pK_d of acetic acid in solution is ~ 4.6 [11]). However, this was the highest value that could be used in order to describe the data in terms of the double layer model, or the basic Stern layer model. A possible source for such a low pK_d value might be the specific adsorption of negative counterions (in this case Cl^- [8]). As well, a higher surface charge ($\sim 600\,mCm^{-2}$) than usual has been observed [61, 85], which could be due to the surface roughness.

The proton binding isotherms of pDADMAC (figure 4.5) are showing a fairly constant charge of the quaternary amine groups, upon the variation of pH. It has to be stressed that pDADMAC does not contribute to the total net charge in the solution, since the charge of the quaternary amine groups is fully compensated by the charge of the counterions Cl^-, and in this respect, pDADMAC acts as a monovalent strong electrolyte. However, when adsorbed to the carboxylate latex surface, these counterions are to a certain extent depleted from pDADMAC, which gives rise to the positive surface charge of the adsorbed pDADMAC [67].

Although the adsorption isotherms from the batch experiments are showing a dependence of the equilibrium adsorbed amount on the pH, a very good reversibility of the titration curves was achieved by fast titration experiments, which was established by comparing the data from the forward and backward titration runs at same pH and ionic strength. This, and the fact that the common intersection points can be easily recognized in the proton binding isotherms, is leading to a conclusion that the adsorbed amounts of pDADMAC did not change to a great extent during the titrations.

The main feature of the proton binding isotherms of the carboxylate latex particles in the presence of adsorbed pDADMAC, is the common intersection point of the curves at different ionic strengths, which indicates the reversal of the surface charge. This can be clearly explained by inspecting figure 4.7. If the latex particles and pDADMAC would be separated in the water medium (with the supporting electrolyte), this mixture would titrate as indicated by the sum

of the components. The particles would be exerting a negative surface charge (or zero, at low pH), while pDADMAC would not contribute to the overall charge (due to the compensation with the counterions). The protons that are exchanged between the particle surface and the solution, would always experience a negative electrostatic potential. The "screening effect" would in that case cause a shift of the proton binding isotherms towards lower pH values upon an increase in the background electrolyte concentration, and there would be no common intersection point [18]. However, the presence of the adsorbed positively charged pDADMAC in the vicinity of the carboxylate sites, is giving rise to a possibility of a surface charge reversal. In this case, the carboxylate surface sites can behave similarly as amphoteric species, upon the electrostatic screening by the background electrolyte. The charge reversal occurs when the sum of the pDADMAC charge experienced by the carboxylate sites and the charge of the protons bound to them, equals the negative charge of the deprotonated carboxylic groups. The pH value of the charge reversal can be referred to as the point of zero charge, pH_{PZC} (or P.Z.C.), where the electrostatic potential at the surface origin (where the carboxylic groups reside) ψ_0, equals zero [78]. This point depends on the surface charge concentration of the carboxylate groups, the surface concentration of the adsorbed pDADMAC, and the solution pH, but does not depend on the background electrolyte concentration. The point of zero charge in the composite system depends on the adsorbed pDADMAC charge, which, in the low range of pDADMAC (less than one pDADMAC site per one surface site), turned out to be tunable by the polyelectrolyte loading. In the pH-range above the point of zero charge, when the surface charge is negative, the surface is acting as a weak acid. Conversely, in the pH-range below the point of zero charge, the surface charge is positive, and the surface is acting as a weak base.

The presence of the point of zero charge in the experimental proton binding isotherm, enables distinguishing the adsorbed from the dissolved pDADMAC charge. The adsorbed charge is the fraction of the added pDADMAC charge,

which has an influence on the surface potential. The dissolved charge, estimated as the excess charge at point of zero charge, does not influence the surface potential. In principle, three contributions to the latter charge are possible, which can not be distinguished from the proton binding isotherms; the charge of the pDADMAC sites which are not adsorbed and thus present in the bulk solution, the pDADMAC charge compensated by Cl^- and OH^- ions which are incorporated in the adsorbed layer, and the charge of the pDADMAC sites, which are adsorbed, but not in the proximity of the surface, whereby their contribution to the surface potential is reduced.

The adsorbed amounts, as calculated from the excess charge present at the point of zero charge [N^+_{diss}], are in a reasonably good agreement with the result of the batch experiments. Neglecting the influence of different sample preparation for the titration and batch experiments, it may be concluded that [N^+_{diss}] actually corresponds to the residual pDADMAC in the solution, and not to the adsorbed sites, which have less influence on the surface potential, due to their distance from the surface, or incorporation of the counterions into the pDADMAC layer. Therefore, for low polyelectrolyte loadings, the majority of the adsorbed pDADMAC charge actually influences the surface potential. Unfortunately, the adsorbed charge can not be determined from the proton binding isotherms at higher loadings.

The presented models, although very simple, are giving some insight into the distribution of charges in the electrical double layer at the particle/solution interface. The basic Stern models with two surface components at the surface (two types of sites, with two different pK values), is not capable of reproducing the experimentally determined point of zero charge (see figure 4.8). This deviation is becoming larger with an increase of the adsorbed amount of pDADMAC. This is due to an overestimation of the pDADMAC charge influence at the surface potential ψ_0. On the other hand, the modified Stern model can give good predictions of the point of zero charge, which is a consequence of the fact that the

pDADMAC sites are modeled to be at a certain distance from the surface (see figure 4.2), such that the surface potential ψ_0 is less influenced by the pDADMAC charge. The presence of the pDADMAC charge which does not influence the surface potential, is in agreement with the picture of the pDADMAC sites as displaced from the surface: as the distance of the positive pDADMAC sites from the surface is increased, their effect on the surface potential ψ_0 decreases. The decrease of the "effectiveness" of the pDADMAC sites, will be compensated by an uptake of protons by the surface (so that the degree of surface protonation is increased). This uptake corresponds to a shift in the bulk pH towards higher values, which explains the difference in the predictions of the point of zero charge between the basic, and modified Stern model.

It is apparent that the modified Stern model, although overly simple, can satisfactorily reproduce the measured proton binding isotherms, in particular, the dependence of the point of zero charge upon the variation of the adsorbed amount of pDADMAC. The trend of the Stern capacitance (see table 4.5), might be pointing out that the center of mass of the adsorbed pDADMAC is becoming more displaced from the surface, with an increasing adsorbed amount. Consequently, the fraction of the pDADMAC sites which do not influence the surface potential increases. Figure 4.6 supports this conclusion, since it shows more dissolved pDADMAC sites at higher loadings (the dissolved amount does not increase with loading at the same rate as the actually adsorbed amount).

In spite of the above successes of the extended Stern model, the quantitative prediction of the proton binding isotherms in the whole pH range, is still lacking. The causes for the discrepancy may be as follows. The model does not assume any particular distribution of the adsorbed pDADMAC sites in the electric double leayer, and the sites are uniformly distributed in a plane at some distance from the surface. Consequently, we are not able to draw more precise conclusions about the actual conformation of the pDADMAC layer from the proton binding isotherms. For example, in the directions parallel to the surface, the distribution

of the adsorbed pDADMAC sites may not be uniform, but patch-wise. In the direction normal to the surface, the distribution might assume different shapes, as some simulation results are pointing out [86, 87], with different proportions between the tails, loops, and trains. Both the lateral, and the vertical distribution of the adsorbed sites could have a pronounced influence on the surface potential. Furthermore, the conformation of the adsorbed pDADMAC is pH- and ionic strength-dependent, and it is very likely that it dynamically changes during the described titration experiments.

The response of the counterions (K^+, and Cl^-) in the diffuse layer to the presence of the adsorbed pDADMAC, can be qualitively predicted by the presented extended Stern model. The charge balance between the surface and the diffuse layer, which has to equal zero at all time, leads to the conclusion that upon the adsorption of pDADMAC, some positive counterions (i.e. potassium ions) have to be depleted from the diffuse layer into the solution. In fact, the coincidence of the point of zero charge, and the isoelectric point (see figure 4.9), is indicating that there is an equal distribution of counterions (K^+, and Cl^-) in the adsorbed pDADMAC layer.

4.7 Conclusion

All of the presented results are demonstrating the usefulness of the potentiometric titrations for studying the charging mechanisms in the system consisting of pDADMAC, adsorbed to oppositely charged, carboxylate latex surface. In combination with the surface complexation models, the experimental proton binding isotherms can give a deeper insight in the surface concentrations of ions and their distributions along the interface. The pDADMAC charge, which has an influence on the surface potential, can be determined from the proton binding isotherms at the point of zero charge. The comparison between the adsorbed amount, as calculated from the proton binding isotherms, and measured independently in the

batch experiments, is showing that at low pDADMAC loading (< 0.6 mg m^{-2}), all the added pDADMAC sites influence the surface potential. However, at higher loadings, this is no longer the case.

The best fitting of the experimental data were achieved by applying an extension to the basic Stern model, where the adsorbed polyelectrolyte sites are considered to be displaced from the surface. The Stern capacitance, obtained from fitting the extended Stern model to the experimental proton binding isotherms, is showing that the distance of the center of mass of pDADMAC to the surface, is increasing with an increasing adsorbed amount.

Chapter 5

pH dependent charging of silica particles in the presence of pDADMAC

5.1 Introduction

In the previous chapter, the proton binding isotherms of weakly acidic carboxylate latex particles in the presence of a strong cationic polyelectrolyte poly(dimethyldiallylammonium chloride) (pDADMAC), have been presented. The measured proton binding isotherms enable distinguishing the charge of the adsorbed pDADMAC, which influences the surface potential, from the pDADMAC charge, which is not adsorbed, or does not influence the surface potential due to compensation with the bulk solution ions, or the Cl^- ions which are present within the adsorbed layer. It was concluded that the latter case may as well occur if some fraction of the pDADMAC charge is displaced from the surface, and is therefore less effective in neutralizing the surface charge. In this chapter, a charging behavior of the silica particles will be studied in the presence of pDADMAC. The emphasis will be made on the effect of the molecular weight

of the polyelectrolyte. In particular, it will be investigated, whether the polyelectrolyte molecular weight influences the effect of the adsorbed positive charge on the surface.

Silica is silicon oxide, and as such, it is amphoteric. This was confirmed in many studies of the charging behavior of silica suspensions [88–91]. The protonation of pure silica can be well interpreted in terms of the 1-pK MUSIC [76, 77] model. The advantage of this model is that it is able to predict the surface charge, according to the actual crystallographic structure of the surface. According to the MUSIC model, theoretically one or two protons can bind to singly, or doubly coordinated oxygens of silicon oxide. The pK values for these four protonation reactions can be calculated (further explanations can be found in the above publications), and it turns out that for silica, the only protonation reaction which takes place in the experimental pH-range of $3.5 < \text{pH} < 9.0$, is that one where a proton is bound to a singly coordinated oxygen. Binding of the second proton to the singly coordinated, and the first proton to the doubly coordinated oxygens, would occur at much lower pH values. Therefore, the surface charge on the pure silica surface originates from the SiO^- surface species, according to the reaction:

$$\text{SiOH} \rightleftarrows \text{SiO}^- + \text{H}^+ \tag{5.1}$$

The pK of this reaction is around 7.5, so at $\text{pH} > 3$, similar to the carboxylate latex particles, silica is weakly acidic, and negatively charged.

The CD-MUSIC model is found to be suitable for describing adsorption, charging behavior, and particularly, surface speciation of the adsorption sites, in the case of adsorption of small molecules to metal oxide surfaces [92–95]. A problem that may arise when studying the pH-dependent charging, is that silica dissolves, and the dissolution rate increases with pH [96]. However, it was established that the dissolution of silica, prepared according to the Stöber procedure, starts playing an important role around $\text{pH} \approx 9$ [74]. Therefore, the experimental window for the potentiometric titration studies, is constrained to

$3 <$ pH < 9.

A very large number of studies, dealing with the polyelectrolyte adsorption on silica (or silicon oxide), are available [66, 67, 83, 84, 97]. The importance of this process can be related to several factors. The first is probably, the natural abundance of silica, which can act as a carrier of the natural organic substances, and small molecules [8]. Another example of application of silica particles, is the preparation of microcapsules by layer-by-layer adsorption of oppositely charged polyelectrolytes [7]. Silicon wafers with a surface oxide layer are suitable for measurements like reflection infrared spectroscopy (total or attenuated) or ellipsometry. Adsorption studies have been carried out with various strong [67, 97] or weak [83] polyelectrolytes, or polyampholytes [98]. Particularly interesting for the present chapter are the potentiometric titration studies, carried out by Shubin [66, 67], where the surface charge was related to the conformation of the adsorbed polyelectrolyte.

The proton binding isotherms, obtained in the present study, will be interpreted in the same way, as was presented in the previous chapter. The dissolved charge will be subtracted from the added amount of quaternary amine sites, in order to obtain the adsorbed charge, which has an influence on the electrostatic potential at the origin of the silica surface (ψ_0), where the protonation sites are situated. According to the MUSIC, the sites can be singly or doubly coordinated with oxygen [77]. In this chapter, the modified Stern model (as presented in the previous chapter) will be used in order to fit the experimental proton binding isotherms. An overall charge will be attributed to the protonation sites of silica, thus the exact speciation will not be discussed.

5.2 Experimental

Stöber silica particles were kindly supplied by the Nippon Shokubai company (Japan). The particles were obtained as powder, which was pre-treated by heating

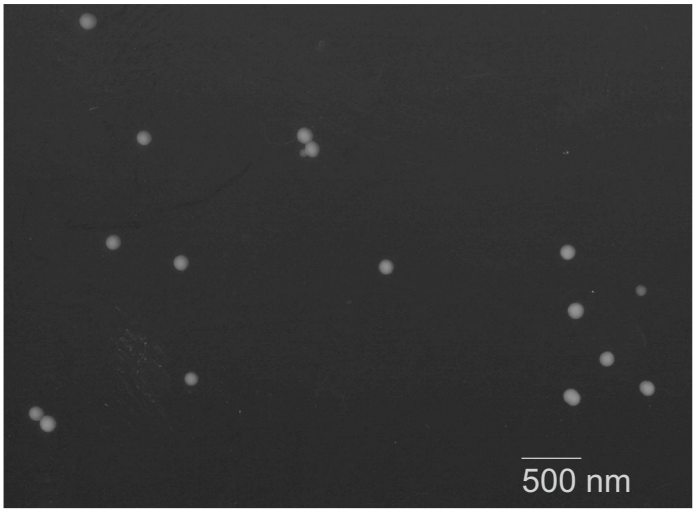

Figure 5.1: The transmission electron micrograph of the heated silica particles which were used for the titrations.

at 800 °C for 24 hours. This procedure was reported as useful for elimination of the microporosity of Stober Silica particles [90, 91]. After the heating treatment, the particles were suspended in MilliQ water to give a 10 % (by weight) stock suspension. The suspension was sonicated 4 × 15 min and shaken in between sonication.

Figure 5.1 is a transmission electron micrograph of the particles, after the heating treatment. The micrograph is showing that the particles are fairly spherical and monodisperse. From the TEM, the particles have a radius of 64 nm. The hydrodynamic radius, calculated from TEM, is 66.5 nm. The hydrodynamic radius, measured with dynamic light scattering equals 69 nm. The surface area, calculated from the diameter measured with TEM, equals 24.3 $m^2\,g^{-1}$. The BET surface area equals to 32.0 $m^2\,g^{-1}$.

The 0.2 % (by weight) stock solutions of high molecular mass $400 - 500$ kDa, and low molecular mass $100 - 200$ kDa poly(dimethyldiallylammonium chloride) (pDADMAC), were prepared with MilliQ water, from the 20 % solutions, which were purchased from Aldrich. The purchased solutions were used without any

further purification. The concentration of the purchased solutions were verified with the total carbon and nitrogen analyis, which have as well shown a correct stoichiometric ratio of carbon and nitrogen.

The adsorption of pDADMAC was carried out in the following manner. First, the silica suspension ($10-20$ ml) was added into a polyethylene container of 30 ml. The measured pH of the pure silica suspension is around 5. Then, pDADMAC solution was added. The concentration of the pDADMAC stock solution is adjusted, so that the addition of pDADMAC is of the order of a few milliliters. The mixture was shaken, and the pH was adjusted to pH $\approx$ 7.5 by carefully (with an automatic burette) adding KOH (0.25 M). The mixture was shaken for several minutes, and transferred into the titration cell. Titrations were performed with the Jonction titrator (see appendix), in the same way as described in chapter 4. The studied pH range was $4 <$ pH < 8.5. Higher pH values were not studied in order to minimize the dissolution of silica, and constant ionic strengths were maintained throughout titrations at 0.01, 0.05, 0.10, 0.50, 1.00, by additions of 3 M KCl and de-carbonized water. The burette concentrations of HCl and KOH were 0.25 M. The titration mixture was degassed with nitrogen, which was previously passed through conc. KOH, water, and 0.1 M KCl solution.

5.3 Data treatment and results

The data treatment of the potentiometric titration experiments was performed in the same way, as described for the pDADMAC-latex system (chapter 4): In a first correction, the charge of all the free Cl^- and K^+ ions, which were added with pDADMAC, and during pH-adjustment for the adsorption, was subtracted from the experimental "raw" proton binding isotherms. The resulting proton binding isotherms showed an excess positive charge, which can be considered as dissolved charge N_d^+iss, at the common intersection point. Following the same argument as described in the data treatment for the pDADMAC-latex system

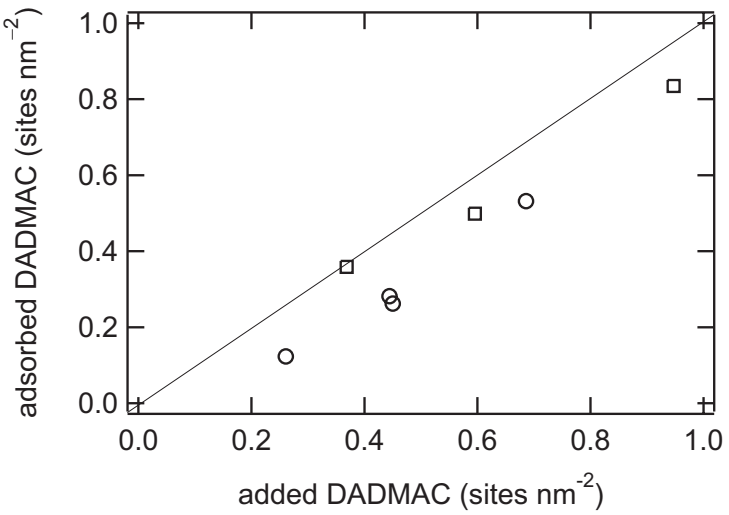

Figure 5.2: The excess positive surface charge, as calculated from the positive charge at the point of zero charge (see text), recalculated into sites per nm^2, is plotted versus the loaded amounts of pDADMAC. ○: low molecular weight pDADMAC (100-200 kDa); □: high molecular weight pDADMAC (400-500 kDa).

(chapter 4), this charge was used to calculate the adsorbed charge. The values of the adsorbed and the dissolved charge are listed in table 5.2. In the second correction, the dissolved charge [N^+_{diss}], was subtracted from the proton binding isotherms, so that the presented data exert a common intersection point at zero surface charge.

In figure 5.2, the adsorbed amount of quaternary amine sites, calculated from the excess charge at the point of zero charge, is presented versus the total added amount of quaternary amine sites. The presented adsorbed amount of the quaternary amine sites does not include the sites which are displaced from the surface, since their influence on the surface potential is mitigated. However, in chapter 4, a good agreement between the adsorbed amount, calculated from the excess charge at the point of zero charge, and the adsorbed amount, measured in batch experiments, was observed. This is pointing out, that the dissolved pDADMAC is the major contribution to the excess charge at the point of zero charge.

The proton binding isotherms are showing typical protonation behavior for Stöber silica particles, pre-treated by heating [91]. The titrations were repeatedly performed with acid and base at the same ionic strength, for pH < 9. Since the proton binding isotherms from titrations with acid, and with base, do not show any significant difference, it can be concluded that in the studied pH range, the dissolution of the pre-treated silica can be neglected. This finding is in agreement with previous findings [90, 91], which show that the dissolution rate of silica is low at pH < 9, and starts growing at higher pH values. The proton binding isotherms of silica which was not pre-treated, have shown differences (hysteresis) between the titrations performed with acid, and base. The same is the case if the pH-range is extended to higher pH-values.

The surface charge of the pre-treated silica is negative in the whole examined pH-range. At pH < 3, silica is positively charged [88, 89], but such low pH was not experimentally examined in the present work. The maximum surface charge at high pH can not be experimentally determined, because the highest experimentally reachable pH is around (or slightly below) pH $= 9$. Above that pH, the dissolving of silica is becoming pronounced [90]. At pH $= 9$, the charged fraction of the protonation sites is around 8 to 15 per cent of the total protonation sites (considering the value of 8 sites per nm^2 for the total surface concentration of the protonation sites [77]), depending on the ionic strength.

A very good description of the experimental proton binding isotherms of pure pre-treated silica suspension, with the basic Stern model can be noticed in figure 5.3. The parameters obtained from fitting are listed in table 5.3. However, it has to be stressed that in this case (as opposed to the case of carboxylate latex particles), the fitting is not free of ambiguity. Namely, the total surface concentration of the protonation sites is calculated from the slope of the proton binding isotherm, which is as well influenced by the Stern capacitance, C_{S}. In other words, in the absence of a clear plateau in the data at high pH, these two parameters are correlated.

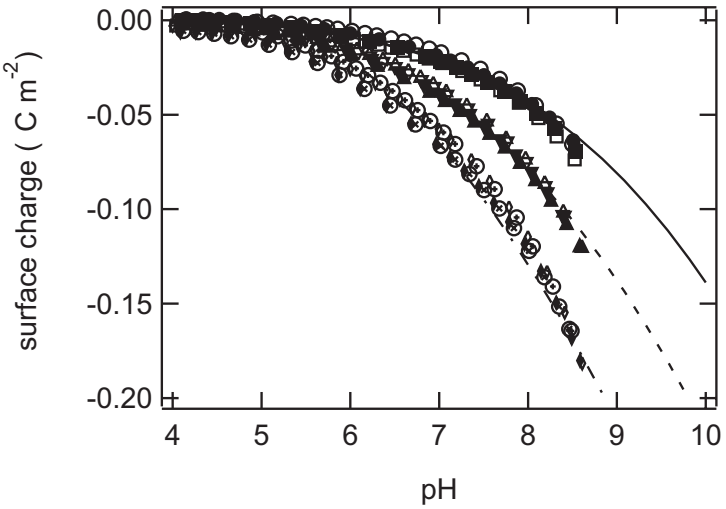

Figure 5.3: Proton binding isotherms of the silica particles. Open symbols represent the forward titrations, and closed symbols the backward titrations. Ionic strengths: $\circ, \square, \bullet, \blacksquare : 0.01\,M$, $\triangle, \triangledown, \blacktriangle, \blacktriangledown : 0.10\,M$, $\Diamond, \odot, \blacklozenge, \otimes : 1.00\,M$. The lines represent the prediction by the basic Stern model, with the parameters enlisted in the table 5.3.

Table 5.1: The parameters of the basic Stern model obtained from fitting the experimental proton binding isotherms of silica, where pK_{d} is the microscopic dissociation constant, and Γ_0 total surface concentration of the protonation sites, from [76] (fitted with the MUSIC model).

pK_{d}	Stern capacitance (Fm^{-2})	Γ_0 (sites nm^{-2})
7.5	3.5	8

Table 5.2: The results obtained from the proton binding isotherms of the composite pDADMAC-silica system. Adsorbed, and the dissolved sites ($[N^+_{diss}]$) are explained in detail in the data treatment section in chapter 4. The Stern capacitance is obtained by fitting the modified Stern model (see chapter 4) to the experimental proton binding isotherms. The upper part of the table refers to pDADMAC with Mw $= 100 - 200$ kDa, and the lower part to pDADMAC with Mw $= 400 - 500$ kDa.

DADMAC loading (sites nm^{-2})	DADMAC adsorbed (sites nm^{-2})	DADMAC dissolved (sites nm^{-2})	C_S (Fm^{-2})	pH_{pzc}
0.26	0.12	0.14	2.90	5.78
0.45	0.26	0.19	1.26	6.71
0.44	0.28	0.16	1.26	6.72
0.68	0.53	0.15	1.10	7.72
0.37	0.36	0.01	1.62	6.78
0.60	0.50	0.10	1.05	7.68
0.94	0.83	0.11	1.05	8.70

The proton binding isotherms of silica particles in the presence of adsorbed pDADMAC are presented in figure 5.4. The upper part of the figure is showing the data for several different loadings of pDADMAC ($M_w = 100-200$ kDa). The lower figures are presenting results, which were obtained with pDADMAC of a higher molecular weight ($M_w = 400 - 500$ kDa). As was observed in the case of carboxylate latex (chapter 4), the proton binding isotherms in figure 5.4 are showing a point of zero charge, which is tunable by the loading of the pDADMAC. The lines in these figures are the best-fittings of the modified Stern model, as described in chapter 4. The parameters obtained from fitting are presented in table 5.2.

Figure 5.5 is showing the point of zero charge, determined from the proton binding isotherms, versus the adsorbed charge of the quaternary amine sites (from pDADMAC), which is expressed as the number of elementary charges (or sites) per surface area. The adsorbed charge was determined by subtracting the excess charge at the point of zero charge, from the total positive charge added

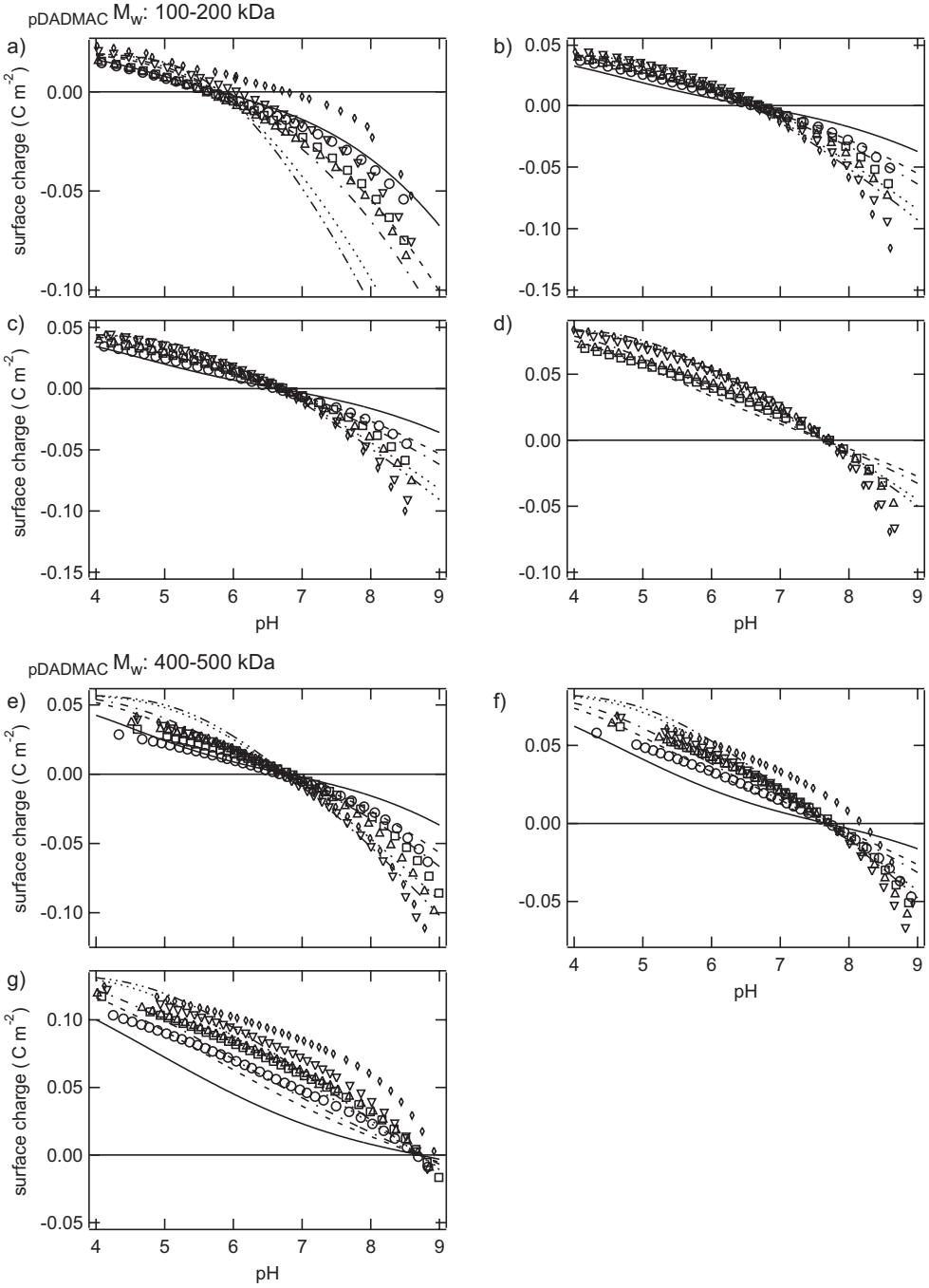

Figure 5.4: Proton binding isotherms of the silica particles in the presence of low molecular weight (top figures), and high molecular weight (bottom figures). Loadings of pDADMAC: a) 0.07 mgm^{-2}, b) 0.12 mgm^{-2}, c) 0.12 mgm^{-2}, d) 0.18 mgm^{-2}, e) 0.10 mgm^{-2}, f) 0.16 mgm^{-2}, h) 0.25 mgm^{-2}. Ionic strengths: $\circ$ 0.01 M, $\square$ 0.05 M, $\triangle$ 0.10 M, $\triangledown$ 0.25 M, $\Diamond$ 1.00 M.

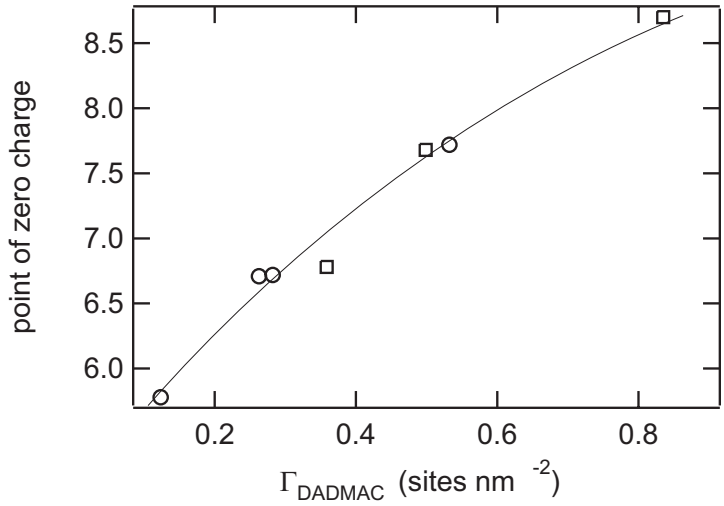

Figure 5.5: The point of zero charge versus the adsorbed positive surface charge, as calculated from the excess charge at the point of zero charge [N_d^+iss] (see data treatment section in chapter 4), for high and low molecular weight pDADMAC. $\circ$: $M_w = 100 - 200\,kDa$; $\square$: $M_w = 400 - 500\,kDa$

as pDADMAC. As was established in chapter 4, the adsorbed charge calculated in this manner, could be lower than the total positive charge carried by the adsorbed pDADMAC molecules, because the influence of the quaternary amine sites on the surface potential decreases with an increasing distance of these sites from the surface origin. However, figure 5.5 is showing a coincidence of the point of zero charge, for both studied molecular weights of pDADMAC, when represented as a function of the adsorbed charge. As will be discussed in the following section, this observation may be pointing out, that the molecular weight of the polyelectrolyte, does not affect the surface density of the charged quaternary amine groups, which compensate the negative charge present at silica surface at the point of zero charge.

5.4 Discussion

The proton binding isotherms of the silica particles, in the presence of adsorbed strong cationic polyelectrolyte pDADMAC, exhibit the point of zero charge, as was observed for the carboxylate latex particles in the presence of pDADMAC. At the point of zero charge, the surface potential equals zero. This fact has important consequences and, in the case of homogeneous surfaces (e.g. metal oxide), can provide an insight into the charge distribution near the surface. In the case of metal oxide, at the point of zero charge, the surface charge density equals zero, and in the case of a monovalent inert electrolyte, the amounts of positive and negative counterions in the diffuse layer are perfectly matching. The aim of the following discussion is to explain the charge distribution at the point of zero charge, for the case of the composite system of a weakly charged surface in the presence of an adsorbed strong polyelectrolyte.

Although amphoteric, bare silica surface can bear only negative charge in the studied pH-range (above 3), which is in agreement with previous findings (e.g. [74, 89]). Since the second protonation step can be discarded above pH = 2, in the case of pure silica, the same charging model can be applied, as for the carboxylate latex particles, which is demonstrated in the figure 5.3. The obtained parameters are in a good agreement with the already published results for the same type of silica [77].

As a simplest model of the silica surface with an adsorbed pDADMAC, let us imagine a situation, where all the quaternary amine sites reside in the plane at the surface origin, together with the protonation sites of silica. Then, at the point of zero charge, where the surface potential equals zero, the number of deprotonated silica sites has to equal the number of the adsorbed quaternary amine groups of pDADMAC. Thus, any positive charge which appears in the proton binding isotherm at the point of zero charge, after subtraction of the excess charge (Cl^- added with pDADMAC, or K^+ added during the sample preparation to adjust

the pH to the adsorption value), could only be attributed to the quaternary amine groups of the dissolved pDADMAC. In this case, the calculation of the adsorbed amount of pDADMAC at the point of zero charge would be straightforward. The adsorbed amount would equal the difference between the loaded amount of pDADMAC, and the amount of elementary charge units present at the point of zero charge.

The basic Stern model, can not reproduce the proton binding isotherms of the composite system, in particular the point of zero charge, as was shown in chapter 4. Therefore, it is sensible to assume that the quaternary amine sites from pDADMAC, do not influence the surface potential with the same efficiency. This could in the first place occur due to a fact, that some of these groups reside at a larger distance from the surface than the others. In this case, the point of zero charge depends on the density distribution of the adsorbed pDADMAC [99], and this complicates the prediction of the adsorbed amount from the point of zero charge. Furthermore, Cl^- ions which may be present in the adsorbed pDADMAC layer, neutralize the charge of the quaternary amine groups to a certain extent, which in turn reduces the effect of the pDADMAC charge on the surface potential.

As discussed in the data treatment, we can express the excess charge, present at the point of zero charge, as the excess amount of the quaternary amine sites. If we subtract the excess quaternary amine sites from the total added pDADMAC sites, we obtain the portion of adsorbed positive charge that affects the surface potential.

Figure 5.5 is showing the same dependency of the point of zero charge upon the adsorbed pDADMAC charge that affects the surface potential, for two different molecular weights of pDADMAC. From this, and in the light of the previous discussion, two conclusions can be made. First, that the surface density of the adsorbed pDADMAC sites, at the point of zero charge, is the same for two different molecular weights of pDADMAC, and at the same time, the Cl^- ions

have the same effect in both. Second, the effect of a difference in the surface density of pDADMAC sites, on the surface potential, for two different molecular weights of pDADMAC, is matched through an exchange of the Cl^- ions with the solution. The two conclusions can not be distinguished from the current experiments. Therefore, it can not be clearly stated whether the difference in the pDADMAC charge, experienced by the silica surface, presented in figure 5.2 for two different molecular weight of pDADMAC, reflects a difference in the adsorbed amount, the density of the adsorbed sites, or an exchange of Cl^- ions with the solution. A combination of these effects is possible as well.

5.5 Conclusion

Silica particles are suitable for studying the charging behavior in a system composed of weakly charged particles and adsorbed strong polyelectrolyte. The presented proton binding isotherms can give important information about the charging behavior in these systems. An interesting feature of the proton binding isotherm is the point of zero charge, which is tunable by the adsorbed amount of pDADMAC. If there are no counterions present within the adsorbed layer, and the strong polyelectrolyte is adsorbed in a conformation where all the sites reside at the surface, the excess charge which is present at the point of zero charge, can be attributed to the polyelectrolyte in the solution.

The coincidence between the point of zero charge, observed with two different molecular weights of pDADMAC, at the same adsorbed pDADMAC charge (i.e. the pDADMAC charge which actually influences the surface potential), is pointing out in two directions. First, the effective charge of the strong polyelectrolyte, is always the same fraction of the total adsorbed polyelectrolyte charge, which is situated in the close vicinity of the surface (the rest of the polyelectrolyte charge is compensated with the counterions). Second, for different molecular weights of polyelectrolyte, the difference in the surface densities of the charged polyelec-

trolyte sites, is matched by a difference in the amount of counterions which are incorporated into the adsorption layer.

Conclusions

Potentiometric titrations have been used to study the charging properties of various systems. These included pure solutions of poly(amidoamine) dendrimers, colloidal suspensions of carboxylate latex and silica particles, and composite systems, where strong cationic poly(dimethyl-diallylammonium chloride) (pDADMAC) is adsorbed onto carboxylated latex, or silica particles.

The methodology of the potentiometric titrations, in determinations of the excess charge in water solutions and suspensions, was presented in chapter 1. To obtain the proton binding isotherms of the above systems, the blank acid-base titration curves were subtracted from the titration curves of the systems of interest. The pH-scale of the proton binding isotherms was calculated from the parameters of the blank titration curves, which were obtained by fitting, and verified through determinations of the pK values of standard systems, namely ethylenediamine and acetic acid. The determined pK values are within ± 0.03 units from the values reported in literature. The blank titration curve parameters include the concentrations of the strong acid and base in the burettes, the slope and offset of the electrode reading versus pH, the common activity coefficient of H^+ and OH^- ions, and the dissociation product of water. A study of the correlations between these parameters has shown that the common activity coefficient, one of the burette reagent concentrations, and one of the electrode parameters are reasonable for fitting. The fitted common activity coefficients have shown to be in agreement with the predictions of the Davies formula. As

well, the blank titration curves were used to verify the titration baselines, which are showing the carbonate content in the titrated system. The amount of the dissolved carbon dioxide was reduced to less than $10^{-5}\,\mathrm{moldm}^{-3}$ by a careful preparation of reagents and degassing with purified nitrogen.

The potentiometric titration study of the protonation of poly(amidoamine) dendrimers is presented in chapter 2. The proton binding isotherms of the high generations are showing two steps, at $7.5 < \mathrm{pH} < 10$ and $4 < \mathrm{pH} < 7$, and an intermediate plateau at $7 < \mathrm{pH} < 8$, with the degree of protonation of 1/2. It was shown that the proton binding isotherms can be very well interpreted with a site binding model, which includes the microcopic protonation constants, and the nearest neighbor pairwise interactions as parameters. The model can be used for assessment of both macroscopic and microscopic protonation mechanism. In the case of poly(amidoamine) dendrimers, the proton binding isotherms can be described even for a large number of protonation sites, by using only six parameters. The cluster parameters can be unambiguously fitted from the experimental proton binding isotherms by starting from G0, where only three parameters are needed, and proceeding towards higher generations, by using always the same values of cluster parameters. In turn, the macroscopic pK values could be calculated from the site binding model. The comparison between the pK values which were obtained by direct fitting of the proton binding isotherms, and the pK values calculated from the cluster parameters, has shown a very good agreement.

Further analysis of the proton binding isotherms of poly(amidoamine) dendrimers was carried out in terms of a microscopic protonation mechanism, where the protonation species are distinguished by the distribution of the bound protons among the sites, as described in chapter 3. It was shown that for high generations, the plateau in the proton binding isotherm at $\theta = 1/2$ corresponds to an intermediate protnation microspecies where the outermost primary amine sites are protonated, while the rest of the sites are deprotonated. The intermediate species is evident at $7 < \mathrm{pH} < 8$. The microcopic protonation mechanism further

reveals that the primary amine groups protonate in the first step, which occurs at $7.5 < \mathrm{pH} < 10$. The inner part of the molecule protonates in the second step, which occurs at $4 < \mathrm{pH} < 7$. The last site to protonate is one of the innermost sites. This occurs at $\mathrm{pH} \approx 3.5$. The mechanism is the same for the low generations of poly(amidoamine) dendrimers (i.e. G0 and G1), except that the proton binding isotherms of these molecules attain a slightly different shape, due to a different proportion between the outermost primary, the innermost tertiary, and the rest of the sites.

A comparison between the protonation mechanisms of three different dendritic polyamine structures is presented in chapter 3. These include the poly(amidoamine) and poly(propyleneimine) dendrimer, and the (2,3) dendrimer, where the structure is the same as in the poly(propyleneimine) dendrimer, but with a short spacer between the innermost two sites. The agreement between the microscopic protonation constants for poly(amidoamine) and poly(propyleneimine) dendrimers is showing that the microscopic pK is inherent to a certain type of the protonation group, and its chemical environment. The comparison of the pair interaction parameters is showing that they depend on the spacer length between the neighboring protonation sites.

The microscopic protonation mechanisms of the three studied dendrimer structures turns out to be different. The poly(propyleneimine) dendrimers protonate with a prominent intermediate microspecies, where the sites in the odd shells, counting from the rim, are protonated. The rest of the sites, which reside in even shells counting from the rim, are deprotonated. This leads to a plateau in the proton binding isotherm at $\theta = 2/3$. The lowest generation of the (2,3) dendrimer protonates with a mechanism which is similar as for the poly(amidoamine) dendrimer, while the higher generations protonate with a mechanism, which is similar to poly(propyleneimine) dendrimers. However, the microspecies, which was observed for poly(amidoamine) dendrimers at $\theta = 1/2$, can be noticed even for high generations of the (2,3) dendrimer, but is less prominent than the mi-

crospecies with the shell-like protonation pattern.

The proton binding isotherms of the carboxylate latex particles in the presence of adsorbed strong cationic pDADMAC are presented in chapter 4. At different ionic strength, the proton binding isotherms are crossing in a common intersection point, where the surface potential equals zero. In this manner, this composite system is showing a behavior, which can be compared with the protonation behavior of amphoteric systems, like the metal oxides. The common intersection point corresponds to the point of zero charge, and can be used to evaluate the amount of adsorbed pDADMAC. For different pDADMAC loadings, the adsorbed amounts obtained in this manner are in a good agreement with the values which were determined in batch experiments. In this system, the point of zero charge is tunable by the amount of adsorbed pDADMAC. However, the point of zero charge can be observed only for low adsorption, where the ratio between the adsorbed pDADMAC sites, and the surface sites, is lower than unity. At higher adsorbed amounts, the surface charge is overcompensated by pDADMAC, and the surface can no longer bind protons in the experimental pH-window. The point of zero charge determined from the proton binding isotherms coincides with the isoelectric point, determined from the electrophoretic mobility measurements.

The proton binding isotherms of the carboxylate latex particles in the presence of adsorbed pDADMAC were interpreted in terms of Stern model. The basic Stern model has shown as inappropriate, since it could not reproduce correctly the point of zero charge. Much better results were obtained by implementing a modification of the basic Stern model, where the pDADMAC sites were treated as displaced from the surface origin. Having in mind the simplicity of this model, the fitting is surprisingly good.

The effect of the molecular mass of adsorbed pDADMAC, on the protonation behavior of silica, is shown in the last chapter. In this case as well, the proton binding isotherms are featured with a point of zero charge, which was used to determine the adsorbed amounts of pDADMAC. For two studied molecular masses,

namely that of 100-200 kDa and 400-500 kDa, the points of zero charge were found to coincide for the same adsorbed amounts. The modified Stern model, as presented in chapter 4, was here as well found to be appropriate for describing the proton binding isotherms.

As a part of this thesis, and with an invaluable effort of the department electronic workshop, an automated titrator was developed and called Jonction titrator. The routines were developed in order to perform potentiometric titrations at pre-set constant ionic strengths. The development of this setup is described in the appendix.

Appendix A

Automated potentiometric titrator

Introduction

In the initial stage of this work, constant ionic strength acid-base potentiometric titrations were performed with the Wallingford titrator, introduced and described by Kinniburgh and Milne [16]. The Wallingford titrator is featured with very good flexibility, and to my knowledge, it is the most widely used setup for this kind of experiments. Although not very user-friendly, this setup can be applied for a variety of titration tasks, including the conductivity titrations.

A new titration system, called "Jonction" titrator, was set up during the later stage of this work, based on the experience with the Wallingford titrator. For the new setup, Mr. Stephane Jeannerret, at the Department of inorganic, analytical, and applied chemistry at the University of Geneva, has built a high-impedancs voltmeter with an A/D converter unit, as a replacement of the robust Microlink 3000 interface of the Wallingford titrator. The rest of the hardware, namely the burettes and the stirrer, are the same. The basic routines for the communication between the hardware and the PC, as well as the electrode reading routines,

were all developed by Mr. Stephane Jeannerret. For all his effort, the author of this thesis owes him a huge credit. The constant ionic strength titration routines have been programmed by the author of this thesis. Our new software is programmed upon the LabView platform, which provides user-friendliness, although it requires a considerable amount of programming time. This text contains a brief description of the Wallingfdord titrator with a summary of my experience with that setup, and a thorough description of our own-built system. However, the main purpose is to provide a user-manual for the Jonction titrator.

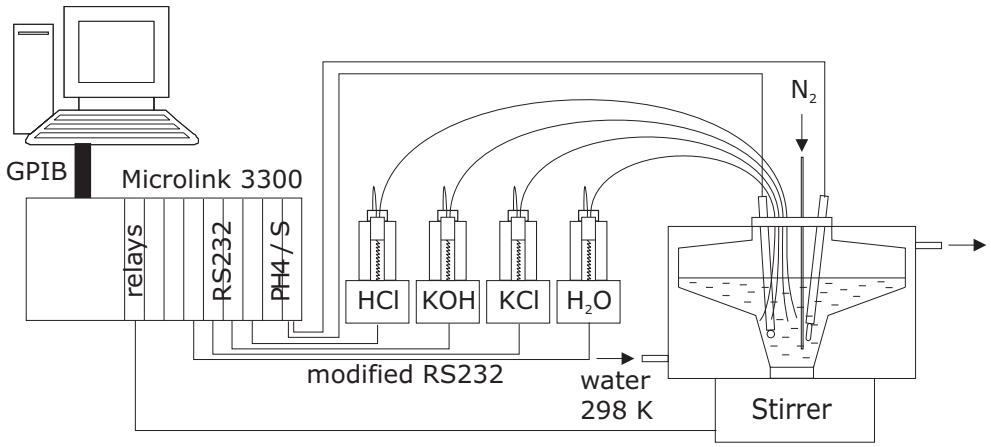

Figure A.1: Wallingford titrator.

Wallingford titrator

Hardware

The Wallingford titrator [16] hardware consists of:

- Four Metrohm 712 Dosimat burettes with tubings
- pH-measurement electrode couple
- Microlink 3300 interface with modules
- Titration cell
- Pure nitrogen degassing apparatus
- Conductivity meter (optional)
- PC

These components are connected according to the scheme depicted in figure A.1:

Metrohm 712 Dosimat burettes and the tubings Metrohm 712 Dosimat burettes consist of the main body, that embeds all the mechanic and electronic parts, and of an exchange unit, that embeds the bottle containing the dispensed liquid, the dispensing cylinder, and tubings. The exchange units can vary in the size of the dispensing cylynder. In this work, both 5 mL and 10 mL exchange units were used, without an observable difference in the precision of the results. An advantage of the 10 mL in front of the 5 mL unit is that the dispensing cylinder is less frequently filled, which in turn may prolongue the lifetime of the exchange unit and the mechanical parts of the burette. Highest care should be made that no air (or gas) is being dispensed, which would produce an error of the measured volume. Therefore, all the tubing connections should be well sealed. Operating the burette is simple, and while the titrator is not running, it can be accessed manually via the touchpad interface. Although the overall impression is that they are reliable and durable, occasional checks are recommended. Tubing fittings every time after disconnecting them, the glass cylinders have to be cleaned if they appear dirty or contain precipitate, and the pistons replaced if damaged. The taps can easily be replaced if they become blocked by some precipitate. A check by an official Metrohm mechanic is recommended (after cca 5000 hours of usage) for all the mechanical and electronic parts within the main body. It is recommended to check the precision of the piston walk on the same occasion. Directions for manually operating and maintaining the burettes can be found in the Metrohm burette manual.

In order to dispense volumes smaller than the size of a drop, the tubing endings were submerged into the solution. To minimize the diffusion flux of the ions through the tubing openings, the tubing endings were made of 0.2 mm inner diameter teflon tubing. Therefore, in order to minimize the dispensing pressure, the dispensing rate should not exceed 5 mL/min. Otherwise, leakages may occur.

Electrodes The pH measurement couple consists of two separate electrodes: glass electrode (Metrohm 6.0123.100) and Ag/AgCl reference electrode (Metrohm 6.0733.100).

pH-measurement couple specifications:

- Glass electrode:

  pH measuring range: 0...14

  Membrane glass type: U Membrane

  resistance: 150...500 MΩ

  Electrode slope: > 97 % of the ideal Nernst value

  Electrode zero point: 0 ± 15 mV

- Ag/AgCl reference electrode:

  Diaphragm: Ceramic pin

  Reference electrolyte: KCl, $c = 3\,\mathrm{M}$

  Diaphragm flow rate: 5...15 μL/h

  Diaphragm resistance: 0.4...0.9 kΩ

The performance of the electrode couple is measured by the stability of the reading expressed as the drift, and the time needed for equilibration after an abrupt change in pH of the medium. A satisfactory drift value is about 2×10^{-4} pH units per minute (ca 0.1 mV / min). This drift criterion should normally be achieved within no more than 5 minutes, except in the region around pH = 7, where the drifts are usually larger, and the equilibration time longer. While the above electrodes have shown good performance in solutions of simple acids or bases, their lifetime is becoming considerably shorter if they are used in suspensions. The problem usually arises from the deposition of the particles or polymers at the glass electrode surface, and at the ceramic diaphragm, which is the electric

contact of the reference electrode with the outer solution. This is very pronounced in the systems containing polyelectrolytes or colloidal particles, and even more in their mixtures.

Generally, the glass electrode is usually conditioned with HCl [100]. However, in the case when the electrodes were immersed into particle suspensions, there is no common way of conditioning, but it rather depends on the composition of the suspension. As a rule of a thumb, a good approach is to tune the pH of the conditioning solution, in order to achieve the conditions where the electrode charge is similar to the charge of the particle. In the case of polyelectrolytes adsorbed to the particles, one should as well consider the polyelectrolyte charge. In that case, one should tune the electrode charge according to the polyelectrolyte. For example, in the case of positively charged polyelectrolyte adsorbed on a negative surface (e.g. pDADMAC adsorbed onto carboxylated latex), the electrodes should be conditioned in 0.1 M HCl. Very unstable response, especially in the basic pH region, was observed after using the electrodes in suspensions of metal oxides (e.g. SiO_2, TiO_2). In the case of silica, this is probably due to deposition at the glass electrode surface, and blocking of the reference electrode ceramic diaphragm by the particles. While a good rinse with a surfactant solution (1 % Hellmanex) is sufficient for the glass electrode, one should condition the reference electrode in 1 M HNO_3 for several hours. Changing the inner solution after conditioning the reference electrode is recommended. Finally, if the electrodes are showing bad response even after conditioning, they should be replaced.

Microlink 3300 interface and PC requirements Microlink 3300 is an interface that provides computer control over all the hardware used in the Wallingford titrator setup. It belongs to a wider family of Microlink 3000 series interfaces, with a GPIB connection to the PC. Other models (3200, 3301, etc.) can be connected via RS 232, Ethernet, or both. The GPIB connection at the PC end can be achieved through a PC card. In that case, one first has to install the driver

software, which is supplied together with the interface.

The Microlink 3300 interface contains power supply and a control card that handles the communication with the computer. It can port a number of various modules, which appear as integrated circuit boards. The modules can serve for various tasks, ranging from time counting, analogue signal aquirement and modulation, high-speed signal scanning, to digital signal processing and device control by means of relays. This gives the Wallingford titrator setup the flexibility to be used in conjunction with various other devices.

The standard Wallingford titrator setup makes use of nine modules. Two pH measurement modules (PH4/S), six RS232 interface modules for burette and conductivity meter communication, and a relay module for the stirrer control. This allows connection and reading of up to eight ISE-reference electrode couples, a conductivity meter, five burettes and the stirrer (which makes use of only one of the eight relays). In principle, the RS232 and relay modules could as well be used for other purposes, but the Wallingford titrator software is not suitable for that.

PH4 / S module This module combines eight high impedance analogue inputs and an integrating A-D converter with a 4.5 digit resolution. The integrating period of 400 ms allows up to 2.5 readings per second, and is sufficiently long to eliminate both 50 and 60 Hz interferences. Eight high impedance inputs can host up to four ion selective - reference electrode couples. The ion selective electrode inputs are BNC sockets, while the reference electrode inputs are standard banana sockets. Other specifications are:

Voltage range: $-1.9999\,\mathrm{V}...1.9999\,\mathrm{V}$

Input current: $10\,\mathrm{pA}$

Input impedance: $1\,\mathrm{T\Omega}$

A/D converter: 4.5 digit precision, dual-slope, integrating

Conversion time: $400\,\mathrm{ms}$

Integration time: $0.1\,\mathrm{s}$ (rejects 50 and 60 Hz)

Accuracy: $\pm 0.03\,\%$ of reading ± 2 l.s. digits

RS 232 module The RS 232 modules are used for the control of the burettes and the conductivity meter. Attention should be paid to the cables that are used to connect the Metrohm 762 Dosimat burettes with the module. The pin assignment is different at the two ends. This is due to the fact that the RS 232 module belongs to data terminal equipment (DTE) standard, while the computer belongs to data communication equipment (DCE) standard. The cables must be adapted according to the scheme which can be found in the instrument manual or [16].

The baud rate, parity, stop bits and XON-XOFF modes are preset by the manufacturer. An address, set by DIP switches that are found on the integrated

circuit board, is assigned to each module, and is normally preset by the manufacturer. It should be adjusted if the ports of the modules are changed. The sequence of the module addresses has to go from lower to higher numbers, from left to right respective to the main frame.

Conductivity meter and conductivity cell (optional) Conductometric titrations are one more option of the Wallingford titrator. For that, one needs a Metrohm 712 conductivity meter connected to the Microlink 3300 interface through a RS 232 module. During this work, it was established that the conductivity meter should be connected at an address which is higher than all the burette addresses. Otherwise, the communication may fail. The settings for the conductivity meter are:

baud rate=9600

data bit=7

stop bit=1

parity=even

handshake=none

RS232 control=ON.

Other conductivity meter specifications are:

Measurement range: 0..20 S/cm

Max. conductivity resolution: 4.5 digits

The conductivity cell used in this work is an epoxy-body Accumet (Cat. no. 13-620-161) cell with two platinum electrodes. The cell constant is 0.1 cm^{-1}. The epoxy sleeve around the platinum plates was removed to achieve a better flow of the solution into the space between the electrodes.

PC Since the Wallingford titrator software is running under DOS, the requirements for the PC are rather minimal: an IBM-compatible PC with installed DOS. However, from my experience, the communication with the Microlink 3200 interface is not achievable with any computer: the reasons could be in the talk-listen delays or data buffering properties of a particular PC. This can change from one PC to another.

Software

The Wallingford titrator software is actually a programming language, with a structure similar to Fortran. The language consists of settings and commands. In the settings, the user can define the features that are constant during an experiment. This includes the hardware settings (e.g. the devices that are used, the burettes settings), and other features like the electrode reading criterion, stirring status etc. The commands can be regarded as subroutines, which can be called from the main routine. The experimental procedure is defined in the main routine, which can contain loops, conditional statements, and calculations. User-defined or pre-defined (e.g. current reading of the EMF, dosed volumes, etc.) variables can be used as arguments for commands or for programming purposes. These programming features provide enough flexibility to develop even very advanced titration routines. More details about this language can be found in [16].

Some minor problems connected with the Wallingford titrator software were spotted in the course of this thesis. The drift reading conditions are not obeyed, and the salt additions upon using the TITRATI command were observed as not precise. The latter can be bridged by programming the constant ionic strength routines from scratch, by using the very neat programming possibility of the Wallingford titrator software. However, for an unexperienced user, this might be time-consuming.

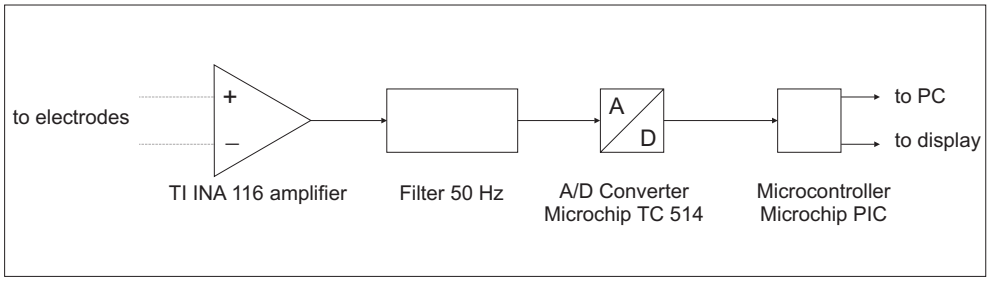

Figure A.2: Scheme of the signal processing by the HighImp4 instrument.

Jonction titrator

As a difference to the Wallingford titrator, the Microlink 3200 interface was eliminated from Jonction titrator setup. Therefore, a voltmeter that communicates directly with the PC through a RS232 connection was constructed by Mr. Stephane Jeannerret. The communication between the burettes and the PC is established directly, by using the RS232 connections as well. Except for the drivers and some simple supporting routines for the burettes, which were found on the web page of National Instruments (http://www.ni.com/support/), all the necessary software was originally developed in the Labview programming language. By the time of this manuscript, the PC control of the conductivity meter reading and the stirrer were not included in our setup. A scheme of our new setup is presented in chapter 1.

Hardware

Highimp4 instrument HighImp4 is an instrument which embeds a high-impedance voltmeter and an A/D converter. The instrument was developed by Mr. Stephane Jeannerret at the Department of inorganic, analytical and applied chemistry at the University of Geneva. All the technical details about this device, and the according low-level Labview programs (drivers) can be found in [101]. The signal processing by this instrument is depicted in figure A.2.

PC requirements To run Labview, the PC should be equipped with a 200 MHz processor unit, 32 MB RAM, and Windows '98 version installed. Though, higher speed processors and more RAM are desirable for code development. From the hardware side, the PC has to be equipped with at least five serial ports (one for the HighImp4, and the rest for the burettes).

Software

The software for Jonction titrator is fully developed under the Labview platform. LabView is a very powerful application software, intended for the control of peripheric instruments by a PC, acquirement and modulation of meter readings, virtual signal processing etc. While the possibilities of this software seem endless, we have used only the least necessary to develop the constant ionic strength potentiometric titration procedures. In general, LabView programs consist of two parts, namely the user interface and the code. The user interface is presented as a console of a virtual instrument, and contains all the input and output variables, organized as controls or indicators. The controls can be modified by the user, and are displayed in forms of buttons for boolean variables, numeric fields or turnable buttons for numeric variables, etc. The indicators are just showing the current values of variables, and are being displayed in forms of led indicators for boolean, numeric fields for numeric variables, graphs for numeric arrays, etc. All the values of these variables are constantly updated in real time.

Jonction titrator program has a hierarchical concept, as shown in figure A.3. The user has to start the main program, which is calling various subroutines. As well as the main program, the subroutines too have an user interface. The user has to be acquainted only with the interfaces of the two highest levels in order to run experiments. While some subroutines are interactive, which means that the user is asked for input, the others are not. These are just displaying some indicator variables, and performing calculations in the background. If it does not

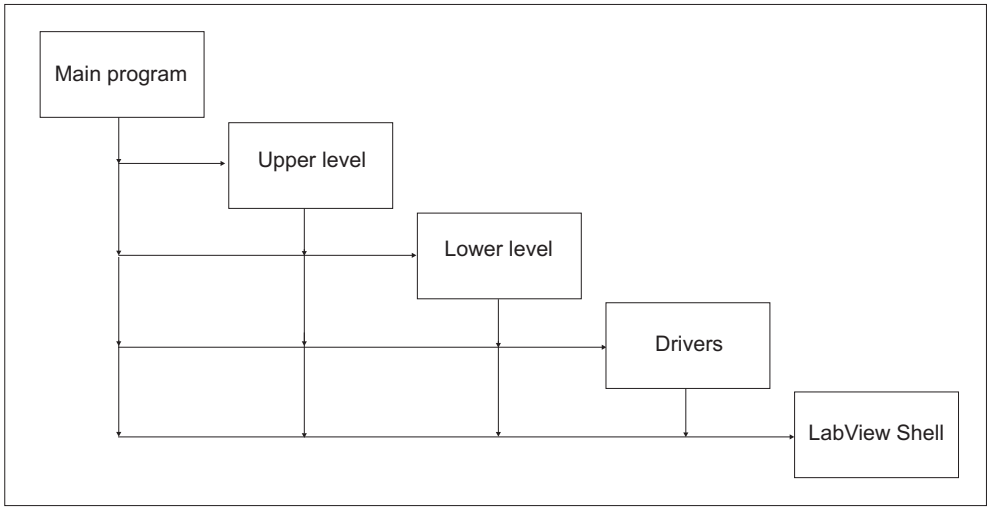

Figure A.3: Scheme of the Jonction titrator software hierarchy. The arrows define the directions in the communication between different levels.

contain any important information, the user interface of a subroutine is hidden while the main program is running.

Experimental modes There are several experimental scenarios (see figure A.4), which are defined by a choice of three boolean controls: titrant additions (constant or dynamic) , direction (one way or forth-back), and ionic strength (variable or constant).

The titrant addition control defines the mode which is used to calculate the titrant additions: in the dynamic mode, for each titration step, the addition is calculated in order to achieve a pre-defined difference in pH which is constant for the whole run (see figure A.5). In the constant mode, the titrant additions are pre-defined and constant (see figure A.5).

The direction selection is possible only in the dynamic mode, and defines whether the dynamic mode will be used for both directions, or the constant mode will be applied during the back-run. This is useful if the back-run is preferred to be accelerated for some reasons. It is emphasized that in all scenarios, the titrator

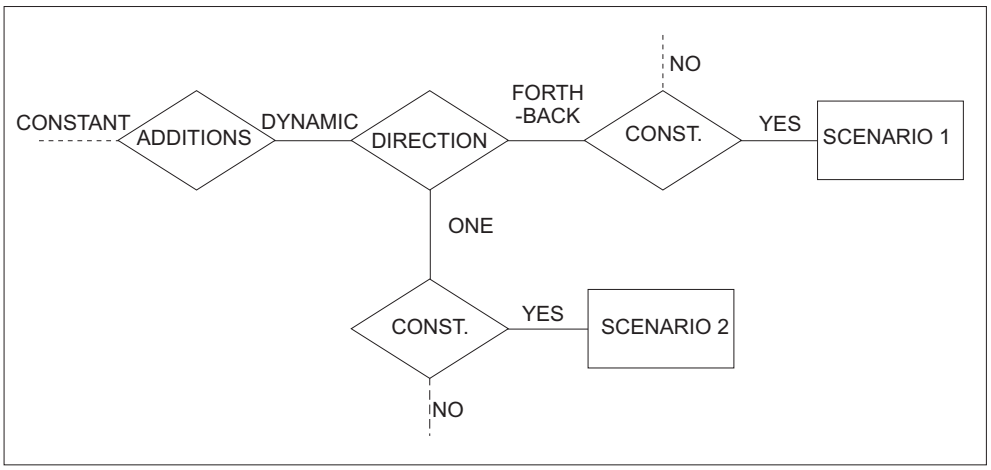

Figure A.4: Experimental scenarios with Jonction titrator. The bare arms in the flowchart denote directions which were still not implemented at the time of this manuscript.

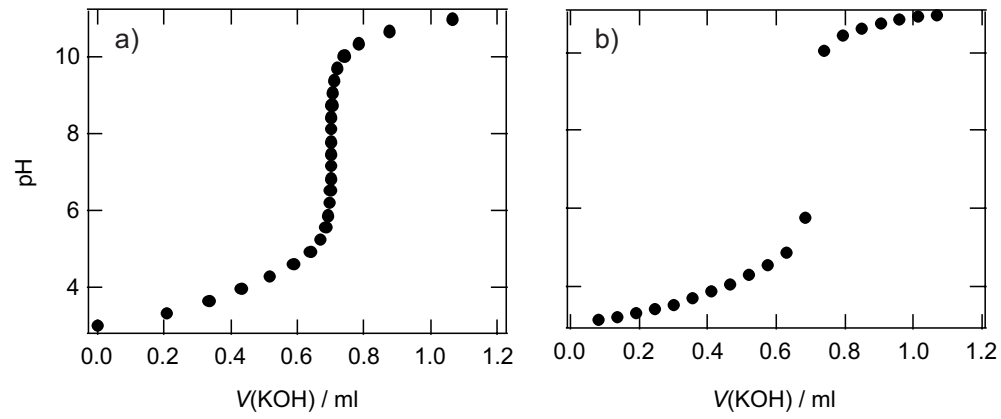

Figure A.5: Titration curves obtained with a) dynamic and b) constant titrant addition modes.

performs forth and back titration runs. The ionic strength control lets the user choose whether the titrator should attempt to maintain a pre-defined constant ionic strength in the system during the titration. A constant ionic strength can be maintained by adding salt or water in order to correct for the change produced by an acid or base addition. The variable ionic stength scenario is previewed for a setup with only two burettes, but so far not implemented, and will therefore be omitted in the further text.

Output files There are several output files of Jonction titrator. The data file and the log file are created automatically during the experiment. There are possibilities to save the experimental parameters and calibration data into files with extensions .par and .cal, respectively.

Data output file (.txt) This file contains the output data, which are written to the file every time a reading has been acquired. The data are organized in columns, in the following order: total volume of the solution in the cell (including the sample), burette1, burette2, burette3, burette4 volumes (in milliliters), calibrated reading value (usually pH, see "Calibrated reading value acquisition"), drift, standard deviation (explanations of these terms can be found in paragraph Calibrated reading value acquisition subroutine).

Log file (.txt.log) The log file serves for recording the actions that were taken during an experiment, and the times when they occurred. As well, at the beginning of this file, all the experimental parameters are found. Actually, most of the reported actions are automatically taken by the program (e.g. acquirements of the electrode reading, salt addition to increase the ionic strength, or changing the direction of the pH change between "forth" to "back", etc.).

Running Jonction titrator

From the software side, all what is needed to run an experiment is to know how to use LabView interfaces of the main program and the upper level subroutines (see figure A.3). In the chapters below follow the descriptions of the experimental steps and the according interfaces, in a sequence as they appear in an actual experiment. The relevant controls and indicators are found in the upper parts of the windows. The lower parts contain only indicators that are of no importance for the user, and are therefore shaded out. In later chapters, more information will be given about the other non-interactive subroutines and the actual code of Jonction titrator program. The experiment usually consists of two independent parts: calibration of the electrodes, and titration. The program needs the calibration parameters for the conversion of the raw electrode reading into pH.

Jonction titrator main program (Titrator_dusko.vi) The main program is contained in the LabView file Titrator_dusko.vi. Opening this file by double-clicking on it will start LabView, and the user interface of the main program will appear on the screen (see figure A.6). The user has to launch the program, by pressing Ctrl+R, or by choosing "Start" from "Operate" menu, or clicking on the white flesh in the toolbar. Immediately after launching, the program initializes HighImp4, which is announced on the screen. After that, the program is calling the subroutine for entering various experimental parameters (see SV_Titr_enter_par_multi_test.vi). The user interface of that subroutine automatically appears on the screen. After user closes that, the subroutine for burette assignment (see Prod_assign.vi) is called. Upon quitting on command, the main program performs burette initialization, where the communication is established and some settings are passed to them (limiting volumes, filling and dispensing rates), which should take less than 5 seconds. After that, the program will initialize the log file, and then wait for further commands. This is announced by

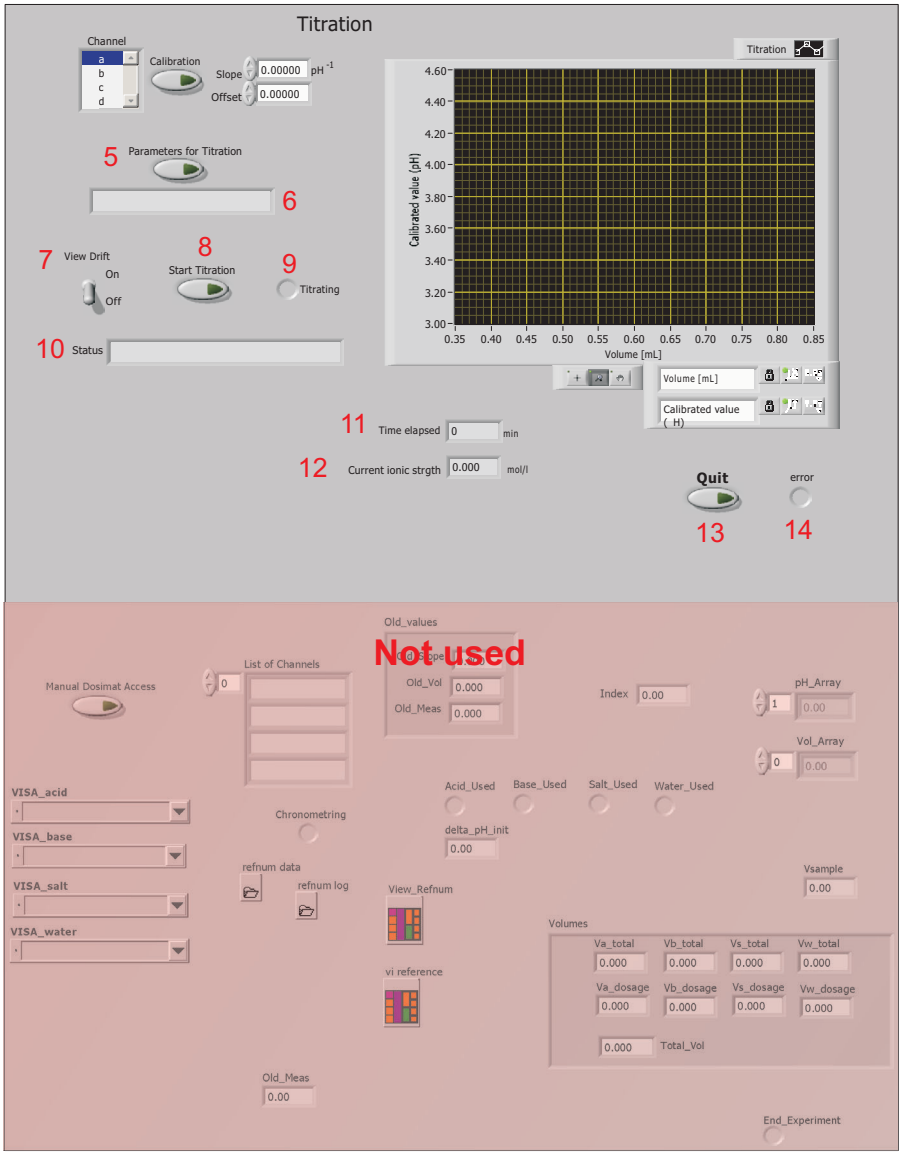

Figure A.6: Main program user interface. The controls in the lower part can not be changed by user.

the message "Idle" in the status indicator. The commands that can be given at this point, by clicking one of the buttons, are: "Calibration", "Parameters for titration", "Titration", or "Quit". Clicking on the "Parameters for titration" button will again launch the subroutine for parameter setting (if a check or change is desired), while the "Quit" button will stop the experiment and LabView will be closed. The button "Calibration" will launch the calibration subroutine (see SV_HighImp4_Set_Calib_Parms.vi). If the calibration parameters are a priori known, the calibration is not necessary. Then the parameter values have to be entered in the "Slope" and "Offset" fields (see figure A.6.). Once the calibration parameters are defined, the titration may be launched, by pressing the "Titration" button. At that event, the timer is started. The program continues by initializing the data file and writing "Start titration", the date and time to it, and filling burette cylinders. The titration starts by an addition of water, salt, and acid or base, in order to achieve the initial pH, ionic strength, and the initial total volume (the calculation of the additions is previously performed by a non-interactive subroutine, see init_dose_calc.vi). After that, an adjustment of the initial pH in the cell is performed (see SV_adjust_pH.vi). Usually, this step is needed only when the initial solution contains some substance undergoing dissociation, and not needed for the blank titrations. Then, the titrations are performed under the conditions that have previously been defined (several possible experimental scenarios are described in figure A.4.). The subroutine which performs the dynamic constant ionic strength titration in one direction, between pre-defined initial and final pH, is SV_titra_dyn_cnst_I_forth1.vi. For the dynamic mode forth-and-back titrations at constant ionic strength, it is invoked in loops where the directions (inner loop) and ionic strengths (outer loop) are varied. After the titrations have been finished at the highest defined ionic strength, the program will close the data file, stop the chronometer, and wait for further commands ("Idle state, waiting for command" is announced in the status indicator). If desired, the experiments can be repeated (the system in the titration cell has

to be exchanged though), or the main program can be quitted by clicking the "Quit" button. In the latter case, the communications with burettes are terminated (the burettes are switched to manual control), the log file is closed, and LabView is quitted. If the program is terminated by choosing "Stop" from the "Operate" menu (Or clicking at the stop icon in the toolbar), the communications with burettes are not properly terminated, and the control over them is not switched to manual. In that case, to gain manual control over the burettes, one needs to reset their power supply.

Here follows the description of the controls and indicators:

1. "Channel" control: Lets the user choose the HighImp4 channel that will be used for the electrode reading.

2. "Calibration" trigger button: The button will start the calibration subroutine, which is described below.

3. "Slope" and "Offset" controls: The two controls let the user enter the parameters of the calibration line, which will be used to convert the reading signal into pH. These fields are used if the calibration line parameters are a priori known, and no electrode calibration is needed.

4. Titration curve graphic: The graphic displays the complete titration curve of the most recent run.

5. "Parameters" button: The button triggers the SV_Titr_Enter_Par_Multi_test.vi subroutine, where most of the important controls for the titration are being set.

6. "Parameter file" indicator: Indicates a filename if the parameters have been saved.

7. "View drift" switch: The switch triggers the window for a graphic that displays electrode reading versus time. This window will be active on the

desktop while the main program is running, until the switch is set to "off".

8. "Start titration" button: The button starts the experiment.

9. "Titrating" led indicator: The indicator is lit on while the experiment is running.

10. "Status" indicator: Indicates the current activity of the instrument.

11. "Time elapsed" indicator: Indicates the time elapsed after the titration was launched by clicking "Start titration" button.

12. "Current ionic strength" indicator: Indicates the ionic strength.

13. "Quit" button: The button terminates the program and LabView.

14. "Error" led indicator: Indicator is lit on if some error occurred during the run.

Global parameters (SV_Titr_enter_par_multi_test.vi) In this subroutine, the user has to define all the paramteres that are used to control the experiment (in the code, they are located in the global parameter cluster (global parameters are the parameters which are accessible to all subroutines). Description of the user interface controls and indicators:

Common controls:

1. "Waiting time after dispensing" control: Lets the user set the time for which the titrator will wait after dispensing acid, base, salt and water. Or example, this time could be needed for mixing.

2. Drift criterion: The user must enter the drift in pH/s (here, pH refers to the unit of the calibrated reading value) that the titrator will use as the reading criterion.

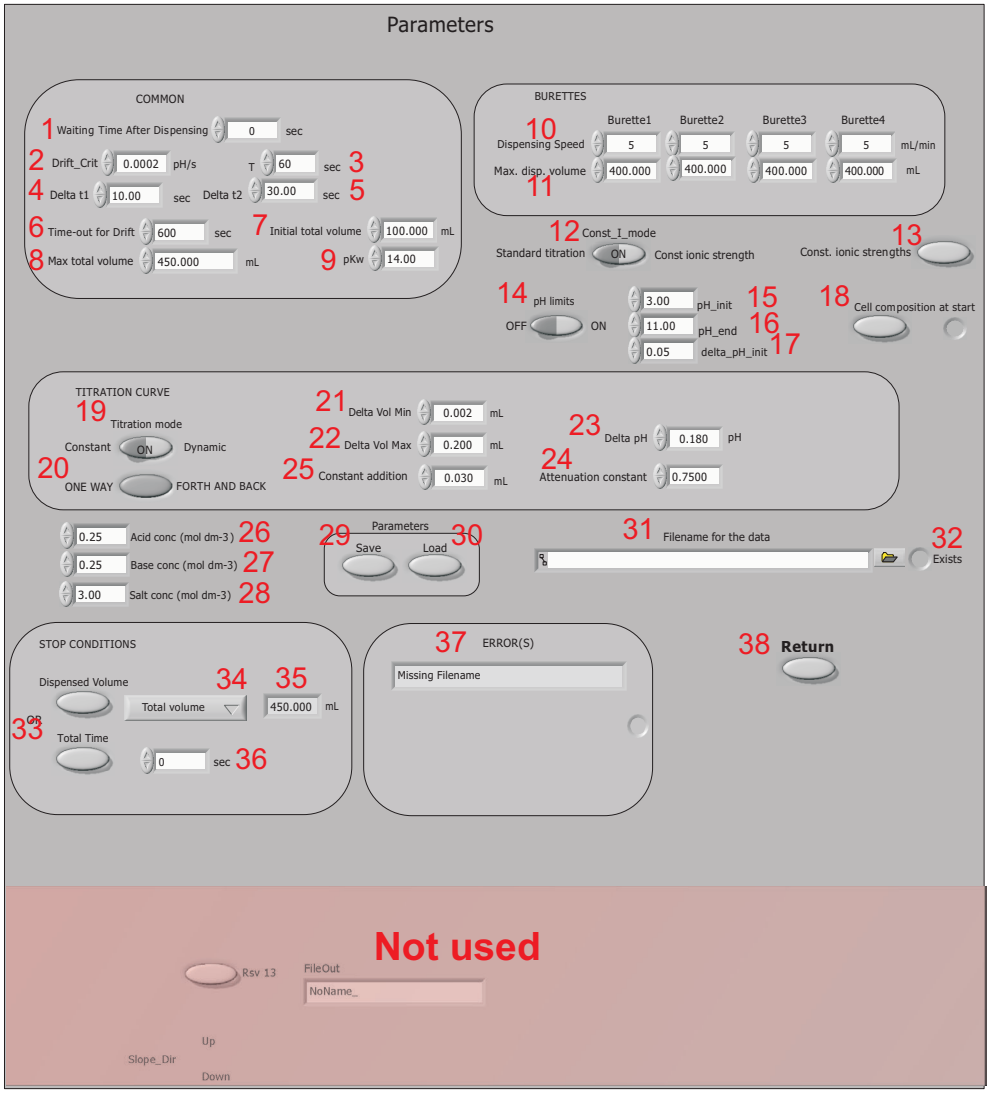

Figure A.7: The user interface of the parameter assignment subroutine.

3. "Drift monitoring time": The control for setting the time during which the drift is monitored. If the reading criterion is weak, this will be the time gap between two readings (see "Calibrated reading value acquisition").

4. "Delta t1": First reading period (see "Calibrated reading value acquisition" paragraph, below).

5. "Delta t2": Second reading period.

6. "Time out for drift": The control for setting the maximum waiting time for satisfying the drift criterion.

7. "Initial total volume": The control for setting the initial volume in the titration vessel. Minimum initial total volume is determined by the cell geometry and the electrodes (the limitation is that the electrodes have to be sufficiently immersed into the solution). For the cell in figure 1.4, it is cca 45 mL. However, this volume has to be larger than the sum of the sample volume and the initial dosages of acid or base and salt. Otherwise, the initial burette additions can not be calculated.

8. "Maximum total volume": The control for setting the maximum volume that can be achieved in the experiment, if the total volume condition is chosen (see control 34). This volume is determined by the size of the cell.

9. "pKw": The control for setting the ionic product of water (depends on the temperature, pKw=14.00 at 298 K).

   Burette settings:

10. "Dispensing speed": The control for setting the dispensing rate. The value depends on the tubing diameter.

11. "Maximum dispensed volume": The security setting for the maximum volume that can be dispensed from a burette during an experiment.

12. "Const_I_mode" switch: Lets the user choose between the constant ionic strength and standard titrations (in spite of the fact that the constant ionic strength are commonly done and could be called "standard").

13. "Constant ionic strengths" button: The button triggers the subroutine where the ionic strengths are being set (Cnst_I_par.vi).

14. "pH limits" switch: Previewed for the choice between the mode where the pH is swept in a pre-defined range, and a mode where the pH range is not defined, so that the experiment is terminated according to the conditions defined through controls 33 to 36, or manually. However, at the time of this manuscript this option was not implemented.

15. "pH_init": The control for setting the initial pH in the experiment. The initial solution is automatically dosed to achieve the initial pH. If the cell contains a substance that undergoes dissociation, manually dosed prior to starting the experiment, the pH will be automatically adjusted to the initial value.

16. "pH_end": The final pH in a titration run.

17. "Delta_pH_init" control: Lets the user set the convergence criterion for the initial pH setting (see SV_cnst_mode.vi).

18. "Cell composition at start" button: The button triggers the subroutine where the user can enter the content of the cell that was manually dosed prior to the current experiment (see cell_comp.vi).

Titration curve settings:

19. "Titration mode" switch: Lets the user choose between dynamic and constant additions mode (see the paragraph about the experimental modes). If the constant mode is used, then the controls 21 to 24 are not accessible.

20. "Direction" switch: Lets the user choose between "One way" and "Froth and back" modes.

21. "Delta vol min" control: The minimum volume of the titrant that can be dispensed in the dynamic mode. It is recommended to set this to a low value (e.g. 0.005 mL).

22. "Delta vol max" control: The maximum volume of the titrant that can be added in dynamic mode. It is recommended to set this to a value between 0.2 and 1.0 mL, depending on the concentrations of acid and base in the burettes.

23. "Delta pH": The control for setting of the aimed pH increment.

24. "Attenuation factor": The control for setting the attenuation factor (see SV_titra_dyn_cnst_I_forth1.vi).

25. "Constant additions": The constant additions of the titrant, used in the constant mode. This value is also used for the first step addition in the dynamic mode.

26. Control for entering the concentration of the acid in the burette

27. Control for entering the concentration of the base in the burette

28. Control for entering the concentration of the monovalent salt in the burette

29. Saving the parameters entered in the fields on the disk.

30. Loading the parameters from a (.par) file.

31. "Filename for the data": The control for entering the filename and the full path for the data file.

32. "Exists" led indicator: Flashes if the data file already exists. In that case, it will be overwritten.

Stop conditions:

33. "Dispensed volume" and "Total time" switches: Let the user choose between two conditions for automatic stopping the experiment: volume and time (see further).

34. If the user chooses the volume condition for terminating the experiment, he has to specify which one: the total volume in the cell (choice 0), or the dispensed volume from one of the burettes (choices 1-4). It is recommended to use the total volume condition, as a prevention from overflowing the cell: if not stopped by finishing the experimental task (see A), the experiment will stop if the total volume of the solution exceeds the maximum value, defined in control 8.

35. Volume indicator: it indicates the volume at which the experiment will be terminated (only if the "Dispensed volume" switch is set to true). If it is the total cell volume, the value from control 8. is displayed. Otherwise one of the values from controls 11. will be displayed, depending on the choice of the burette in 34.

36. Here, the total time stop condition value is being set (only if the "total time" condition was chosen in 33).

37. Error indicator: Some of the common errors in the parameter values, which can be recognized by the program, are indicated. If there are errors, the led indicator in this field flashes.

38. "Return" trigger button: Terminates the subroutine.

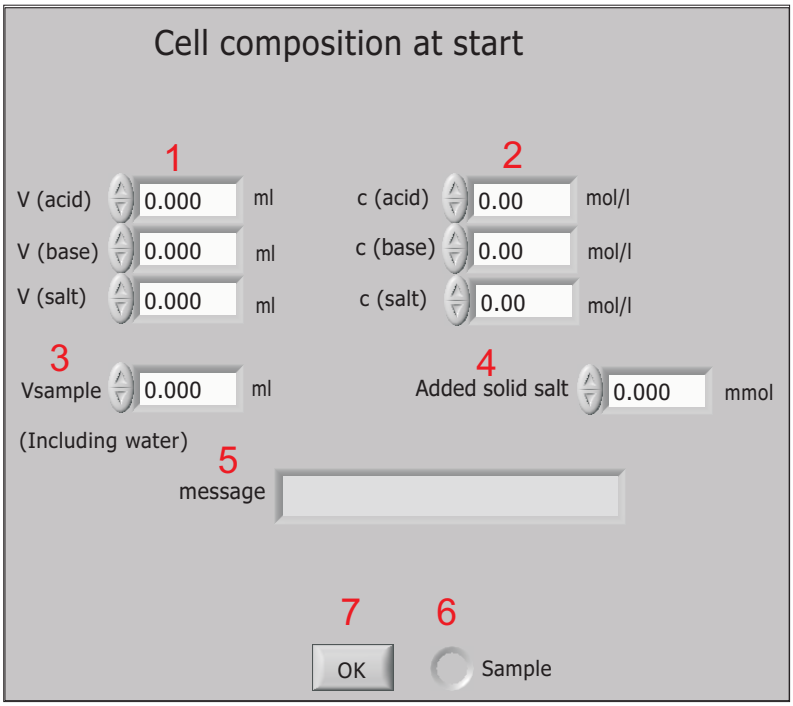

Figure A.8: The user interface for defining the initial cell composition.

Cell composition at start (cell_comp.vi) In this subroutine, the composition of the cell prior to the titration experiment has to be defined. The cell can contain strong acid or base, 1:1 salt in form of solution or solid, water or some unknown liquid sample. In the case of strong electrolytes, the volumes and the concentrations of the added solutions have to be transmitted to the program, so that it could account for the ionic strength change caused by this. Water and unknown sample are just accounted as an extra volume.

Description of the controls and indicators:

1. "V(acid)", "V(base)" and "V(salt)": The controls for input of volumes of strong acid, strong base and salt (1:1), respectively, added to the cell prior to the titration experiment.

2. "c(acid)", "c(base)" and "c(salt)" controls: The input of concentrations of

the strong acid, strong base and salt solutions that were added to the cell prior to the titration experiment.

3. "V(sample)" control: Input of the total volume of all the components added to the cell prior to the titration experiment, including water and weak electrolytes.

4. "Added solid salt": The control for input of the moles of solid 1:1 salt added to the cell prior to the experiment.

5. "message": If a value smaller than 0 has been entered in the above controls, an error message will be indicated.

6. "Sample" led indicator: Flashes if an entry was made in the above controls.

7. "OK" button: Triggers quitting from the subroutine.

Burette assignment (prod_assign.vi) In this subroutine, acid, base, salt or water can be assigned to each burette. The burette numbers are defined by their VISA addresses (in LabView, every external device has to be assigned a logical address), which are in turn related to the ports where they are connected. It is logical that one keeps the order of the burettes at the bench in the sequence of their visa addresses, such that burette1 is the one on the left, and burette4 the one on the right side. However, it does not matter which solution is contained in which burette, as long as all of them are different. This was done in order to provide the freedom for the user to exchange the upper units of the burettes without having to intervene in the titrator code. A warning will appear in the message box if the burettes are ambiguously assigned (e.g. acid assigned to more than one burette). This subroutine closes upon clicking the OK button.

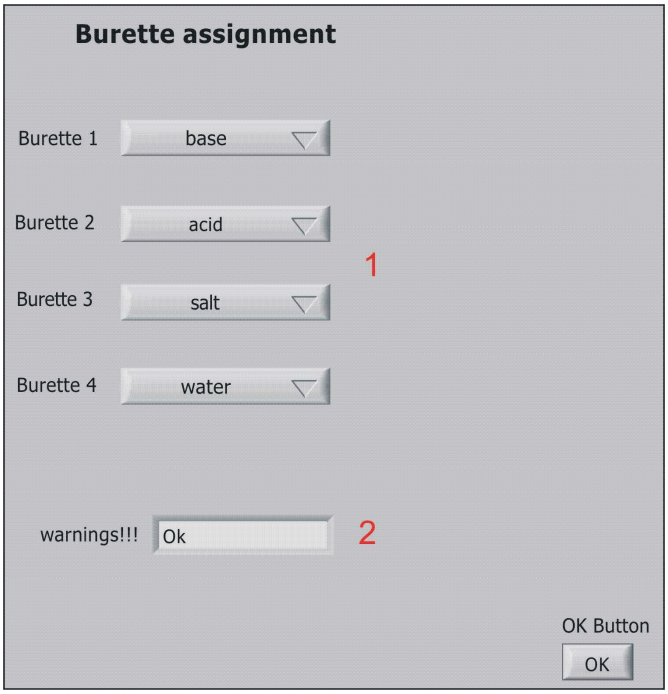

Figure A.9: The user interface for burette assignment.

Description of controls and indicators:

1. "Burette n" control: Here, the user has to assign acid, base, salt and water to each burette (i.e. VISA address).

2. "Warnings": Indicates a warning if the same solution is assigned to different burettes. Otherwise, "OK" is displayed.

Calibration (SV_HighImp4_Set_Calib_Parms.vi) Due to the analog-digital conversion, the values sent to the PC by the HighImp4 instrument, are not calibrated on the absolute voltage scale, but rather some "raw" values. For the calibration, standard buffer solutions are needed, thermostated to the experimental temperature. The a priori known values can be given in pH units, millivolts etc., which will in turn determine the units of the calibrated signal. To update the calibration, the user has to enter a known value in the field at right, and then click on the field at left.

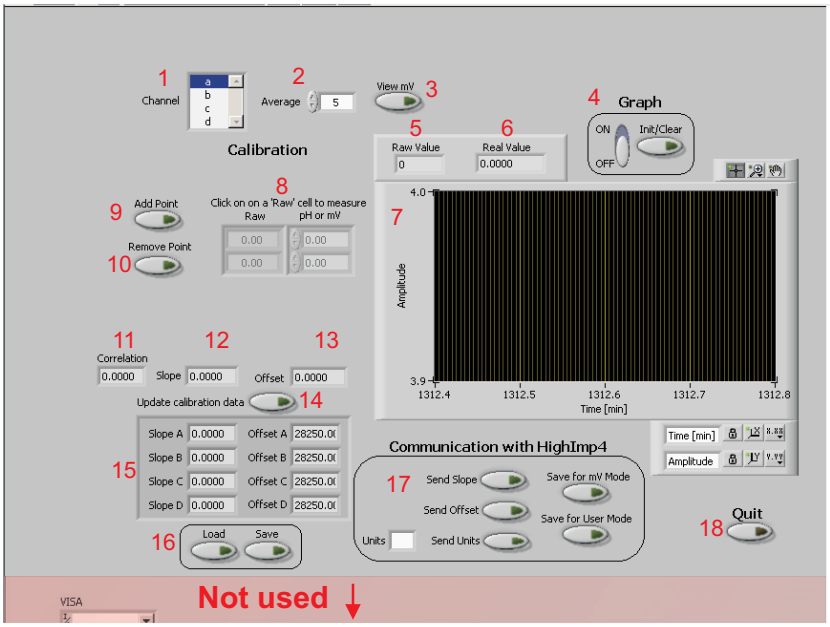

Figure A.10: The user interface for the electrode calibration.

Controls and indicators:

1. "Channel" selection: lets the user choose the voltmeter channel that will be used for the electrode reading and calibration.
2. "Average" control: the user can choose the number of points for block-averaging
3. "View mV" switch: sets the value displayed in the graphic. It can be in millivolts (obtained by a rough internal calibration of the instrument), or the calibrated signal, obtained from the raw values by using the current values of the calibration parameters.
4. "Graph" controls: the switch to the left is used to display the time dependency of the reading value in the graph below, and the one to the right to clear the graph.
5. "Raw value" indicator: indicates the currently read raw value at the preset channel.
6. "Real value" indicator: indicates the current calibrated signal.
7. Display for the time dependency of the reading value (in millivolts or calibrated value, depending on the position of the switch 3).
8. The array of calibration points, i.e. the raw values (left) and some calibrated values that are known a priori (right).
9. "Add point" buttons: the user can set as many as ten calibration points.
10. "Remove point" button: To remove points.
11. "Correlation" indicator: indicates the coefficient of correlation for the calibration data.

12. "Slope" indicator: the slope of the calibration line.

13. "Offset" indicator: the offset of the calibration line.

14. "Update calibration data" button: upon pressing, the calibration parameters (slope and offset) are saved for the experiment.

15. Indicators of the calibration parameters for each channel.

16. "Load" and "Save" buttons: serve for loading the parameters from a file or saving them.

17. "Communication with HighImp4" buttons: serve to transfer the calibration parameters and the used units to the voltmeter, which will change the value displayed on the voltmeter display.

18. "Quit" button: serves to quit the calibration subroutine, and return to the main program.

pH adjustment subroutine (SV_adjust_pH.vi) Controls and indicators:

1. "Current measure" indicator: the user can read the current c.r.v.

2. "Split dose" led indicator: flashes when the titrant dose was decreased by half (see SV_cnst_mode.vi).

3. "Exit" led indicator: flashes when the convergence criterion was satisfied and the subroutine automatically closed.

4. "View drift" switch: the user can turn on the time dependency of the calibrated signal graphic (same as switch 7 in Titrator_dusko.vi).

5. "Variable regulation" switch: turns on the controls for the below variables.

6. "Convergence criterion" control: (same as 17 in section SV_Titr_enter_par_multi_test.vi).

7. "Initial pH" control: the user can adjust the pH that is being set. However, this will not affect the initial pH variable set in the subroutine for entering the parameters (SV_Titr_enter_par_multi_test.vi).

8. "Constant addition" control: the user can adjust the additions of the acid or base used in the pH adjustment procedure.

Dynamic mode titration procedure(SV_titra_dyn_cnst_I_forth1.vi) Commands and indicators:

1. "Current volume" indicator: indicates the volume of the titrant dispensed in the current titration run.

2. "Current measure" indicator: displays the last acquired c.r.v. (pH).

3. "Index" indicator: indicates the number of the data point currently acquired (or the total number of acquired points in the current titration run).

4. "Limited" led indicator: indicates whether the calculated addition volume was inside limits which were set as parameters, or it had to be corrected (see the chapter about the dynamic titration procedure).

5. Titration curve graphic: all the points [c.r.v., titrant volume] of the current titration run are displayed.

6. "Error" led indicator: this will indicate some errors that may occur during the titration (e.g. a burette was not properly assigned to the titrant solution, the maximum dispensing volume for the titrant burette was exceeded, etc.).

Algorithms

Data acquisition subroutine (SV_read_all_and_write_to_data.vi) The flowchart of the data acquisition subroutine is presented in the figure A. The

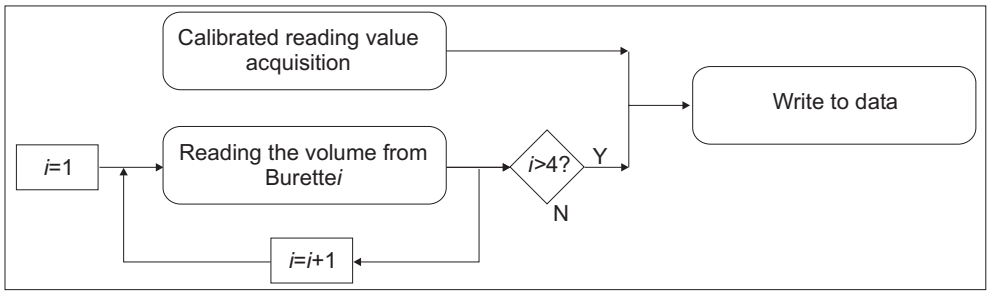

Figure A.11: The data acquisition subroutine flowchart.

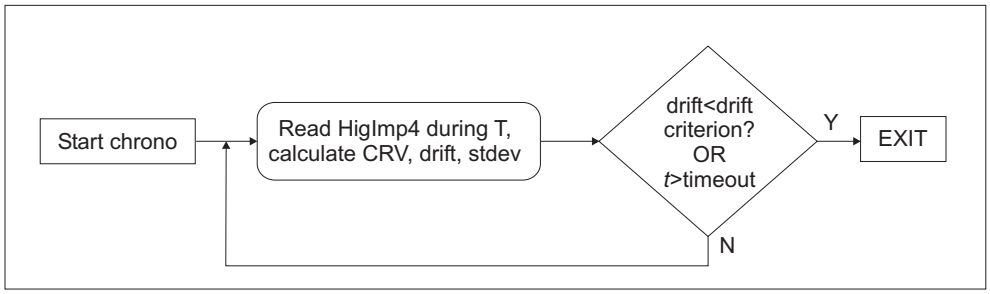

Figure A.12: The calibrated reading value acquisition flowchart.

c.r.v. is acquired simultaneously as the volumes from all the burettes. These values are being written to the data file. The time delay for this subroutine is given by the time delay for the c.r.v. acquisition.

Calibrated reading value acquisition subroutine (SV_HighImp4_Acq_Drift.vi) The flowchart of the c.r.v. acquisition subroutine is depicted in the figure A.12.

The core of this subroutine is the middle part, where the c.r.v. (Calibrated reading value), drift and standard deviation are being calculated. The calibrated reading value is the value acquired as a valid reading, according to the drift or time-out criterion, in the units of the calibrated signal. The calculation is done in the following manner: The raw signal is continuously acquired and recalculated into the calibrated signal during a time T (see figure A.13). Time T is divided

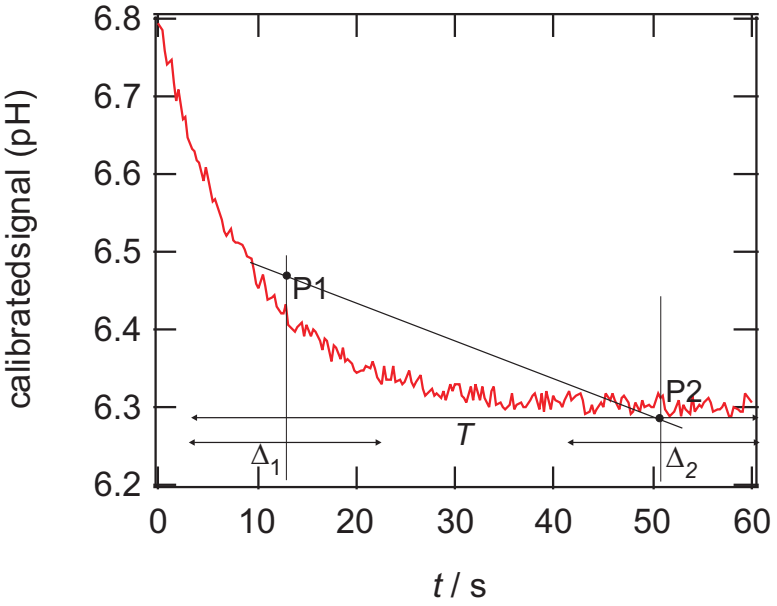

Figure A.13: Calibrated signal versus time during one reading period T. Depicted are the two significant time periods Δ_1 and Δ_2. P1 and P2 are the points for the drift calculation.

into three parts: Δ_1, Δ_2 and $T - \Delta_1 - \Delta_2$. The c.r.v. is the mean value of the calibrated signal acquired during Δ_2. The drift is the slope of the straight line through two points: [mean of the calibrated signal acquired during Δ_1, Δ_1 / 2] and [mean of the calibrated signal acquired during Δ_2, $T - \Delta_2$ / 2]. Standard deviation is calculated from the calibrated signal acquired during Δ_2.

The formulas for calculating the c.r.v., drift and standard deviation of the signal are:

$$\mathrm{crv} = \frac{\int_{T-\Delta 2}^{T} pH \cdot dt}{\int_{T-\Delta 2}^{T} dt}$$

$$\text{drift} = \frac{\frac{\int_0^{\Delta 1} pH \cdot dt}{\int_0^{\Delta 1} dt} - \frac{\int_{T-\Delta 2}^{T} pH \cdot dt}{\int_{T-\Delta 2}^{T} dt}}{T - \frac{\Delta 1 + \Delta 2}{2}} \tag{A.1}$$

$$\text{stdev} = \frac{\sqrt{\int_{T-\Delta 2}^{T} (pH - crv)^2 \cdot dt}}{\int_{T-\Delta 2}^{T} dt} \tag{A.2}$$

The input global parameters for this subroutine are: the drift criterion (drift_crit), drift monitoring interval (T), first and second data acquisition interval (Δ_1 and Δ_2) and the maximum waiting time (TO_drift).

Dynamic mode addition calculation (SV_Dynamic_Disp_d.vi) The dose of a titrant is calculated from the two recent points in the titration curve by using the formula:

$$\text{addititon} = \frac{\text{c}_{\text{att}} \cdot \Delta\text{pH} \cdot (\text{V}_2 - \text{V}_1)}{\text{pH}_2 - \text{pH}_1} \tag{A.3}$$

where V_2, V_1, pH_1 and pH_2 are the volumes and the pH values of the two most recent data points, respectively (see figure A.13). The attenuation constant c_att was introduced to decrease the overshootings that cause a lower data density before the equivalence point. Conversely, undershooting and consequent accumulation of data points appear after the equivalence point. Therefore, c_{att} has to be assigned the highest possible value, but which still sufficiently attenuates the overshooting (usually, 0.7-0.8 is a good choice, but this depends on the concentrations of the solutions in the burettes). The method is depicted in figure A.14

Input global parameters: The aimed pH increment (Dyn_delta_E), attenuation factor (C_slope)

Calculation of the dosages for the initial solution In this subroutine, the initial volumes of the acid (Va), base (Vb), salt (Vs) and water (Vw), are cal-

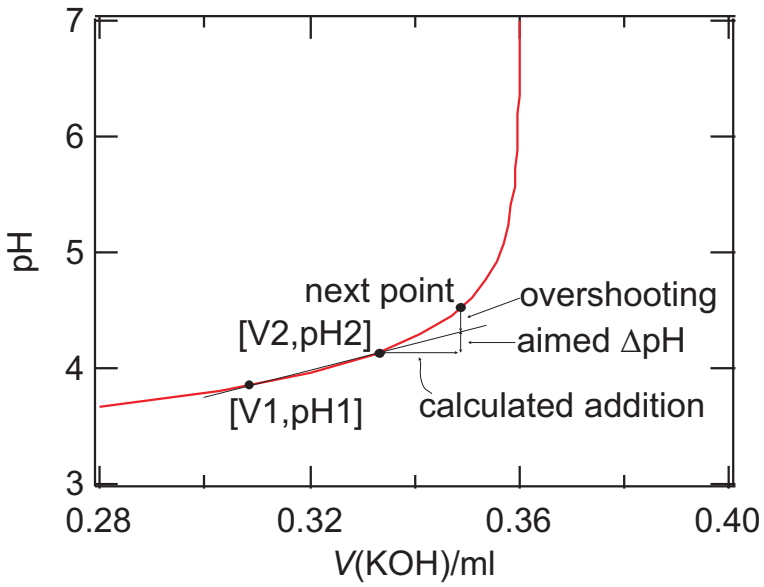

Figure A.14: Dynamic addition calculation. The red line is the titration curve (blank HCl-KOH titration), [V1,pH1] and [V2,pH2] are the two recently measured data points.

culated according to the initial pH (pHinit), initial ionic strength (I(1)), total volume (Vtinit), sample volume (Vsample), and all the components that were added to the cell prior to the experiment: Va_in, ca_in and Vb_in, cb_in are the volumes and concentrations of added of acid and base solutions, respectively, Vs_in and cs_in are the volume and concentration of added salt solution, ns_in is the amount of added solid salt in moles, and Vsample is the total volume of all added solutions (for example, it can include the volume of some sample of a weak acid, and the volumes of the acid and base added to the cell previously). The initial pH, ionic strength, total volume, sample volume, and the concentrations of the burette solutions of acid (ca), base (cb), salt (cs) are set in the global parameter subroutine. The initial additions of acid, base, salt and water additions are calculated in the following manner: First the acid or base addition is calculated, according to the initial pH:

$$\mathrm{Va} = \frac{\mathrm{Vtinit} \cdot (10^{-\mathrm{pHinit}} - 10^{\mathrm{pHinit}-\mathrm{pKw}}) - \mathrm{ca\_in} \cdot \mathrm{Va\_in} + \mathrm{cb\_in} \cdot \mathrm{Vb\_in}}{\mathrm{ca}} \quad \text{(A.4)}$$

$$\mathrm{Vb} = \frac{\mathrm{Vtinit} \cdot (10^{\mathrm{pHinit}-\mathrm{pKw}} - 10^{-\mathrm{pHinit}}) - \mathrm{cb\_in} \cdot \mathrm{Vb\_in} + \mathrm{ca\_in} \cdot \mathrm{Va\_in}}{\mathrm{cb}} \quad \text{(A.5)}$$

If the calculated acid or base addition is smaller than 0 (pHinit ≤ 7, then Vb ≤ 0, otherwise if pHinit ≥ 7, then Va ≤ 0), it is set to 0 for further calculation. Then, the salt addition can be calculated:

$$\mathrm{Vs} = \mathrm{Vtinit}\frac{2 \cdot \mathrm{I} \cdot \mathrm{Vtinit} - \mathrm{sum}}{2 \cdot \mathrm{cs} \cdot \mathrm{Vtinit}} \quad \text{(A.6)}$$

$$\begin{aligned} \mathrm{sum} \;=\; & \mathrm{ca} \cdot \mathrm{Va} + \mathrm{cb} \cdot \mathrm{Vb} + \mathrm{ca\_in} \cdot \mathrm{Va_in} + \\ & + \mathrm{cb\_in} \cdot \mathrm{Vb\_in} + \mathrm{absacid} + \mathrm{cs\_in} \cdot \mathrm{Vs\_in} + \mathrm{ns\_in} \cdot 1000 \end{aligned} \quad \text{(A.7)}$$

$$\mathrm{absacid} = |\mathrm{ca} \cdot \mathrm{Va} + \mathrm{ca\_in} \cdot \mathrm{Va\_in} - \mathrm{cb} \cdot \mathrm{Vb} - \mathrm{cb\_in} \cdot \mathrm{Vb\_in}| \quad \text{(A.8)}$$

Finally, the water addition is the difference between the initial total volume (Vtinit) and the acid (Va), base (Vb), salt (Vs), and sample additions (Vsample):

$$\mathrm{Vw} = \mathrm{Vtinit} - \mathrm{Vsample} - \mathrm{Va} - \mathrm{Vb} - \mathrm{Vs} \tag{A.9}$$

Input global parameters: initial pH (pHinit), initial ionic strength (I(1)), total volume (Vtinit), sample volume (Vsample), Va_in, ca_in, Vb_in, cb_in, Vs_in, cs_in, ns_in and Vsample (see the above definitions).

The pH adjustment procedure (Constant addition mode) This subroutine is used to adjust the pH to the pHinit value at the beginning of the experiment, or in the scenario with one-way titrations (see A). Constant volumes of the titrant (V_ad_dose) are added until the pH exceeds the initial value (pH_init). Then, the addition volume is split by half, and the titrant is changed (to acid if initially it was base, and vice-versa). This procedure is repeated until the convergence criterion ($|\mathrm{pH\_init} - \mathrm{pH}| \leq \mathrm{delta\_pH\_init}$) is satisfied.

Input global parameters: the initial pH (pH_init), constant titrant addition (V_ad_dose), the convergence criterion for the procedure (delta_pH_init)

Ionic strength adjustments In the constant ionic strength mode, this subroutine is called after each acid or base addition. It calculates and doses the salt (Vs) or water (Vw) additions needed to correct for the ionic strength changes. The formulas for the calculation are:

$$\mathrm{Vs} = \frac{\mathrm{I} \cdot \mathrm{Vt} - \mathrm{cs} \cdot \mathrm{Vst} - \mathrm{cs\_in} \cdot \mathrm{Vs\_in} - \mathrm{ns} \cdot 10^3 - \frac{1}{2} \cdot \mathrm{sum}}{\mathrm{cs} - \mathrm{I}} \tag{A.10}$$

$$\mathrm{sum} = \mathrm{ca} \cdot \mathrm{Va} + \mathrm{ca\_in} \cdot \mathrm{Va\_in} + \mathrm{cb} \cdot \mathrm{Vb} + \mathrm{cb\_in} \cdot \mathrm{Vb\_in} + \mathrm{abs} \tag{A.11}$$

$$\mathrm{abs} = |\mathrm{ca} \cdot \mathrm{Va} + \mathrm{ca\_in} \cdot \mathrm{Va\_in} - \mathrm{cb} \cdot \mathrm{Vb} - \mathrm{cb\_in} \cdot \mathrm{Vb\_in}| \tag{A.12}$$

$$\mathrm{Vw} = \frac{\mathrm{sum1}}{2 \cdot \mathrm{I}} - \mathrm{Vt} \tag{A.13}$$

$$\begin{aligned} \mathrm{sum1} \quad = \quad & \mathrm{ca} \cdot \mathrm{Va} + \mathrm{ca\_in} \cdot \mathrm{Va\_in} + \mathrm{cb} \cdot \mathrm{Vb} + \mathrm{cb\_in} \cdot \\ & \mathrm{Vb\_in} + \mathrm{abs} + 2 \cdot \mathrm{cs} \cdot \mathrm{Vs\_t} + 2 \cdot \mathrm{cs\_in} \cdot \mathrm{Vs\_in} + 2 \cdot \mathrm{ns} \cdot 10^3 \end{aligned} \tag{A.14}$$

Input global parameters: Ionic strength

Acknowledgements

I dedicate this thesis to my parents.

Special thanks to prof. Michal Borkovec, for all his support.

As well, I would in particular like to thank the following people, whose help was invaluable:

Mr. Stéphane Jeannerret.

Dr. Cécile Géhin-Delval.

Dr. Jörg Kleimann.

Dr. Claire Chassagne.

Dr. Motoyoshi Kobayashi.

Mr. Francois Bujard.

All the guys from the group, for discussion, support and friendship (Last but not least).

List of Figures

List of Tables

Bibliography

[1] Dautzenberg H., Jaeger W., Kötz J., Philipp B., Seidel Ch., and Stscherbina D. *Polyelectrolytes*. Carl Hanser Verlag, Munich, Vienna, New York, 1994.

[2] Zimmermann R., Kratzmuüller T., Erickson D., Li D. Q., Braun H.G., and C. Werner. *Langmuir*, 20:2369–2374, 2004.

[3] Scherrenberg R., Coussens B., van Vliet P., Edouard G., Brackman J., de Brabander E., and Mortensen K. *Macromolecules*, 17:456–461, 1998.

[4] Biesheuvel M. P. and Cohen Stuart M. A. *Langmuir*, 31:2785–2791, 2004.

[5] Hoagland D. A., Smisek D. L., and Chen D. Y. *Electrophoresis*, 17:1151–1160, 1996.

[6] Borkovec M., Jönsson B., and Koper G. J. M. In E. Matijevic, editor, *Surface and Colloid Science*, volume 16. Kluwer Academic/Plenum Publishers, New York, 2001.

[7] Decher G. *Science*, 277:1232–1237, 1997.

[8] Stumm W. and Morgan J. J. *Aquatic Chemistry*. John Wiley and Sons, New York, 1996.

[9] Hill T.L. *Statistical Thermodynamics*. Dover, New York, 1986.

[10] Atkins P. W. *Physical Chemistry*. Oxford University Press, Oxford, 1994.

[11] Smith R. M. and Martell A. E. *Critical Stability Constants*, volume 6. Plenum Press, New York, 1989.

[12] Contescu C., Jagiello J., and Schwarz J. A. *Langmuir*, 9:1754–1756, 1996.

[13] Miyake S. *Talanta*, 13:1253, 1966.

[14] Avdeef A. *Analytical Chemistry*, 50:2137–2142, 1978.

[15] Toren E. C. Jr. *Analytical Chemistry*, 40(402R-413R), 1968.

[16] Kinniburgh D. G. and Milne C. J. Guide to the wallingford titrator. Technical, British Geological Survey, 1992.

[17] Nag fortran library, mark 18, 1997.

[18] Baes C. F. Jr. and Mesmer R. E. *The Hydrolysis of Cations*. Krieger, Malabar, 1986.

[19] Press W. H., Teukolsky S. A., Vetterling W. T., and Flannery B. P. *Numerical Recipes in Fortran*. Cambrige University Press, Cambridge, 1986.

[20] Gans P. and O'Sullivan B. *Talanta*, 51:33–37, 2000.

[21] Sun L. and Crooks R. M. *Journal of Physical Chemistry B*, 106:5864–5872, 2002.

[22] Vögtle F., Gestermann S., Hesse R., Schwierz H., and Windisch B. *Progress in Polymer Science*, 25:987–1041, 2000.

[23] Ottaviani M. F., Monalti F., Romanelli M., Turro N. J. A., and Tomalia D. *Journal of Physical Chemistry B*, 100:11033–11042, 1996.

[24] Haensler J. and Szoka F. C. *Bioconjugate Chemistry*, 4(372-379), 1993.

[25] Kukowska-Latallo J. F., Bielinska A. U., Johnson J., Spindler R., Tomalia D. A., and Baker J. R. *Proceedings of the National Academy of Sciences*, 93:4897–4902, 1996.

[26] Prosa T. J., Bauer B. J., and Amis E. J. *Macromolecules*, 34:4897–4906, 2001.

[27] Nisato G., Ivkov R., and Amis E. J. *Macromolecules*, 33:4172–4176, 2000.

[28] Ramzi A., Scherrenberg R., Joosten J., Lemstra P., and Mortensen K. *Macromolecules*, 35:827–833, 2002.

[29] Ottaviani M. F., Valluzzi R., and Balogh L. *Macromolecules*, 35:5105–5115, 2002.

[30] Chen W., Tomalia D. A., and Thomas J. L. *Macromolecules*, 33:9169–9172, 2000.

[31] Betley T. A., Banaszak Holl M. M., Orr B. G., Swanson D. R., Tomalia D. A., and Baker J. R. *Langmuir*, 17:2768–2773, 2001.

[32] van Duijvenbode R. C., Koper G. J. M., and Böhmer M. R. *Langmuir*, 16:7713–7719, 2000.

[33] van Duijvenbode R. C., Borkovec M., and Koper G. J. M. *Polymer*, 39:2657–2664, 1998.

[34] van Duijvenbode R. C., Rajanayagam A., Koper G. J. M., Baars M. W. P. L., de Waal B. F. M., Meijer E. W., and Borkovec M. *Macromolecules*, 33:46–52, 2000.

[35] Kabanov V. A., Zezin A. B., Rogacheva V. B., Gulyaeva Z. G., Zansochova M. F., Joosten J. G. H., and Brackman J. *Macromolecules*, 31:5142–5144, 1998.

[36] Koper G. J. M., van Genderen M. H. P., Elissen-Roman C., Baars M. W. P. L., Meijer E. W., and M. Borkovec. *Journal of the American Chemical Society*, 119:6512–6521, 1997.

[37] Borkovec M. and Koper G. J. M. *Analytical Chemistry*, 72:3272–3279, 2000.

[38] Huang Q. R., Dubin P. L., Moorefield C. N., and Newkome G. R. *Journal of Physical Chemistry*, 104:898–904, 2000.

[39] Welch P. and Muthukumar M. *Macromolecules*, 31:5892–5897, 1998.

[40] Pericet-Camara R., Papastavrou G., and Borkovec M. *Langmuir*, 20:3264–3270, 2004.

[41] Niu Y., Sun L., and Crooks R. M. *Macromolecules*, 36:5725–5731, 2003.

[42] Borkovec M. and Koper G. J. M. *Journal of Physical Chemistry*, 98:6038–6045, 1994.

[43] Borkovec M. and Koper G. J. M. *Macromolecules*, 30:2151–2158, 1997.

[44] van Duijvenbode R.C., Rajanayagam A., Koper G.J.M., Borkovec M., Paulus W., Steuerle U., and Haussling L. *Physical Chemistry Chemical Physics*, 24:5649–5652, 1999.

[45] Noszal B. *Journal of Physical Chemistry*, 90:4104–4110, 1986.

[46] Rabenstein D. L. *Journal of the American Chemical Society*, 95:2797–2803, 1973.

[47] Rabenstein D. L. and T. L. Sayer. *Analytical Chemistry*, 48(1141-1146), 1976.

[48] Mernissi-Arifi K., Schmitt L., Schlewer G., and Spiess B. *Analytical Chemistry*, 67(2567-2574), 1995.

[49] Felemez M., Bernard P., Schlewer G., and Spiess B. *Journal of the American Chemical Society*, 122:3156–3165, 2000.

[50] Zhang X. X., Oscarson J. L., Izatt R. M., Schuck P. C., and Li D. *Journal of Physical Chemistry*, 104:8598–8605, 2000.

[51] Yamamoto K., Higuchi M., Shiki S., Tsuruta M., and Chiba H. *Nature*, 415:509–511, 2002.

[52] Sideratou Z., Tsiourvas D., and Paleos C. M. *Langmuir*, 16:1766–1769, 1999.

[53] Lee I., Athley B. D., Wetzel A. W., Meixner W., Baker Jr. J. R., Tomalia D. A., and Baker J. R. *Macromolecules*, 35:4510–4520, 2002.

[54] Perrin D. D., Dempsey B., and Serjeant E. P. *pKa Prediction fpr Organic Acids and Bases*. Chapman and Hall, London, 1981.

[55] Russel W. B., Saville D. A., and Schowalter W. R. *Colloidal dispersions*. Cambridge University Press, Cambridge, 1989.

[56] de Gennes A. *Scaling Concepts in Polymer Physics*. Ithaca, NY, 1979.

[57] Fleer G. J., Stuart M. A., Scheutjens J. M. H. M., Cosgrove T., and Vincent B. *Polymers at Interfaces*. Chapman and Hall, London, 1993.

[58] Tran Y. and Auroy P. *Journal of the American Chemical Society*, 123:3644–3654, 2001.

[59] Belloni L. *Journal of Chemical Physics*, 119:7560–7565, 2003.

[60] Evans D. F. and Wennerström H. *The Colloidal Domain*. Wiley-VCH, New York, 1999.

[61] Behrens S. H., Christl D. I., Emmerzael R., Schurtenberger P., and Borkovec M. *Langmuir*, 16:2566–2575, 2000.

[62] Yu W. L., Bouyer F., and Borkovec M. *Journal of Colloid and Interface Science*, 241:392–399, 2001.

[63] Bouyer F., Yu W. L., Robben A., and Borkovec M. *Langmuir*, 392-399(17):5225–5231, 2001.

[64] Vermeer A. W. P. and Koopal L. K. *Langmuir*, 14:4210–4216, 1998.

[65] Rojas O. J., Ernstsson M., Neumann R. D., and Claesson P. M. *Langmuir*, 18:1604–1612, 2002.

[66] Shubin V. and Linse P. *Macromolecules*, 30:5944–5952, 1997.

[67] Shubin V. *Journal of Colloid and Interface Science*, 191:372–377, 1997.

[68] Goloub T. P., Koopal L. K., and Bijsterbosch B. H. *Langmuir*, 12:3188–3194, 1996.

[69] Vermeer A. W. P. and Koopal L. K. *Journal of Colloid and Interface Science*, 212:176–185, 1999.

[70] Vermeer A. W. P., van Riemsdijk W. H., and Koopal L. K. *Langmuir*, 14:2810–2819, 1998.

[71] Haronska P., Vilgis T. A., Grottenmüller R., and Schmidt M. *Macromolecular theory and simulations*, 7:241–247, 1998.

[72] Blaakmeer J., Böhmer M. R., Cohen Stuart M. A., and Fleer G. J. *Macromolecules*, 23:2301–2309, 1990.

[73] Schudel M., Behrens S. H., Holthoff H., Kretzschmar R., and Borkovec M. *Journal of Colloid and Interface Science*, 196:241–253, 1997.

[74] Healy T. W. and White L. R. *Advances in Colloid and Interface Science*, 9:303–345, 1978.

[75] Davies J. A., James R. O., and J. O. Leckie. *Journal of Colloid and Interface Science*, 63:480–499, 1978.

[76] Hiemstra T., van Riemsdijk W. H., and Bolt G. H. *Journal of Colloid and Interface Science*, 133:91–104, 1989.

[77] Hiemstra T., de Wit J. C. M., and van Riemsdijk W. H. *Journal of Colloid and Interface Science*, 133:105–117, 1989.

[78] Kallay N. and Blesa M. A. *Advances in Colloid and Interface Science*, 28:111–134, 1988.

[79] Prelot B., Janusz W., Thomas F., Villieras F., Charmas R., Piasecki W., and Rudzinski W. *Journal of Physical Chemistry B*, 106:13280–13286, 2002.

[80] Berne B. J. and Peccora R. *Dynamic Light Scattering*. Wiley, New York, 1976.

[81] O'Brien R. W. and White L. R. *Journal of the chemical society - Faraday transactions II*, 74:1607–1626, 1978.

[82] Wagberg L., Pettersson G., and Notley S. *Journal of Colloid and Interface Science*, 274:480–488, 2004.

[83] Meszaros R., Thompson L., Bos M., and de Groot P. *Langmuir*, 18:6164–6169, 2002.

[84] Szekeres M., Dekany I., and de Keizer A. *Colloids and Surfaces*, 141:327–336, 1998.

[85] Shubin V., Samoshina Yu., Menshikova A., and Evseeva T. *Colloid and Polymer Science*, 275:655–660, 1997.

[86] Beltran S., Hooper H. H., Blanch, H. W., and Prausnitz J. M. *Macromolecules*, 24:3178–3184, 1991.

[87] Park S. Y., Barrett C. J., Rubner M. F., and Mayes A. M. *Macromolecules*, 34:3384–3388, 2001.

[88] Bolt G. H. *Journal of Physical Chemistry*, 61:1166–1169, 1957.

[89] Tadros Th. F. and Lyklema J. *Journal of Electroanalytical Chemistry*, 17:267–275, 1968.

[90] Yates D. E. and Healy T. W. *Journal of Colloid and Interface Science*, 55:9–19, 1976.

[91] Wells J.D., Koopal L. K., and de Keizer A. *Colloids and Surfaces*, 166:171–176, 2000.

[92] Hiemstra T. and van Riemsdijk W. H. *Journal of Colloid and Interface Science*, 179:488–508, 1996.

[93] Meeussen J. C. L., Filius J. D., Hiemstra T., and van Riemsdijk W. H. *Journal of Colloid and Interface Science*, 244:31–42, 2001.

[94] Boily J-F., Persson P., and S. Sjöberg. *Geochimica et Cosmochimica Acta*, 64:3453–3470, 2000.

[95] Rietra R. P. J. J., Hiemstra T., and van Riemsdijk W. H. *Geochimica et Cosmochimica Acta*, 63:3009–3015, 1999.

[96] Hiemstra T. and van Riemsdijk W. H. *Journal of Colloid and Interface Science*, 136:132–150, 1990.

[97] Mahltig B., Rehahn M., and M. Stamm. *Polymer Bulletin*, 45:501–508, 2001.

[98] Mahltig B., Gohy J-F., Jerome R., and Stamm M. *Journal of Polymer Science B*, 39:709–718, 2001.

[99] Ennis J., Sjöström L., Akesson T., and Jönsson B. *Journal of Physical Chemistry*, 201:2149–2164, 1998.

[100] Eisenman G., Bates R., Mattock G., and Friedman S. M. *The Glass Electrode*. Wiley, New York, 1965.

[101] Jeannerret S. Highimp4 user's guide. Technical report, Department of inorganic, analytical and applied chemistry, University of Geneva, 2004.